THÈSE

PRESENTÉE À

L'UNIVERSITÉ DE NEUCHÂTEL

FACULTÉ DES SCIENCES
INSTITUT DE MICROTECHNIQUE

ET À

L'UNIVERSITÉ BORDEAUX I

ÉCOLE DOCTORALE DES SCIENCES PHYSIQUES ET DE L'INGÉNIEUR
LABORATOIRE IMS

Par Guilherme BONTORIN ALVES

POUR OBTENIR LE GRADE DE

DOCTEUR ÈS SCIENCES

SPÉCIALITÉ : Électronique, Microtechnologie

MATRICE D'ÉLECTRODES INTELLIGENTES
Un Outil pour Améliorer les Performances Spatiotemporelles des Systèmes Hybrides (Vivant-Artificiel), en Boucle Fermée et en Temps Réel.

Soutenue le : **24 septembre 2010**

Acceptée sur proposition du jury:

Prof. Dr. Sylvie RENAUD	**Co-Directrice de thèse**
Prof. Dr. Peter SEITZ	**Co-Directeur de thèse**
Prof. Dr. Ricardo Augusto DA LUZ REIS	**Rapporteur**
Dr. Michel DUMAS	**Rapporteur**
Prof. Dr. Bogdan NICOLESCU-CATARGI	**Examinateur**
Dr. Luca BERDONDINI	**Examinateur**

– 2010 –

Université de Neuchâtel unine

FACULTE DES SCIENCES
Secrétariat-Décanat de la faculté
- Rue Emile-Argand 11
- CP 158
- CH-2009 Neuchâtel

IMPRIMATUR POUR LA THESE

Matrice d'électrodes intelligentes : un outil pour améliorer les performances spatio-temporelles des systèmes hybrides (vivant-artificiel), en boucle fermée et en temps réel

de M. Guilherme BONTORIN ALVES

REALISEE EN COTUTELLE AVEC

L'UNIVERSITE DE BORDEAUX I

et

L' UNIVERSITE DE NEUCHATEL (CH)

FACULTE DES SCIENCES

La Faculté des sciences de l'Université de Neuchâtel, sur le rapport des membres du jury

Mme. S. Renaud (co-directrice de thèse, Uni. Bordeaux I),
MM. P. Seitz (co-directeur de thèse, EPFL), L. Berdondini (ITT Gênes I),
M. Dumas (Uni. Montpellier), M. Nicolescu-Catargi (CHU Bordeaux), R. Reis (UFRGS, Brésil)

autorise l'impression de la présente thèse.

Neuchâtel, le 28 septembre 2010

Le doyen:
P. Kropf

■ Téléphone : +41 32 718 21 00 ■ E-mail : secretariat.sciences@unine.ch ■ www.unine.ch/sciences

To my mother,

ACKNOWLEDGMENTS

This PhD thesis was supported by the European Union through the projects:

- Neuroversity: Marie Curie - RTN-CT-2005-019247;

- Facets: FP6-2004-IST-FETPI-015879;

- Neurobit: IST–2001-33564;

- Idea: FP6-516432

And, many people have also supported me directly during my PhD thesis. All my gratitude goes to:

- Sylvie RENAUD, a very dedicated and special thesis supervisor and person, for her extraordinary and continuous support during all these years, my Master and my PhD theses.

- Jean TOMAS, Kilian IMFELD, Christian ROBERT, Milena KOUDELKA-HEP, and Peter SEITZ, for their supervision, help, and advice at all stages of the work;

- Pascal FOUILLAT, Pierre-André FARINE, and Nico F. DE ROOIJ heads of, respectively, IMS (Intégration du Matériau aux Système), ESPLAB (Electronics and Signal Processing), and SAMLAB (Sensors, Actuators, and Microsystems) laboratories, for the opportunity and freedom to work in their respective laboratories;

- Ricardo Augusto DA LUZ REIS and Michel DUMAS, for accepting the invitation to be external reporters on the manuscript and their useful remarks;

- Lucas BERDONDINI, Bogdan NICOLESCU-CATARGI, for accepting the invitation to be in the jury;

- Jochen LANG, Gwendal LE MASSON, Jaap VAN PELT, Bernard VEYRET, Matthieux RAOUX, André GARENNE, and Gilles CHANPENTIER; for their assistance and useful conversations about the biologists' way-of-life and philosophy;

- Sébastien MOUTAULT, Jean-Luc DUMAS, and Patrice TESSON, my colleagues, for organizing and proposing my teaching;

- Sandrine PIFFARETTI and Chrystel PLUMEJEAU, for setting up all the administrative tasks and preparing my PhD viva very efficiently;

- All my colleagues from the IMT and Neuron teams, including: Adeline ZBRZESKI, Adel DAOUZLI, Adam QUOTB, Alexis BOEGLI, Bilel BELHADJ, Colin LOPEZ, Filipo GRASSIA, Florian KOLBL, Jean-Batiste FLODERER, Laure BUHRY, Noëlle LEWIS, Olivia MALLOT, Timothé LEVI, Sylvain SAÏGHI, Yannick BORNAT, Youssef BOUTAIB (Youhoo! ™), etc.; for their friendship, assistance, and especially for their help grounding me in the electronics way-of-life;

- All my fellow students from ENSEIRB and from the IUT-Bordeaux 1, for keeping me in touch the with learning process and for their fresh point of view.

- All my friends on this journey, including: Armando COSENTINO, Anna SCOLEGHI, Aroun GUIRY, Aurore MOUTIER, Beatriz STIRNER, Bruno FOLADOR, Bruno and Janine INOCENTE, Cecilia MEZZOMO, Chau DOAN, Daniel MINEAU, Franciane GOMIG, Ha VU, Hélène BAUDOUIN, Heather LAWRENCE, Juliana STEFANNI, Ketleen ZANI, Linda GYSIN, Loïc CALCERRADA, Luiza RAFAGNIN, Patrice ANTOINNETE, Xia CHEN, Yu-Chi CHANG, …

- My closest family, Palmiro, Helena and Altamiro BALDÃO, for all their help, support and for everything they have done, given, conceived, been, …

- And, lastly, the most important, my mother: Angela BONTORIN, for absolutely EVERYTHING!

All my apologies to you, the ones I have forgotten in this speedy and short Monday morning. Please, feel free to complete:

- Special thanks and apologies to:

who I have unfortunately and mistakenly forgotten on this Monday morning.

TABLE OF CONTENTS

MOTIVATION 1

INTRODUCTION 7

I. HYNET: BOTTOM-UP APPROACH 9
A. NATURAL NEURAL NETWORK 9
B. ARTIFICIAL PART: CLOSING THE LOOP IN REAL-TIME 14
II. DESIGN: TOP-DOWN SPECIFICATIONS 16
A. BIOLOGY 17
B. ELECTRONICS 19

HYNET 23

I. SYSTEM PARTS 25
A. BIOWARE 25
B. HARDWARE 26
C. SOFTWARE 26
II. THE CLOSED-LOOP 26
A. ACQUISITION 27
B. CLOSING THE LOOP WITH THE SOFTWARE 31
C. STIMULATION 36
III. TIME PERFORMANCES 37
A. ACQUISITION 37
B. STIMULATION 38
C. CLOSED-LOOP 39
IV. DISCUSSION 40

PREAMPLIFIER 41

I. DESIGN 43
A. INPUT SIGNAL 44
B. MULTIELECTRODE ARRAYS (MEAS) WITH ACTIVE PIXEL SENSORS (APSS) 44
C. OPERATIONAL AMPLIFIER (OPA), HIGH CUTOFF FREQUENCY AND STABILITY 46
D. LOW CUTOFF FREQUENCY 47
E. NOISE CONSIDERATIONS 49
II - MEASUREMENTS 51
A. DRY MEASUREMENTS 51
B. DRY MEASUREMENTS SIMULATING WET MEASUREMENTS 55
C. WET MEASUREMENTS 56
III. DISCUSSION 57

DETECTOR 59

I. DESIGN 61
A. SIGNAL 62
B. DETECTION METHOD 62
C. THE CIRCUIT 66
II. MEASUREMENTS 69

A. DRY MEASUREMENTS 72
B. DRY SIMULATING WET MEASUREMENTS 72
C. WET MEASUREMENTS 74
III. DISCUSSION 75
A. THE DECISION MODULE 75
B. ADAPTATION MODULE 76
C. THE DETECTOR 76

CONCLUSION 79

I. THE HYNET 81
II. THE INTELLIGENT PIXEL 82
III. BIOELECTRONICS 84

REFERENCES 87

APPENDIXES 99

I. THE FIRST GENERATIONS OF PREAMPLIFIERS 101
II. LIST OF AUTHOR'S PUBLICATIONS 107
CHAPTERS IN BOOKS 107
PAPERS IN PEER-REVIEWED INTERNATIONAL JOURNALS 107
PAPERS IN PEER-REVIEWED INTERNATIONAL CONFERENCE PROCEEDINGS 107
MASTER THESIS 107
III. RÉSUMÉ EN FRANÇAIS 109
A. HYNET 109
B. LE PIXEL INTELLIGENT 112
C. CONCLUSION 117
IV. RESUMO EM PORTUGUÊS 119
A. HYNET 119
B. PIXEL INTELIGENTE 122
C. CONCLUSÃO 126

TABLE OF FIGURES

Figure 2.01 Characteristics of a Hynet. 9
Figure 2.02. An electrogenic cell, the neuron, and its anatomical parts: 9
Figure 2.03. The cell membrane and some of its channels. 10
Figure 2.04. Action potential (or spike) generation. 11
Figure 2.05. Synapse. 12
Figure 2.06. A chemical synapse. 13
Figure 2.07. The data flow in the Hynet closed-loop blocks 14
Figure 2.08. Potential solutions for the biological part of a Hynet and our final choice. 19
Figure 2.09. Potential solutions for the electronics part of a Hynet. 20
Figure 2.10. Hynet configurations related to next chapters of this manuscript: 21
Figure 3.01. The Hynet closed-loop. 25
Figure 3.02. Detailed view of the Hynet closed-loop. 26
Figure 3.03. Real-time monitoring of neural bursting activities induced by stimulations. 30
Figure 3.04. Four steps to describe a closed loop experiment. 31
Figure 3.05. The Condition Descriptor. 32
Figure 3.06. Timer Descriptor: the GUI window. 33
Figure 3.07 The Pattern Descriptor. 34
Figure 3.08. The Linker. 35
Figure 3.09. The command window of the ReTA application closing the loop. 36
Figure 3.10 Data propagation delays of the acquisition chain 38
Figure 3.11 Propagation delays for the stimulation chain 39
Figure 3.12. Data propagation delays of the complete Hynet closed-loop. 39
Figure 4.01. Location of the preamplifier. 43
Figure 4.02. A Passive MEA. 45
Figure 4.03. An MEA with the APS (Active Pixel Sensor) approach. 45
Figure 4.04: Schematic of the operational amplifier (OPA). 47
Figure 4.05. The OPA and its feedback circuit. 49
Figure 4.06. The Integrated Circuits (IC) design. 52
Figure 4.07. Characteristics of the alpha preamplifier: gain and phase. 53
Figure 4.08. Schematic of the experiment for dry simulating wet measurements. 56
Figure 4.09. Comparison between the signals amplified with the MCS chain and our amplifier 56
Figure 4.10. Schematic data flow for wet measurements. 57
Figure 4.11. Recordings of pancreatic ß-cells activity in a hyperglycemic (15 mM) medium. 57
Figure 5.01. The Intelligent Pixel (iP) schematic. 61
Figure 5.02. The activity detection circuit and its constituting blocks. 63
Figure 5.03. The activity detector. 66
Figure 5.04. The decision circuit. 67
Figure 5.05 The adaptation block. 68
Figure 5.06. The IC design. 70
Figure 5.07. Test of the adaptation. 72
Figure 5.08. Schematic of the experiment for dry simulating wet measurements. 73
Figure 5.09. Test of the detector with dry simulating wet signals. 73
Figure 5.10. Schematic of the experiment for wet measurements. 74
Figure 5.11. Recordings of pancreatic ß-cell activity in a hyperglycemic (15 mM) medium. 74
Figure F.01. La boucle Hynet. 109
Figure F.02. Détails de la boucle fermée. 110
Figure F.03. Le logiciel de fermeture de boucle. 111
Figure F.04. Délais de propagations des modules du Hynet. 112
Figure F.05. Location du pixel intelligent. 112
Figure F.06. Le pixel intelligent. 113
Figure F.07. Le schéma électrique du préamplificateur. 113
Figure F.08. Mesures avec des signaux neuronaux simulés. 114
Figure F.09 Le schéma du detector 115
Figure F.10. Test de l'adaptation. 116
Figure F.11. L'enregistrement de l'activité des cellules Bêta du pancréas dans un milieu hyperglycémique. 117
Figura P.01. O laço Hynet. 119
Figura P.02. Detalhes do laço fechado. 120
Figura P.03. O programa de fechamento de laço. 121
Figura P.04. Tempo de propagação dos módulos do Hynet. 121

Figura P.05. Localização do pixel inteligente. 122
Figura P.06. O pixel inteligente. 122
Figura P.07. Diagrama do pré-amplificador. 123
Figura P.08. Medidas com sinais neurais simulados. 124
Figure P.09 O diagrama do detector. 125
Figure P.10. Teste da adaptação. 125
Figura P.11. Registro da atividade de células Beta do pâncreas em um meio hiperglicêmico. 127

TABLE OF TABLES

Table 2.1 Examples of Hynets and their Biological and Electronics Implementation 20
Table 4.1 Main electrical characteristics of the alpha *amplifier.* 53
Table 4.2 Comparison of Alpha, Beta and Gamma amplifiers characteristics. 54
Table 4.3 Comparison of characteristics for Alpha, Beta, Gamma and literature amplifiers. 55
Table 5.1. Activity detectors from the literature. 63
Table 5.2 Characteristics of the detector. 71
Table 5.3 Detector's settings for each series of measurements. 75
Table 6.1 Review of major improvements provided to the research groups by this thesis project. 84
Table F.1 Principales caractéristiques électriques du préamplificateur 114
Table F.2 Caractéristiques du détecteur. 116
Table F.3 Résumé des principales améliorations apportées par ce travail à chacune des équipes. 118
Tabela P.1 Principais características do pré-amplificador. 123
Tabela P.2 Características do detector. 126
Tabela P.3 Resumo das melhorias apresentadas neste trabalho para cada um dos grupos. 127

CHAPTER 1
MOTIVATION

"One of the biggest problems the world must confront and solve is the unification of every field: politics, economics, demographics, religion, sociology, ..."

Pietro Ubaldi (1886–1972), Italian-Brazilian philosopher. In chapter 16 of "God's Law".

Bioelectronics, which is not a recent research field, aims to provide tools for the improvement of human life. The 18th century marks the beginning of studies in "animal electricity". Luigi Galvani (1737 – 1798) is one of the most popular pioneers (Foccacia07). He traveled across Europe with an interesting public demonstration: an electrical source was connected to dead frog's legs and: Surprise! They moved. Electricity was creating animation, "life". In the 20th century, Electronics emerged as a technology-based science that deals with methods to convey information and control devices by the use of the electrical flow.

Bioelectronics is the application of electronics knowledge and tools to biology and medicine. It is a multidisciplinary field, related to biology, medicine, physiology, physics, chemistry, mathematics, etc. These sciences interact, mixing, evolving, and allowing us to explore, control and, hopefully, improve human life.

At the beginning of this thesis, I will start by citing some of the tools designed in bioelectronics. Some are commercially available, *e.g.*:

1) Neural stimulator: this tool improves comfort. For example, it helps to control chronic pain (by stimulation of the spinal cord), control and treat chronic depression, reduce epileptic seizures (by stimulation of the vagus nerve), and treat urinary incontinence (by stimulation of the sacral nerve) (Nsanze05).

2) Brain stimulator: this tool stimulates the basal ganglia and reduces the motor dysfunctions in Parkinson disease. Nowadays, prostheses are based on open-loop systems (fixed stimulation patterns). They are functional, but the next generation stimulator will take into account the level of disorder and adapt the stimulation pattern. It decreases neural damage and increases battery and device lifetime (Robert09).

3) Cochlear Prostheses: this tool restores auditory function. It is based on the stimulation of the spiral ganglion or auricular nerve, depending on which system is still functional in the patient. The next generation prostheses will stimulate directly the cortex hearing area (Loeb03).

Examples of prototype tools (near to commercial use) are:

4) Neuromuscular Reanimation: this tool reanimates muscular movement, normally by the stimulation of a motor neuron. Modern prostheses use multiple sensors to integrate the natural feedbacks. (Loeb01).

5) Brain machine interface: this tool acquires and processes the activity of the brain. The machine "reads" the mind to interface brain activity with computers, robots or artificial limbs. (Nicolelis01)

And in the domain of academic research, we can cite:

6) Visual prostheses: this tool tries to stimulate the retina, the optical nerve, or the visual cortex. A main issue with these prostheses is the number of cells involved in the image processing. For example: a healthy retina owns about 100 million photoreceptors, the optical nerve has about a million axons, and about 70 % of the brain is involved with image processing (comprehension, memory, association, …). So the number and the density of stimulating channels are challenging issues (Weiland05).

7) Determination of insulin needs: the electrical activity of Pancreatic Beta Cells conveys information about the needs on insulin. These cells are intrinsic biosensors more performant than standard chemical sensors, as, unlike glucose, they also take into account hormonal and activity levels. Processing Beta cells electrical activity may be the basics for a new generation of implants for insulin control in diabetes (Raoux10).

8) Cognitive prostheses: Some experiments partially simulate and interface with small and low complexity neural networks. For example, (Beger05) presents a substitution of a part of hippocampus. Further prostheses would offer remedies for the cognitive and memory loss accompanying Alzheimer's disease, the speech and language deficits resulting from stroke, and the impaired ability to execute skilled movements following trauma to brain regions responsible for motor control. This may be a starting point for the "memory prostheses".

This is succinct and non-exhaustive list of bioelectronics' applications (a longer list is presented in (Bontorin06)). Some characteristics of these systems are common, such as natural-artificial interface, large-scale and high-density channels, large amount of data, real-time processing.

Hynet, or hybrid (living-artificial) networks, are extremely demanding systems when considering the pre-cited characteristics. *Hynet* are real-time, closed-loop systems with a living and an artificial part. During my thesis project, I designed and used a *Hynet*. I focused on improving its spatiotemporal performances to offer a performing experimental platform to examine the intrinsic dynamics of electrogenic cells' circuitry. This is done by the conscien-

tious and high integration of electronics functions on the acquisition chain, to create “intelligent” multielectrode arrays.

Chapter 2 (Introduction) introduces the definitions and basic aspects to understand space-time aspects on hybrid living-artificial systems. Chapter 3 (Hynet) describes the initial real-time closed-loop system based on cultured neural networks. Chapter 4 (Preamplifier) shows how to increase the number and the density of acquisition channels. Chapter 5 (Detector) proposes a solution to filter useless data and maintain the real-time feature while increasing the number of channels and amount of data. Chapter 6 (Conclusion) opens the field to further works and concludes the dissertation.

CHAPTER 2
INTRODUCTION

"In which we begin not to understand"

Gaston Leroux (1868-1927), French journalist and writer.
In "The Yellow House Mystery".

This dissertation presents my work on the development of a particular type of hybrid system, the Hybrid Network. I define a Hybrid Network (*Hynet*) (Fig 2.01) as a real-time closed-loop "Hybrid System".

A "Hybrid system" has two parts: a living one and an artificial one. "Closed-loop" means that these two parts communicate with each other in bidirectional mode, and that each one receives controlling inputs from the other. "Real-time" means that this communication is fast enough to avoid damage (loss or delay) on the data flow.

When these three characteristics are effective, the artificial and the living parts form a network, named a *Hynet*. We will see how a *Hynet* proves to be an efficient and adaptable experimental support to explore the dynamics and the adaptation process of electrogenic cells.

This introduction is divided into two parts. The first part shows the bottom-up design of a *Hynet* for a neural network. The second part presents a top-down view of the main design characteristics of the *Hynet*.

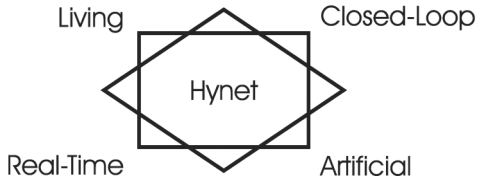

Figure 2.01 Characteristics of a Hynet. A real-time closed-loop system for interactions between living and artificial elements.

I. Hynet: bottom-up approach

A. Natural neural network

In a neural network, the basic element is the neuron. A neuron is an electrogenic cell from the nervous system. It processes and transmits information by electrochemical signaling. For this work, we use biophysical point models for the neurons.

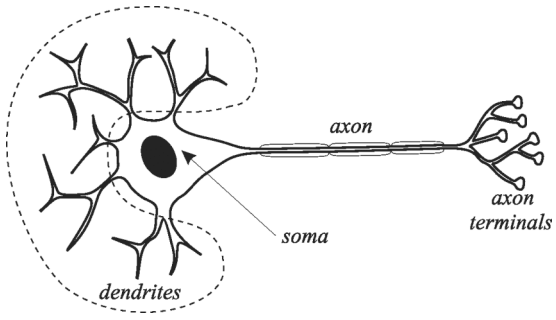

Figure 2.02. An electrogenic cell, the neuron, and its anatomical parts: dendrites, soma, axon, and axon terminals.

Anatomically, a neuron is composed of (Fig .02):

- dendrites: the branched projections of a neuron that act to conduct the electro-chemical stimulation received from other neural cells to the soma.

- soma: the cell body, which contains the nucleus.

- axon: a long, slender projection of a nerve cell, or neuron, that conducts electrical impulses away from the neuron's cell body or soma.

- axon terminals: branched projections of a neuron that act to conduct the electro-chemical stimulation to other cells.

The neural information is represented by electrochemical potential between the inside and the outside of the neuron.

At the resting equilibrium, the intracellular medium has an excess of potassium ions (K^+) and the extracellular one has an excess of sodium ions (Na^+). This misbalance of charges is maintained by: (a) the impermeability of the cell membrane to these ions and (b) an active (energy consuming) exchange of those ions by a pump (Fig. 2.03). At the resting point the membrane potential is about – 65 mV (the reference is the extracellular medium).

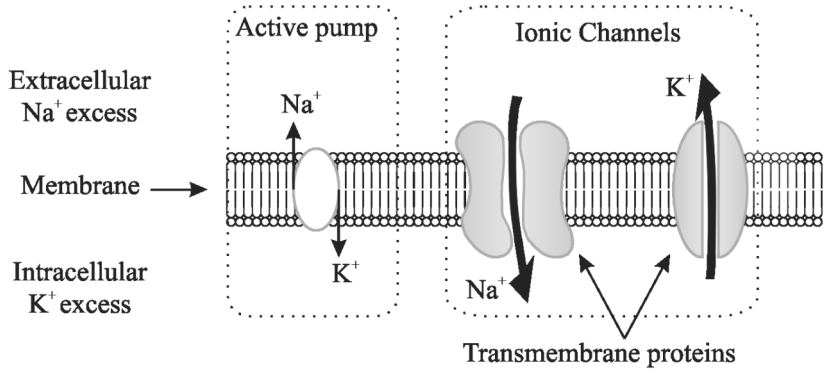

Figure 2.03. The cell membrane and some of its channels. The active pumps maintain a resting potential on the membrane. They transport the sodium (Na+) and potassium (K+) ions opposite to the gradient of concentration. It creates a potential energy across the membrane that is used by the ions to cross opened channels.

The cell membrane contains ion channels. They are selective to a determined type of ion. For example, the sodium channels pass only sodium ions, only under certain conditions on the membrane potential. The transfer of ions tends to restore the potential equilibrium (against the misbalance). At the resting point (Fig 2.04.A), sodium and potassium channels are closed.

If the electrical potential increases above the threshold, the sodium channels open (Fig 2.04.B). Sodium ions migrate into the cell and the membrane potential increases quickly (depolarization).

The increase of cell potential makes sodium channels close (Fig 2.04.C), and potassium channels open (Fig 2.04.C'). Potassium ions migrate out of the cell and as a consequence the membrane potential decreases. The low potential closes the potassium channel (Fig 2.04.D, hyperpolarization). Finally, the active pump slowly brings the membrane potential to the resting point.

This process generates an electrochemical wave, called an *action potential* or a *spike*. A cell presenting an action potential is said to be *firing* or *spiking*. I will use the verbs *fire* and *spike* in the rest of the text.

The action potential carries the information. Generated at the soma, this process is repeated through the axon until its terminations. Here, this information will be transmitted to other neurons.

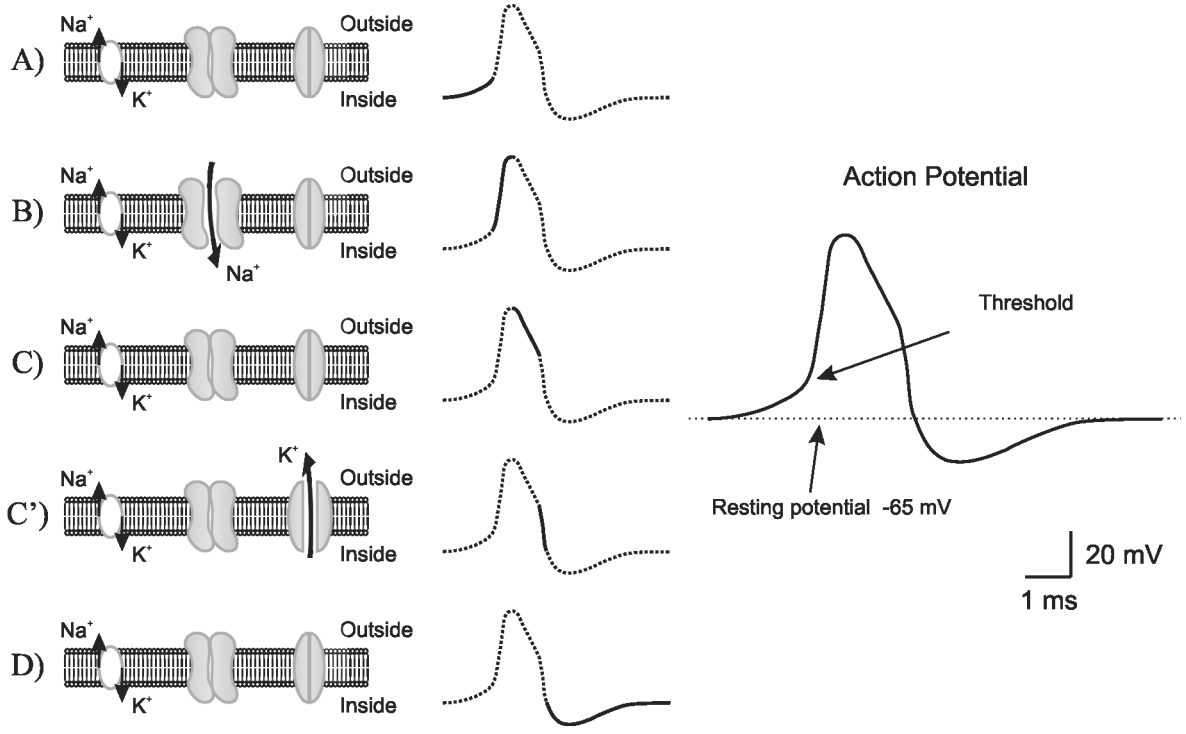

Figure 2.04. Action potential (or spike) generation. The potential energy across the membrane is used to transport the sodium and potassium ions through their respective channels. The sequential opening and closing of sodium and potassium channels creates the action potential.

Once the action potential reaches the axon terminals, it passes to another neuron through a synapse (Fig 2.05). Information passes by synapses, from the presynaptic neuron to the postsynaptic one.

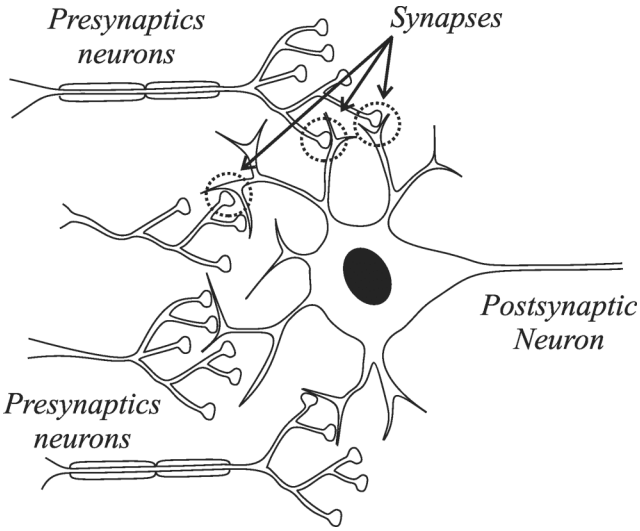

Figure 2.05. Synapse. The space between the presynaptic axonal terminals and the postsynaptic dendrites.

There are three different kinds of synapses: a. electrical, b. chemical, and c. neuromuscular. We will only cite chemical synapses in the context of our project (Fig 2.06). The mechanism involved in chemical synapses is the release of neurotransmitters, triggered by a presynaptic cell, to receptors on the postsynaptic cell. The process is the following:

When the presynaptic cell spikes, its membrane depolarization induces calcium channels to open, increasing the Ca^{++} concentration inside the cell. This concentration induces vesicles, which are filled with neurotransmitters, to fuse with the cell membrane. This expels the neurotransmitters inside the synaptic cleft (the narrow space between the presynaptic and the postsynaptic neurons). Some of these neurotransmitters bind chemical receptors on the postsynaptic cell membrane. These active receptors hyperpolarize or depolarize the postsynaptic cell, and eventually trigger a spike.

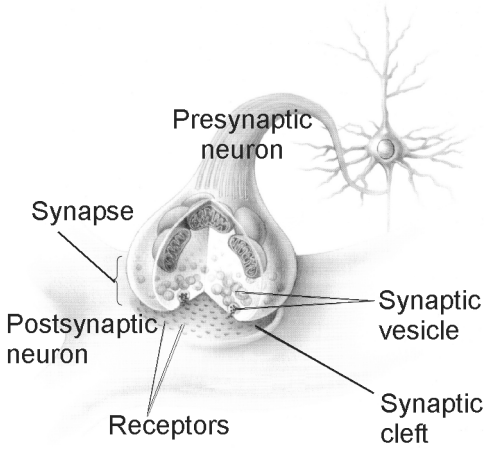

Figure 2.06. A chemical synapse. Expulsed vesicles by the presynaptic neuron liberate chemical substances sensed by the postsynaptic neuron receptors, and induce changes in the membrane voltage.

If an action potential in the presynaptic neuron causes a depolarization of the postsynaptic membrane, the synapse is called excitatory. The synapse is also said to "conserve" the signal, and "facilitate" the formation of an action potential in the postsynaptic neuron (the potential is closer to the spiking threshold level).

Also, if the firing of the presynaptic neuron causes the hyperpolarization of the postsynaptic membrane, this synapse is called inhibitory. We also say that this synapse is in opposition to the signal, and prevents the formation of an action potential in the postsynaptic neuron (the potential is further from the spiking threshold level).

The potential in the postsynaptic membrane changes according to the income of electrochemical information. If the membrane potential exceeds the threshold, an action potential is created (a neuron spikes or fires).

In addition to the inhibitory/excitatory categories, synapses can differ in their efficiency. More "efficient" synapses have more effect (more depolarization or more hyperpolarization) on the postsynaptic membrane. This efficiency is coded by the "synaptic weight". Synaptic weights change in the course of the neural network's life, by complex biological mechanisms of learning or plasticity (Gerstner02, Hebb49).

Each neuron has one or more presynaptic neurons. We consider synapses to transmit "information", coded as the variation in the membrane potential, by a hyperpolarization or a depolarization. Once the membrane potential exceeds a spiking threshold, an action potential is generated as described above. Each neuron can also be presynaptic to other neurons, so the data can in turn be transmitted to other neurons depending on synaptic weights, resulting in a global network handling information transmission.

B. Artificial part: closing the loop in real-time

The artificial part communicates with the living network to form a living-artificial closed-loop. The artificial part tasks are: to acquire the activity of the living part, to process the data, and to apply the relevant stimulation pattern (Fig 2.07)

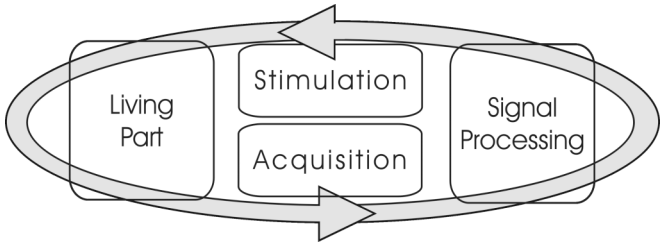

Figure 2.07. The data flow in the Hynet closed-loop blocks: living part, acquisition, signal processing, and stimulation.

Based on these three tasks, different declinations appear in the literature (Table 2.1), depending on the application.

(Chapin99) designed a Hynet to determine whether simultaneously recorded motor cortex neurons can be used for real-time device control. In this experiment, rats were trained to position a robot arm and obtain water by thinking on pressing a lever.

(Reger00) developed a *Hynet* between a brain of a lamprey and a small mobile robot. The mobile robot acted as an artificial body that delivers sensory information to the neural tissue and received command signals from it. The purpose of this system was to investigate the behavioral, computational and neurobiological mechanisms of sensory-motor learning.

(Jung01) presented a *Hynet* between a lamprey's spinal cord and an integrated circuit that mimicked the spinal motor pattern generation. The artificial part succeeded in establishing a persistent and stable oscillation similar to the natural one.

(Le Masson02) reconstructed a thalamocortical circuit using hardware and software neuron models connected to an *in vitro* preparation. The resulting experiments show that combining the gain control of feedback inhibition and the modulation of membrane excitability enables thalamic circuits to finely tune the gating of spike transmission from sensory organs to the cortex.

(Carmena03) demonstrated that primates can learn to reach and grasp virtual objects by controlling a robot arm through a closed-loop brain–machine interface (BMI). Using visual feedback, monkeys succeeded in producing robot reach-and-grasp movemented even when their arms did not move.

(Nowotny03) demonstrated that spike-timing dependent plasticity (STDP) enhanced synchronization (or entrainment) in a *Hynet* composed of a spike generator, a dynamic clamp emulating an excitatory plastic synapse, and a chemically isolated neuron from the Aplysia abdominal ganglion.

(Oprisan04) showed a *Hynet* composed of one bursting biological neuron and one bursting model neuron coupled using the dynamic clamp. The aim was to determine why elements of central pattern generators phase lock in a particular pattern in given conditions.

(Berger05) presented a biomimetic system with silicon neurons which function was to process information transmission between cortical brain regions, in the context of replacing the CA3 region of a Hippocampal slice.

(Whittington05) presented a *Hynet* that controlled and analyzed cardiac culture on planar MicroElectrode Arrays (MEA). Its aim was to study cardiac cell physiology, to improve the speed and accuracy of traditional open-loop stimulation protocols, pharmacological screening, and to improve biosensors based on acquiring electrical activity of cardiac cultures.

(Potter06) presented an interesting setup with embryonic rat neurons deposited on MEAs. The neural culture controlled external devices, such as virtual robots, actual robots or drawing robotic arms. The setup was also a tool for fundamental research in the burst control, stimuli efficiency, or plasticity and learning.

(Novelino07) showed a *Hynet* where embryonic rat neurons cultured on MEA were connected to a robot, simulating an “embodiment”. The aim was to study the biological neural processes of learning and adapting to unpredicted situations, the underlying computational properties, and the information coding.

The *Hynet* systems we designed in our group are related to three applications. The first one is the *Hynet*, for *Hybrid Neural Network*. The living part of *Hynet* is composed of embryonic rat neurons on an MEA compose the living part. The artificial part processes the data from the culture and sends electrical stimuli. This setup is a basis for the study of complex learning and plasticity rules. It is detailed in the next chapter of this document.

The second one is the *Wave-Hynet*, for the study of the functional influence of electromagnetic waves, such as those generated on Global System Mobile (GSM) at 1.8 GHz, on neural networks. We are also looking for the therapeutical influence of waves therapeutically.

The third one is the *Gluc-hynet* where the living part consists of pancreatic beta cells on MEAs. This system processes the electrical activity of the cells (used as complex glucose bio-sensors) to evaluate online the insulin need.

In all these systems, the purpose of creating a hybrid network is to integrate the artificial and the living parts within a single cellular network. Consequently, the artificial part must "listen to" and "talk to" the living part "coherently". By coherent, we mean that the system must avoid any data flow damage (loss or unacceptable delay).

Real-time is our key word for optimizing communication. (Joseph88) defines a real-time system as a system whose computations and actions satisfy defined time constraints. This time constraint is represented by a deadline (DL), which is defined by the application. (Burns01) defines two different DL for real-time systems. They are: (a) the Soft DL: this DL that can be missed without compromising the system's integrity; (b) the Hard DL: this DL's failure implies an error, and compromises definitely the task. These two deadlines are defined to determine the minimal performances of the processing system (Lu02).

The way the cells encode significant information defines the useful bandwidth of the signal. Through the Nyquist-Shannon theorem, we find the minimum sampling frequency and its respective period. Within this sampling period (*i.e.* within the time step between 2 acquisitions) the online data processing must be executed in order to ensure real-time.

The **closed-loop period** is the time taken by the system between the acquisition and the related feedback answer. This corresponds to a hard deadline (DL) and missing it implies an error.

To illustrate soft deadlines in *Hynet*, we can mention the monitoring of acquired data: even if real-time monitoring is highly appreciated, a delay will not compromise the integrity of the experiment. This is a soft DL and missing it will only result in a warning.

This summarizes the main required aspects of a *Hynet*: hybrid living-artificial, closed-loop and real-time. From this global vision, we need to better analyze specific parts of the system in order to design and to implement.

II. Design: Top-down specifications

In all bioelectronics systems, the developer's specifications spread to both, biological and electronics fields. Concerning biology, global solutions are: *in vivo* or *in vitro* experiments, acute slice or dissociate cultures, and intracellular or extracellular interfaces. From the

electronics point of view, rough implementation categories are: software or hardware, discrete components or integrated circuits (IC), and digital or analog.

A. Biology

The first specification to define is *in vivo* vs. *in vitro*. "*In vivo*" occurs when the electronics device is connected to cells in a living body. "*In vitro*" happens when the cells are extracted or cultured externally and maintained in a physiological medium. The main advantages of *in vivo* are that the cell environment is close to normal; they are embodied in their functional system and act as input/output access to that system. But the disadvantages are the animal stress, the eventual anesthesia, and the body aggression by unnatural materials. On the other hand *in vitro* has the advantages of: cheaper maintenance, easier handling, and shorter access to cells. However the drawback is the absence of *in vivo* elements, such as physiological regulations and antibodies.

The second choice is about: acute slice or dissociated culture. Acute slices maintain the cells in the same network configuration as is the living body. However they have a short life time. This is the case of studies on the hippocampus network. On the other hand, dissociated cultures are more relevant to studies on learning and plasticity. In this case the cells are separated at the beginning of the experiments and are expected to reconnect and build a network over a long period of time (days or weeks).

Finally, a standard configuration choice is the intracellular vs. extracellular interface. An intracellular electrode pierces the cell. This access provides a measure of the neuron membrane voltage with a good signal to noise ratio (SNR), but connections are restricted to a small number (a few units) and a limited duration (a few hours). Extracellular electrodes acquire the signal through capacitive coupling, without perforating the cellular membrane. This increases the cell lifetime and the duration of the experiment (a few weeks, even months). Classical technological solutions for extracellular electrodes are Multi Electrodes Arrays (MEAs) which provide multiple access points to the biological preparation (from tens to thousands).

Extracellular acquisitions present two essential drawbacks. The first one is low amplitude. The intracellular activity potential amplitude is in the 100 mV range for neurons and 20 mV for β-cells. But extracellular potentials are in the $\pm 100\,\mu V$ range for neurons. (Harrison07a, Chay97). The second one is high noise level, when compared to the signal amplitude. Low amplitude signals are more sensitive to noise, as noise can more easily hide the

signal. One issue is the DC offset (extremely low frequency signal) that is in the range of 100 mV (Harrison07a). The other issue is that the quality of extracellular measurement highly depends on the relative localization of the electrodes and the cells. These drawbacks can be handled by a careful design of electronics for conditioning and processing the cell's signal.

In experiments, the biological context is mostly defined by the specifications of the considered applications. In our case, we need to consider a *Hynet* with neurons and with β-cells, and the most sensitive specifications are: a. the number and the density of access points; b. the duration of the experiment.

Large scale is vital to study neurons and β-cells in their network functionality and in the context of plasticity and learning (Morin05, Chao05). For example, (Palti96) highlights that the whole islet of β-cells acts as a unit to determine the needs on insulin. Also, (Wagenaar06) shows the complexity of the study of learning and plasticity at the network level and the importance of apparatus for multisite acquisition.

High resolution is another important feature: knowing the activity of a single individual (cell or small part) is fundamental to determine its contribution on the collectivity (*i.e.* population, network, islet…). High spatial resolution is the base to the study of signal propagation inside the collectivity and inside the individual (Streit06, Georgopoulus86).

Long-term is necessary for the study of plasticity in networks, in the context of cells embodiment or for statistic coherence. Even if short experiments provide insights for the study on cell-to-cell plasticity, the network evolution has to be considered over long dynamics and "inertia" (Potter06, Bakkum04).

These three characteristics, large scale, high resolution, and long-term, imply using extracellular access to biological cells. *In vitro* experiments are always preferred for initial studies on a given topic, because of their simplicity in terms of technology but also on terms of ethics compared to *in vivo* experiments. In the case of studies at the cell network level, we prefer dissociated cells; and for the study of an already-shaped network or functional unit, we privilege acute slices.

For the experiments described in this manuscript, all the living parts are *in vitro* preparations, of dissociated cultures, and with extracellular access (Fig 2.08).

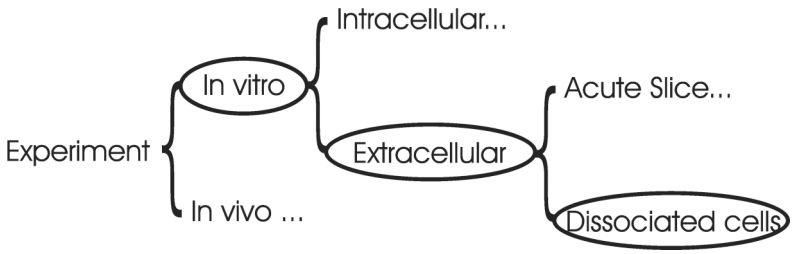

Figure 2.08. Potential solutions for the biological part of a Hynet and our final choice.

B. Electronics

The artificial part of a *Hynet* can be implemented in different forms. The first choice to make is between software and hardware. It corresponds to the way the instructions or commands are described. Software implies a high level of description that is implemented on standard hardware, usually a program (software) running in a computer (standard hardware). This solution has the advantages of: reconfigurability, development time, and price.

The use of custom hardware increases the performances of the system (silicon area, power consumption, computing speed), but it also increases the development cost and time.

A custom hardware implementation can be based on discrete components, configurable IC (such as FPGA – field programmable gate array), semi-custom IC, and full-custom IC. These solutions respectively present increasing performances and higher development costs.

Lastly, the signal can be coded and processed in digital or analog mode. The digital implementation of values and time are discrete. The digital noise comes from two aspects. First, the number of bits determines the signal resolution. Second, the synchronization and technological performances define the minimum delays. Both determine the value and time resolutions. In the case of analog implementation, values and time are continuous. One wire conveys the signal, independently of the resolution. Physical laws of hardware elements (transistors) are used to implement processing equations. The processing is naturally real-time if the dynamics of the equations are correctly replicated by physics. Noise comes from physical characteristics such as thermal fluctuation. This limits the resolution of the signal. Even with computer assisted design, the analog development time and cost are higher than the digital one.

Table 2.1 Examples of Hynets and their Biological and Electronics Implementation

Author	Cells	Interface	Feedback	Computing
Chapin 1999	*in vivo*	extracellular	visual	digital
Reger 2000	*in vitro*, acute	extracellular	discrete hardware	digital
Jung 2001	*in vitro*, acute	intracellular	integrated hardware	analog
Le Masson 2002	*in vitro*, dissociated	intracellular	integrated hardware	analog
Carmena 2003	*in vivo*	extracellular	visual	digital
Nowotny 2003	*in vitro*, dissociated	intracellular	software	digital
Oprisan 2004	*in vitro*, dissociated	intracellular	software	digital
Berger 2005	*in vitro*, acute	extracellular	integrated hardware	digital
Whittington 2005	*in vitro*, dissociated	extracellular	software	digital
Potter 2006	*in vitro*, dissociated	extracellular	software and discrete hardware	digital
Novelino 2007	*in vitro*, dissociated	extracellular	software	digital
This work 2010	*in vitro*, dissociated	extracellular	software	digital and analog

Technological choices for the artificial part of a *Hynet* are mostly a matter of finding a good compromise between the expected (necessary) performances and the development time and cost. Our purpose is to discuss our choices to fulfill *Hynet*'s needs: the acquisition of electrogenic living cells'activity and the processing of the data in real-time (Fig. 2.09)

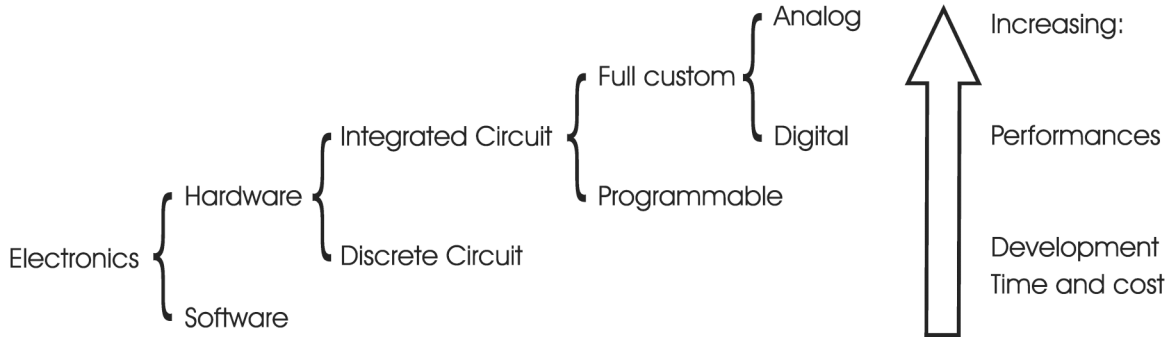

Figure 2.09. Potential solutions for the electronics part of a Hynet. In order to increase the performances of a system, the development time and cost may also increase.

In the next chapter, we present our *Hynet* system, and its performance as a hybrid (living-artificial) real-time closed-loop. This system presents a low development time and cost: analog hardware is limited to a minimum. Chapter 4 (Preamplifier) presents a solution to increase the number and the density of the acquisition channel, with a full-custom integrated

preamplifier. Therefore, we achieve a large-scale and high-density acquisition and we increase the amount of raw data. In Chapter 5 (Detector), we intend to keep the system's real-time feature. The solution is to process the data on-line and in analog mode. The last Chapter (Conclusion) concludes and presents perspectives for the next generation of *Hynets* (Fig. 2.10).

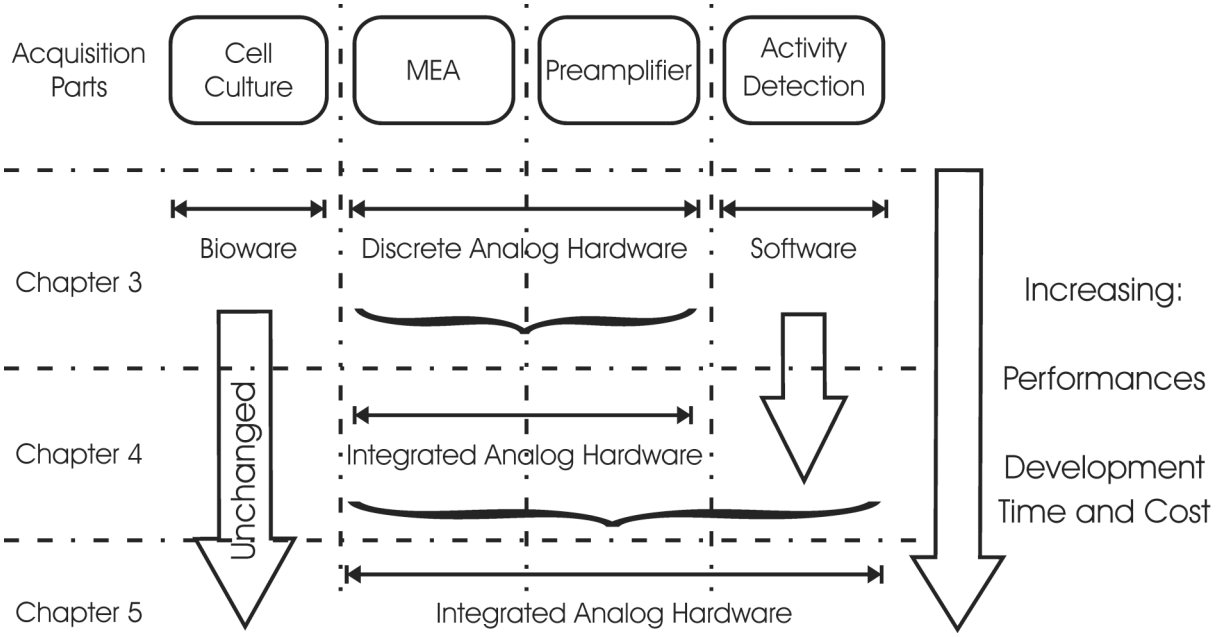

Figure 2.10. Hynet configurations related to next chapters of this manuscript: 3 – Hynet, 4 – Preamplifier, and 5 – Detector. By increasing the development time and cost, we increased the performances of the original *Hynet*.

CHAPTER 3
HYNET

"If we knew what it was we were doing, it would not be called research, would it?"

Albert Einstein (1879-1955), Swiss-American theoretical physicist.

This chapter presents my contribution to the *Hynet* system developed during this thesis project. The parts of the closed-loop system are: bioware, hardware, and software. The data flow starts at the bioware level, passing through the hardware to the software. A friendly user interface guides the user to configure the experiment. The online software processes the data and eventually sends the relevant stimulation. This command passes through the hardware back to the bioware.

The number of acquisition channels on the bioware is limited by the commercial hardware used for the first amplification and by the software data processing. At the beginning of my project, the *Hynet* system was under development. The hardware part was under test and the software part partially written. I participated in both; the hardware validation and the software design. I entirely realized the work presented on section II.B (Closing the loop).

I. System parts

The two parts, artificial and living, of the hybrid network (*Hynet*) communicate in bidirectional mode with each other: each provides outputs and receives controlling inputs from the other. The hardware and software parts of the artificial system run the bioware data acquisition, its processing, and the generation of feedback stimulation patterns. In this section, the three components of *Hynet* are: bioware, hardware, and software (Fig. 3.01).

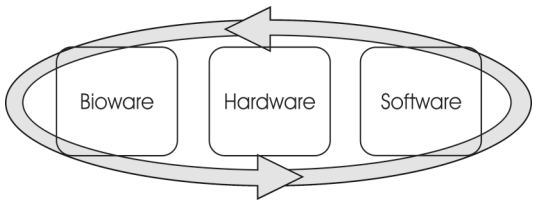

Figure 3.01. The Hynet closed-loop. The bidirectional communication path between the bioware and the software passes through the hardware.

A. Bioware

The first component of the system is the biological material that provides the signal for acquisition and is electrically stimulated.

In the case of Hybrid Neural Networks (Garenne10), we use dissociated rat embryonic cortical cell cultures. Each MEA is plated with approximately 10^5 cells. After plating, the cells naturally tend to interconnect and create a complex neural network covering the MEA. The culture generally exhibits spontaneous spikes and bursts after 10-12 div (days-*in vitro*). In the case of insulin delivery control (Raoux10), we use cloned ß-cells from mice. They are

cultivated for 6 div before the acquisition. The cells are routinely kept healthy and active for more than 3 months.

B. Hardware

The second stage of the system is implemented on hardware, as a bridge between the bioware and the software. With the exception of the MCS (MultiChannel System™) suite (detailed later), all elements are custom made and assembled into a customized rack. This rack controls analog and digital signals, and it has an independent power supply and electrical references from those of the culture and of the computer. Hardware elements consist of a series of boards plugged into a modular and autonomous rack that conveys buses of shared data. All boards are configurable and work in real-time.

C. Software

The software is programmed in C++ and runs in a Windows XP™ environment. It contains four basic parts, three of which are graphical user interfaces (GUIs) that work offline and offer visual supports to control and monitor the experiment. The fourth one is the Real-time Application (ReTA) which recovers the information from the GUIs and from the hardware, and pilots the hardware. ReTA is the heart of the software part, and as such must be monitored to work in real-time.

II. The Closed-loop

We detail in this section the tasks of the artificial part of the *Hynet* (Fig. 3.02). They are: A. the acquisition of biological data, B. the data processing resulting in decisions and stimulation patterns to close the loop, and C. the generation of electrical stimulation signals.

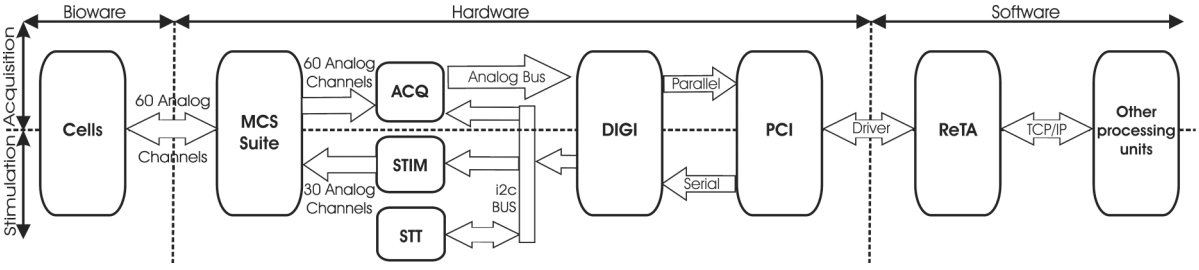

Figure 3.02. Detailed view of the Hynet closed-loop. The acquisition begins by the MultiChannel Systems (MCS) suite, with 60 analog channels. Signals are amplified by the ACQ boards and digitized by the DIGI board. The PCI board conveys the digitized signals to the software domain. The Real-Time Application (ReTA) processes the data and can pass it to other processing units by a TCP/IP communication. The stimulation flow starts at the software level, initiated by an external processing unit or by the ReTA. The PCI board sends the control commands serially to the DIGI board. The Stimulation Trigger (STT) and Stimulation boards (STIM) convert the digital signals into 30 analog signals that are applied to the culture by the channels of the MCS Suite.

A. Acquisition

The hardware unit measures electrical signals from the cultures on the MEAs and conveys them to the software. Incoming analog signals have a low amplitude (10 ~ 100µV, mainly in the 100 Hz – 10 kHz bandwidth) and a high noise level (up to 1 mV in lower frequencies and about 10 μV_{rms} in the 100 Hz – 10 kHz band). The hardware outputs digital signals, with a 12 bit resolution and 40 kHz sampling frequency per acquisition channel. The hardware is composed of: the MCS suite, and boards identified as *ACQ* boards, *DIGI* boards and a *PCI* board (Fig. 3.02).

1) MCS suite: The bioware is plated on a multielectrode array, MEA200-30 from MultiChannelsSystems (MCS) (diameter 30µm; interelectrode distance is 200µm). The 60-electrode signals are available as parallel analog outputs of the MEA200-30. This MEA is inserted in the MEA1060 preamplifier from MCS, with a voltage gain of 1200. The preamplifier is connected to the BBMEA breakout box (for physical connections) from MCS. This system provides an easy access to the 60 recording analog channels (MEA System User Manual ref.06).

2) *ACQ* board: we designed these boards to filter, isolate optically, and amplify the analog signals from bioware. Each ACQ board manages 4 channels with a high-pass filter (0.1 Hz cut-off frequency) and an individually controlled gain tunable between 1 and 12 700. The gain's control signal uses a serial i2c protocol (Inter-Integrated Circuit (Irazabal03)). For a complete 60-channel recording system, 15 ACQ boards are necessary. The amplified signals are conveyed to an analog bus.

3) *DIGI* board: this controls a subset of the rack's channels. More precisely, it manages:

3.a) the digitalization of the biological signals. The board is equipped with a Xilinx® FPGA (configurable digital circuit) that controls 2 Analog-to-Digital Converters (ADC). Each ADC converts each one of the 8 channels with a resolution of 12 bits and sampling frequency of 40 kHz. This sampling rate is specified to ensure a high quality reconstruction of the neurons dynamics for offline processing. Furthermore, as the A/D conversion is implemented within the rack, no analog signal is conveyed inside the digital environment of the computer, which limits the noise.

3.b) the data transfer between the rack boards and the computer PCI (Peripheral Component Interconnect) board. The acquisition data is transferred in parallel mode, as it may

correspond to a large data flow if all channels are active; stimulation data, which is more sparse, is transferred serially. Both are clocked at 16MHz.

3.c) the control of the i2c bus, that manages the data, control and clock signals for the acquisition boards (*ACQ*) and for the stimulation boards (*STIM* and *STT* detailed further).

Each *DIGI* board controls 16 acquisition channels and 8 stimulation channels. For a 60 acquisition and 30 stimulation channels *Hynet* system, 4 boards would be necessary.

4) *PCI* board: this board is the bridge between the rack and computer's PCI (Peripheral Component Interconnect) bus. The necessary data transfer rate for a 60 channels *Hynet* is approximately 5 MiB/s, (with 12 bits - 40 kHz sampling per channel), well below the 133 MiB/s (133.220 bytes per second) of the PCI transfer protocol. The PCI driver module is written in C++ and runs on Windows XP™.

The hardware we developed for the *Hynet* is not competitive with current commercial system (MEA System User Manual ref.06, BioMEA ref.09) in terms of static performances; but although individual boards process less channels, the user can customize the experiment thanks to the modular architecture and the boards' configurability (Bontorin07a).

However the real benefit of the system lies in the real-time features of the processing (including the software) that are not present in commercial systems.

The biological signals are available to the software, which is designed as a Real-Time Application (*ReTA*). Its functions are:

1) Raw signal monitoring: data from 60 channels can be displayed in real-time on the computer screen (Fig. 3.03.A). A zoomed view can also be selected for a single channel (Fig. 3.03.C).

2) Events detection: three types of patterns are extracted from the raw neural data: spikes, bursts, and stimulus artifacts.

A spike is a short electrical depolarization of a cell membrane. Extracellular spikes often reach amplitudes of 50µV eil (equivalent input level). After hardware processing, noise amplitudes are estimated to be about 15µV eil. Thanks to this level difference between spikes and noise, spikes can be detected by thresholding the signal, but the optimum threshold AC and DC may differ over the channels or even evolve over time.

ReTA presents two techniques to set the threshold. The first one is to define it as a fixed voltage value, defined by the user (for example by looking at the monitored signal). The second use the standard deviation (SD) of the signal as an estimation of the noise. The threshold is defined as a multiple (n) of SD. "n" is normally set in between 3 and 5, in order to avoid spike detection errors (false negative or false positive detection).

In order to present less than 1 ‰ of false positive decisions (the system interprets noise as a spike), "n" is usually set to be larger than 3. The maximum value is 5, after which the false negative decisions (true spikes are not detected) are too frequent (Garenne10). SD is continuously updated on line.

For our application, a "*burst*" is a pattern of N spikes on the same channel in a temporal window of duration W. For example, if a channel has three or more spikes (N = 3) in less than 10 ms (W = 10), this event is considered to be a burst. Both values, N and W, are programmable by the user before the experiment.

To implement burst detection, we create at the start of the experiment a circular buffer for each channel where a burst detection is required. Taking into account the sampling frequency (f) of the acquisition, the number of elements of a buffer is (W.f). After each acquisition sampling, the buffer is updated; depending on the values of the first element and the new element, the total number of spikes (S) is changed; the first element is overwritten by the new element; and the pointers of last and first elements are increased. If the total number of spikes in the buffer reaches the number of spikes in a burst ($S \geq N$), a burst is validated for the current timestamp.

Stimulus artifacts are detected by a simple thresholding method. Biologically effective stimulations generate artifacts that saturate the acquisition channel. Consequently, the threshold is relatively easy to fix before the experiment.

3) Events detection monitoring: The three types of events can be monitored online. The events evolution over time is indicated by color coding (Fig. 3.03.B). Inactivated channels are white. Once an event is detected, the corresponding channel passes immediately to red, and then progressively lightens: it provides visual information about signal propagation in the culture.

4) Statistics computing: the online detected events are also used to compute statistics, such as instantaneous firing rate (IFR), inter-burst interval histogram (IBI), inter-spike inter-

val histogram (ISI), and post-stimulus-time histogram (PSTH). These statistics are commonly used in neurophysiology experiments. They are also plotted online (Fig. 3.03 D and E).

5) Storage: All the data are stored on the hard disk for offline analysis. The raw signal is stored in a 12 bits format, and a transtyping operation is done to save space disk. Events and Statistics are stored as timestamps in a text file.

6) Channels selection: To optimize the computational load, the user can configure processing on an individual channel. Useless channels can be deactivated, keeping more resources for *ReTA* or other real-time programs running on the same machine.

7) TCP/IP interface: In order to share the information with other programs, a TCP/IP (Transmission Control Protocol/Internet Protocol) interface is included in *ReTA*. The packages are configurable: they provide the timestamps and statistics of a selected event.

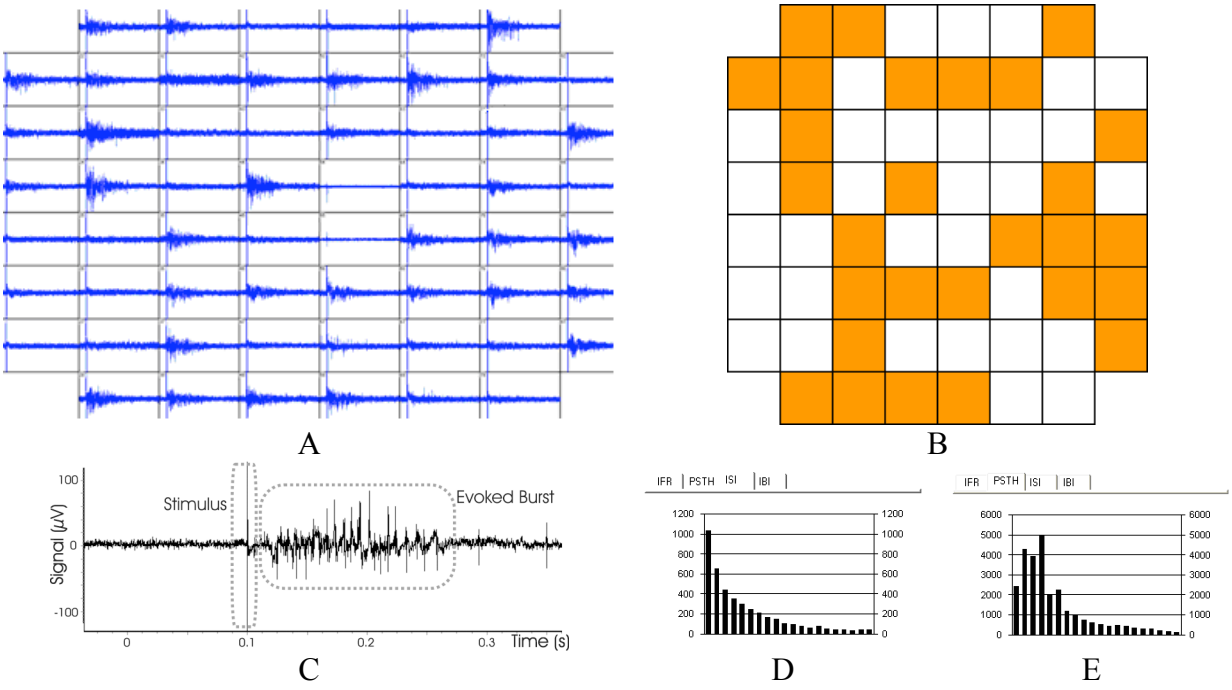

Figure 3.03. Real-time monitoring of neural bursting activities induced by stimulations. (A) 60 raw signals in 1-second windows. (B) Bursts detection figure on the 60 channels; white: no burst detected; grey: burst detected within the last 0.25 s. (C) A zoomed view of one channel. We highlighted the stimulus and evoked burst. (D) Inter-Spike Interval (ISI) and (E) Post-Stimulus Timing Histogram (PSTH) for one channel. IFR stands for Instantaneous Firing Rates, IBI stands for Inter-Burst intervals; IFR and IBI are not presented here.

B. Closing the loop with the software

Our methodology to configure the closed-loop experiment comprises four software steps (Fig. 3.04):

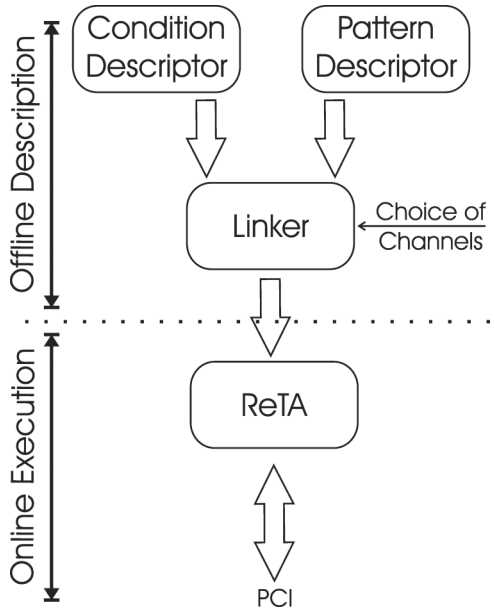

Figure 3.04. Four steps to describe a closed loop experiment. The first step (Condition Descriptor) is the definition of the acquisition pattern that triggers a stimulation. The second (Pattern Descriptor) is the definition of the stimulation signal. The third (Linker) associates the relevant channels with the previous descriptions. The last step (ReTA) reads this configuration and processes on-line the data to and from the PCI.

1) The first step is to run the Condition Descriptor that configures the events in the acquisition that launch a stimulation pattern. A pattern can be launched: (a) continuously and/or periodically during all the experiment; (b) only at the beginning of the experiment (*e.g.* for a training or calibration task); (c) in response to a manual user request (*e.g.* by clicking a button); (d) in response to requests from another program, received through a TCP/IP interface; the purpose of this feature is to allow *ReTA* to interact with other programs; or (e) if a condition in the acquisition is reached. The condition in the acquisition can be defined as a complex input pattern. This pattern is defined by a sequence of time intervals (ΔT). Each interval has a quantity of spikes, bursts or statistics (N) and a test (equal, greater, lower). Fig. 3.05.A shows the window of our Condition Descriptor. Fig. 3.05.B shows a complex condition based on a spike detection. These patterns are stored in a file, which can be stored in a library.

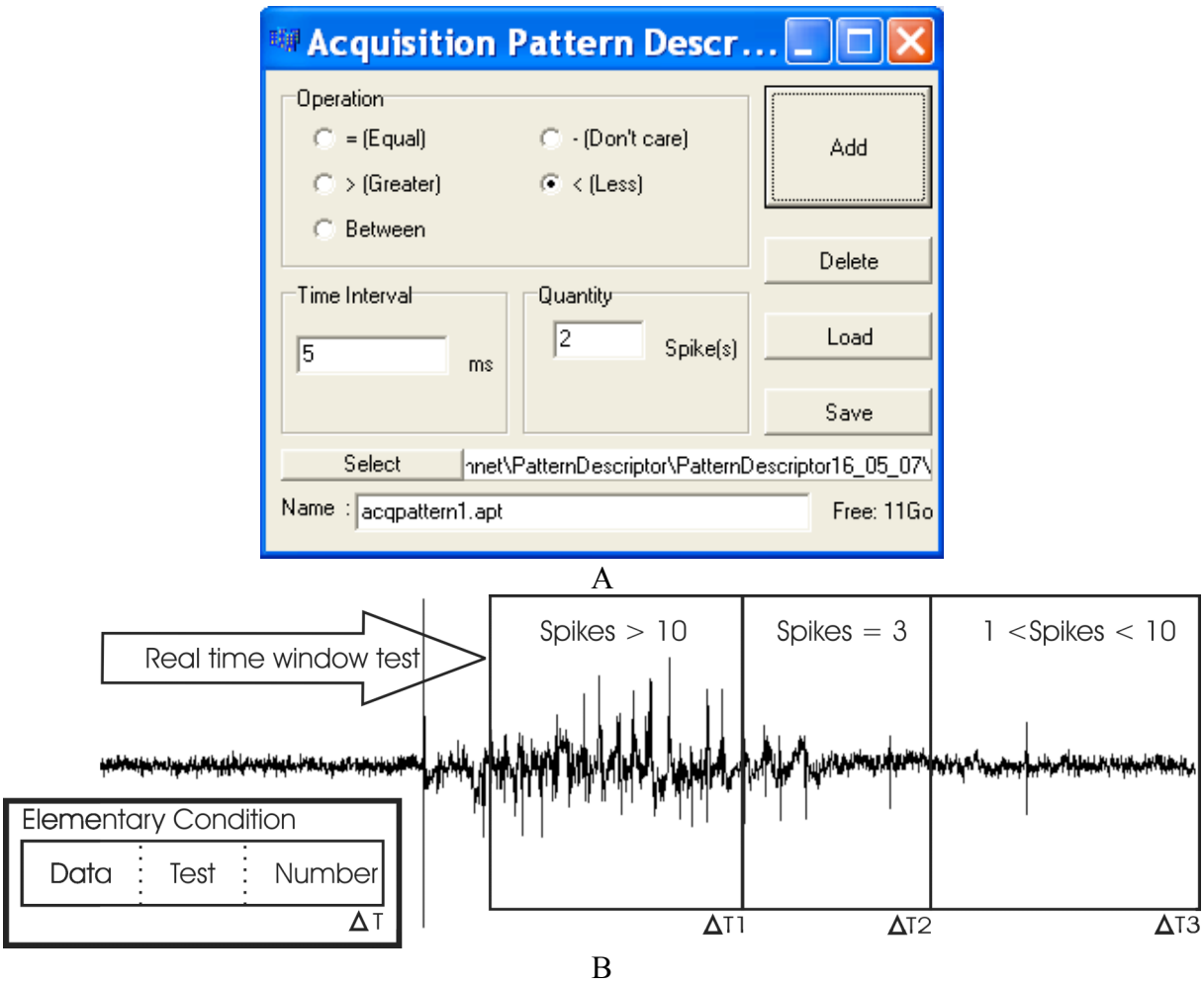

Figure 3.05. The Condition Descriptor. A. The GUI window and B. An example of condition setting. Three information compose one elementary condition: the data we are looking for (spike or statistics), the logical test (equal, less, greater, …), and the time interval ΔT. Each complex condition is composed of one or more basic conditions. In this example the complex condition is composed of 3 elementary conditions. The first is the detection of more than 10 spikes over ΔT1; the second is the detection of exactly 3 spikes over ΔT2, and the last is the detection of at least 1 and less than 10 spikes over ΔT3. During the acquisition, a theoretical window sweeps the signal to look for the condition.

A special input condition is the timer, whose Timer Descriptor block accounts for a delay (constant or random). It can be combined with conditions and/or stimuli pattern. Fig. 3.06 shows the GUI to configure the timer.

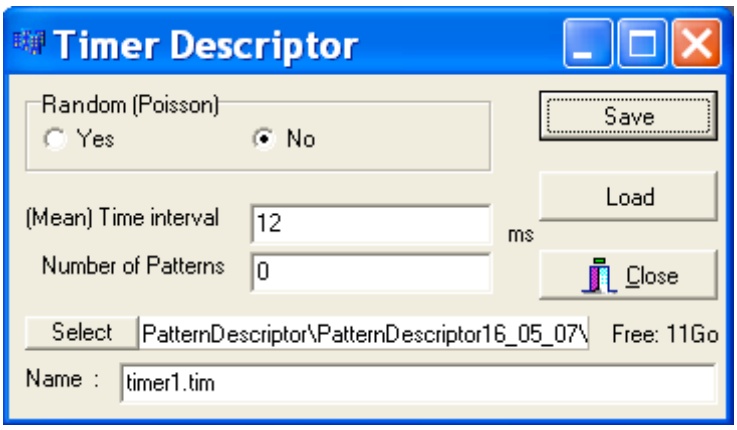

Figure 3.06. Timer Descriptor: the GUI window. The user can chose between a fixed time interval and a Poisson distribution for the timing of events.

2) The second step uses the Pattern Descriptor and configures the stimulation patterns. The basic element of the pattern is the pulse. Bipolar voltage pulses, starting with the positive cycle, have been reported in the literature to be efficient (with respect to measurements of the responsiveness of neuronal cultures) and secure (considering the mean life time of neuronal cells) (Wagenaar04, Merrill05). Four parameters are tunable in a bipolar pulse: the positive (V+) and the negative (V-) voltage levels, and the positive (TV+) and the negative (TV-) widths. The pulse width varies from 50 µs to 3.27 s, with a 50 µs step, and the pulse levels range varies from 0 to ±10 V, with a 4 mV step. In a second level of abstraction, pulses can be repeated inside a "group". Two parameters are configurable in a group: the number of pulses and the pulse period. The last level of abstraction is the pattern, composed of the repetition of groups with a defined group period. Fig. 3.07 presents A. the GUI for the configuration of the stimuli pattern and B. the associated stimulation signal and its parameters. These patterns are stored in a file, which can also be stored in a library.

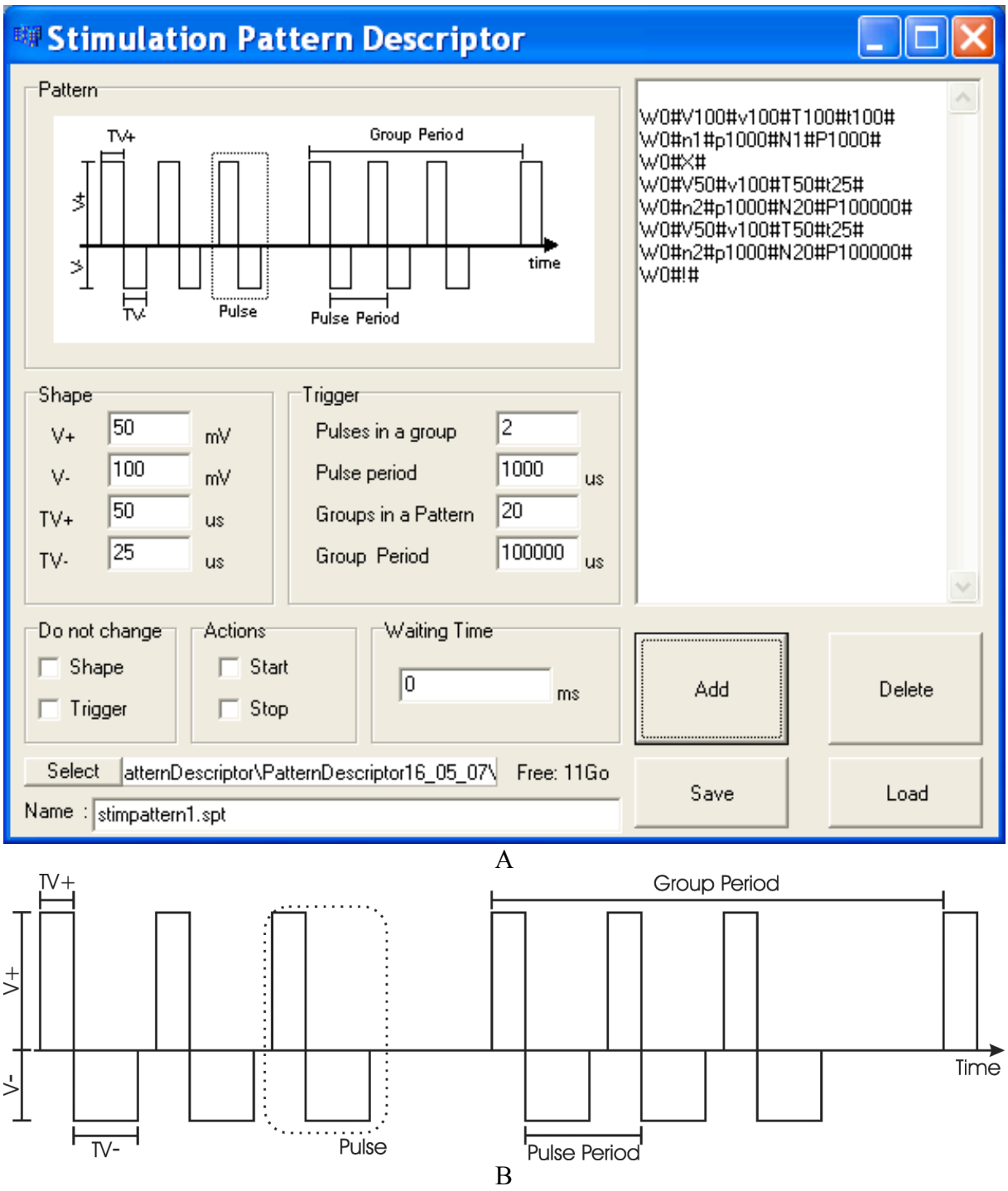

Figure 3.07 The Pattern Descriptor. A. The GUI window and B. Example of a stimulation pattern and its parameters. Four parameters are tunable in a bipolar pulse: the positive (V+) and the negative (V-) voltage levels, the positive (TV+) and the negative (TV-) time widths. Two parameters are configurable in a group: the number of pulses and the pulse period. The last level of abstraction is the pattern, composed of the repetition of groups with a defined group period.

3) The third step uses the Linker and defines the relationships between the conditions defined in step 1, the pattern described in step 2 and the stimulation channel. With this modular configuration, experiments can be designed with a reuse methodology, based on library elements (conditions, stimulation patterns from previous experiments). Logical AND, OR, and PIPE conditions, timers, and/or patterns are programmed at this stage. Fig. 3.08 presents A. the GUI for the linker and B. an example of linking.

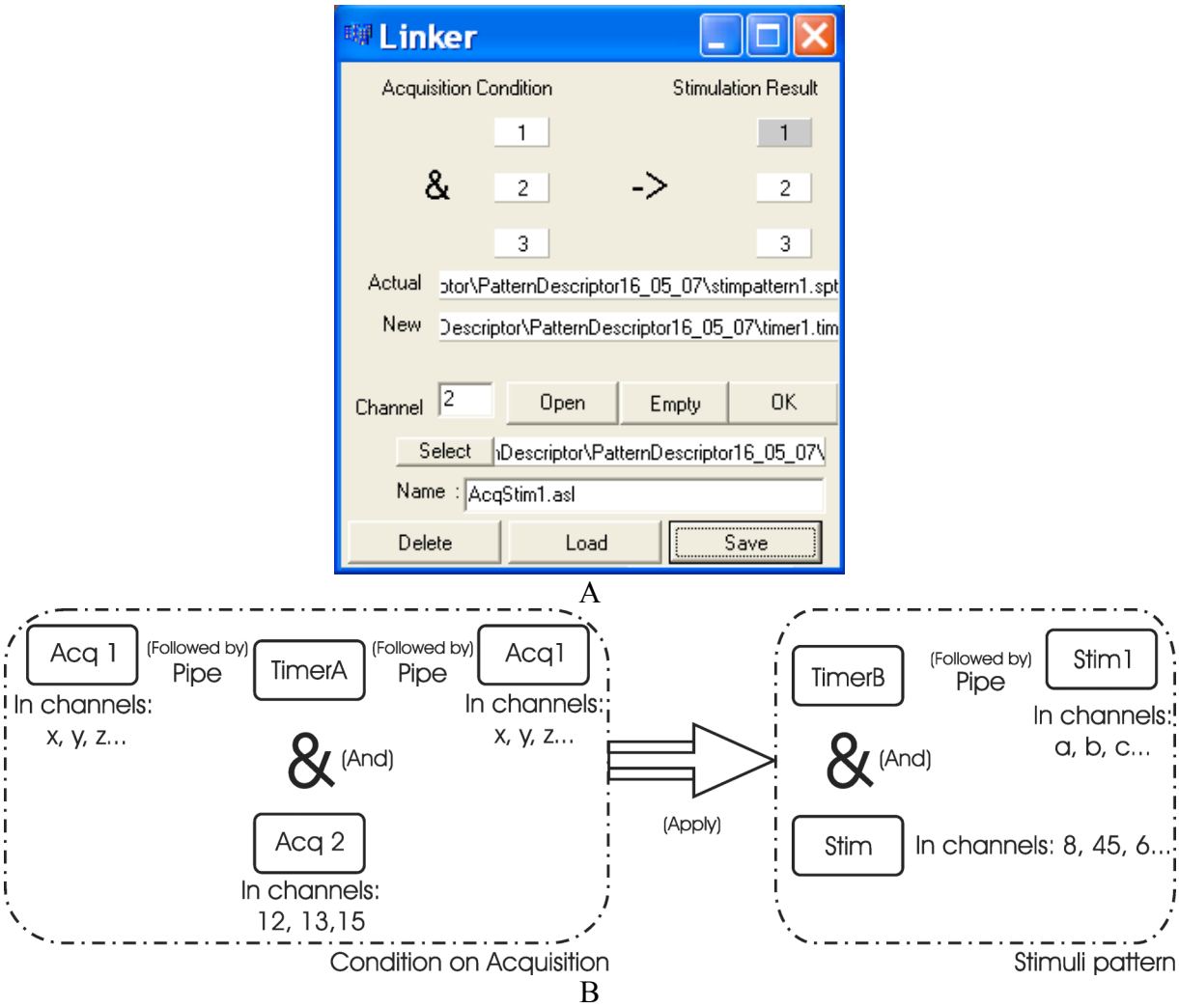

Figure 3.08. The Linker. A. The GUI window. B. An example of linking. The library elements from the previous steps (conditions, stimulation patterns and timers) are linked using logical functions AND, OR, PIPE conditions and the channels numbers. The Linker also relates the acquisition patterns (left part of the figure) to the stimulation patterns (right part of the figure).

4) The last step is the launching of the real-time application (*ReTA*). It interprets the command files of the Linker, launches the different threads and circular FIFOs, establishes the TCP/IP communication, and drives the PCI (Peripheral Component Interconnect) card. Fig. 3.09 presents the command window of the main GUI of the *ReTA* , effectively closing the

loop of the experiment. In the center of the window, a panel displays the number of detected conditions (from step 1) or sent stimulations (from step 2) from and to the hardware.

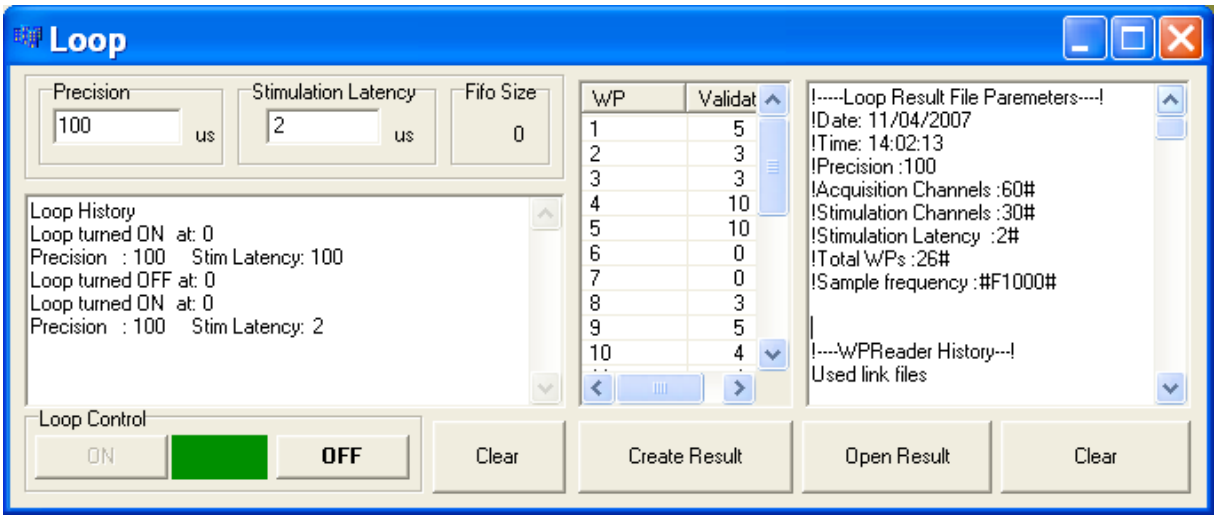

Figure 3.09. The command window of the ReTA application closing the loop. The left part of the window presents the current status of the loop and its parameters. In the center box, the number of conditions detected or stimulations launched are updated in real-time. This interface generates and reads reports of the experiments (right part of the window).

C. Stimulation

After the Acquisition hardware and the Software, the Stimulation hardware completes the closed loop pathway.

The Stimulation hardware is the bridge back from the software to the bioware. The first blocks of the Stimulation hardware is the same *PCI* and *DIGI* boards as described for the acquisition. The *DIGI* board controls two types of boards used for stimulation: the Stimulation Trigger (*STT*) boards and Stimulation (*STIM*) boards (Fig 3.02):

1) Stimulation Trigger (*STT*) Boards: these are in charge of triggering the stimulation signal (a biphasic stimulation pulse as described in the previous section). They provide individual trigger sequences for each channel. An *i2c* local bus controls this process. The resulting stimulation patterns can be configured by: the number of pulses in a group; number of groups in a pattern; periods of pulses and groups (Fig. 3.07.B), as configured in the step 2 of the software. Each *STT* board triggers 2 *STIM* boards, corresponding to 8 stimulation channels. A 32-channel stimulation setup requires 4 *STT* boards.

2) Stimulation (*STIM*) Boards: these generate analog stimulation signals, which are applied to the MEA electrodes. Each board individually controls 4 stimulation channels. For a

32-channel stimulation system, 8 boards are necessary. Individual cables for each channel convey signals to the MCS suite.

The MCS suite is the same suite as the one used by the acquisition flow. The MEA has a parallel access for the acquisition and the stimulation of each of the electrode sites. The user configures the distribution of the stimulation channels among the 60 electrodes by on-board hardware switches.

We intentionally limited the number of stimulation channels to 30, as single stimulations are proven to already have an effect on a population of neurons distributed covering more than one channel. In any case, the number of stimulation channels could easily be increased on our system by adding more *DIGI*, *STT*, and *STIM* boards.

III. Time performances

A. Acquisition

In extracellular measurements, as is the case of MEAs, the typical data bandwidth is about 3 kHz for spike detection (Henze00), which implies a Shannon frequency of 6 kHz (Shannon49). We chose to run our system with a minimum 10 kHz sampling rate (and then a period of 100 µs), to ensure a correct reconstruction of biological signals in real-time. A higher sampling rate (*e.g.* 40 kHz) would give more information about spike shapes, which is not a priority for the experiments we plan.

Thanks to its tunable architecture, our acquisition system can provide different outputs changing its processing delay. We present the delays related to different experiments (A to E in Fig. 3.10), going from 25 µs (A) to 60 µs (E).

The simplest experiment (A) consists of an offline analysis. In this case, only the raw data storage and monitoring must be in real time. The mean delay is 25µs (A). In this case the sampling frequency can be tuned to 40 kHz, increasing detail in the spike waveform.

Adding other real-time processes increases the delay. The most resource demanding online detection (event detection on all channels in a 10 ms burst window) adds 15 µs (B). One statistic function requires 15 µs (C).

The delay to send data to the TCP/IP layer is 5 µs on average. Raw data is not sent because it is too resource demanding. If event detections (D) and statistics (E) are sent, the process delays are, respectively, 45 µs and 60 µs.

In the most complex experiment, all the information (event and statistic) is sent to the TCP/IP layer with a mean delay of 60 µs. If we stick to the initial specification, for real-time, of a 100µs global delay, 40 µs are still available for user-defined additional functions.

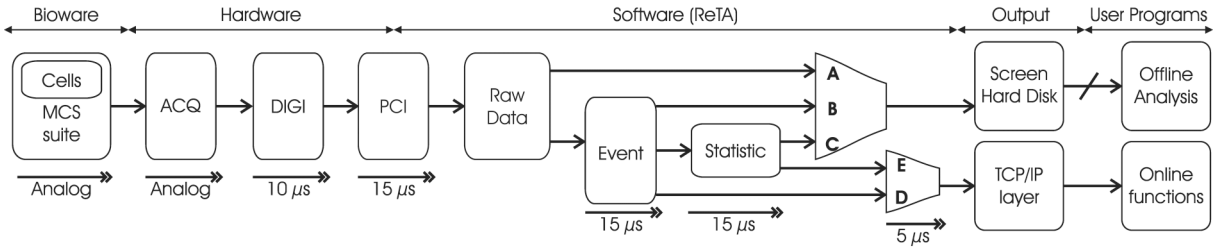

Figure 3.10 Data propagation delays of the acquisition chain as described in Fig. 3.02 for different experimental configurations (A to E). The simplest experiment's delay is 25 µs for real-time raw data storage and monitoring (A). The most complex analysis requires 60 µs (E).

B. Stimulation

Stimuli can originate from three different sources: (a) offline data programmed before the beginning of the experiment; (b) user action; and (c) requests from another program received by the TCP/IP interface. In terms of timing, (a) and (b) are directly implemented from the *ReTA*. For (c) we must take into account the time necessary for *ReTA* to access the data from the TCP/IP layer. Once the *ReTA* "knows" that it must launch a pattern, the mean time for processing through the PCI driver is about 5 µs. With 1 µs more, the data pass the PCI bus and access the *DIGI* boards. These delays suppose a PC with only *ReTA* running besides the Operating System (OS): the PCI bus must be permanently available for the *Hynet*. In any case, these delays are controlled and all buffers are monitored (software access to internal registers and timings). If the delay for a task is too long, a warning/error sequence is launched.

From *DIGI* boards to *STIM* and *STT* boards, the programming time is 5 µs (fixed delay). Analog signals are transferred from the *STIM* boards to the cultures, with propagation delays that are negligible when compared to digital ones. The total delay for the stimulation chain is therefore 16 µs on average (Fig. 3.11).

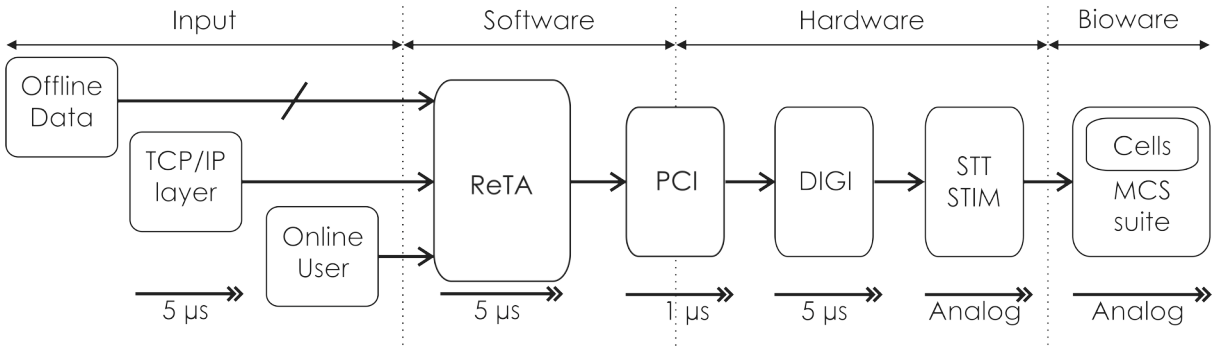

Figure 3.11 Propagation delays for the stimulation chain (as described Fig 3.03). The total mean delay, from the command in the TCP/IP layer to the biological cells, is 16 µs.

C. Closed-Loop

"Real-time" in a *Hynet* system is a strict constraint: it implies that within the time step between 2 acquisitions, all the online processing on the available data has been executed (and has generated a consequent stimulation). The "closed-loop period" is the time taken by the system between the acquisition and the related feedback stimulation. This period should not bypass the maximum sampling period.

The propagation times across the modules of *Hynet* are summarized in Fig. 3.12. The software environment is Windows XP™ running on a Bi-Xeon, 4 GB RAM, 3 GHz PC. Measurements were made individually for each block.

A 10 kHz sampling frequency corresponds to a 100 µs period available for the loop. By summing the digital modules' delays (as the analog ones are negligible), we obtain a closed-loop period of 46 µs. In this case, we have the simplest acquisition chain (25 µs), a closing loop sequence (5 µs), and the simplest stimulation chain (16 µs). More than 50 µs are then available for the software at each time step, to close the loop.

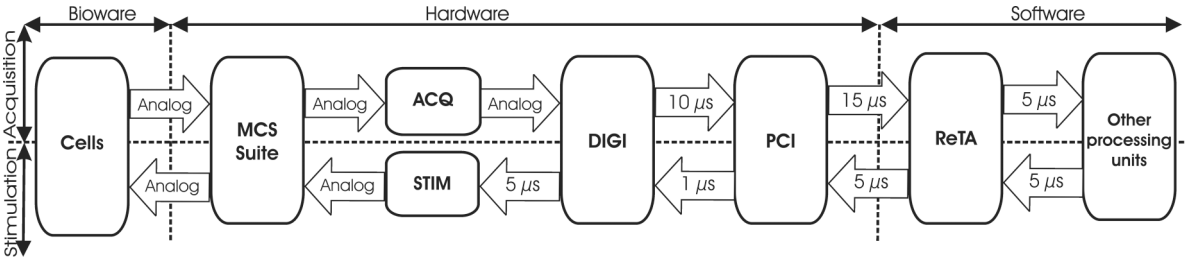

Figure 3.12. Data propagation delays of the complete Hynet closed-loop. The minimum closed-loop processing period is 46 µs. For our specification (10 kHz sampling frequency), more than 50 µs are then available for the software during each period to close the loop.

Into this time interval of 50 µs, the ReTA can process a complex experiment as described in section II.B (Closing the loop with the software). The processing time for the closing loop depends on the complexity of the task. For example, we have applied on all 60 channels a condition composed of two terms. The first one is a spike firing rate between 2 and 10 in a time interval of 20 ms; the second term is a resting time (no spikes) during the following 20 ms. If the condition is fulfilled by any of the 60 channels, the system triggers a stimulus in all of the 30 stimulation channels. The average computation time for this test is 26 µs.

IV. Discussion

This *Hynet* system conveys fewer channels than current commercially available systems from Multichannel Systems or BioLogic Science instruments (MEA System User Manual ref.06, BioMEA ref.09). Its great advantage is the real-time closed-loop. This feature is until now only present in research laboratories, with an equivalent number of acquisition, and similar (double) stimulation channels (Potter06, Novelino07).

To increase the number of acquisition channels, we integrated the preamplifier function, which is one of the factors that limit large-scale acquisition. The next chapter presents this integration.

CHAPTER 4
PREAMPLIFIER

"Perplexity is the beginning of knowledge."

Kahlil Gibran (1883 - 1931), Lebanese-American poet, philosopher, and artist.

The previous chapter describes our closed-loop system working in real-time with a user-friendly interface. This system uses commercially available items, the MEA (MultiElectrode Array) and the preamplifier, both from MCS (Multichannel systems).

The use of commercial components speeds up the design process of the system. Until 2005, commercially available amplifiers and MEAs were limited to 60 channels, and our system had the strong advantage of processing these 60 channels in a real-time closed-loop.

The IMT Institute, in Neuchâtel (Switzerland), has the expertise in designing high-density large-scale MEAs (Imfeld08b). I was supervised by IMT during the second third of my PhD project, and was able to design a new preamplifier compatible with more-than-four-thousand-electrode MEAs. In this chapter, I describe this design and show how we can use it to upgrade our Hynet system, enhancing therefore the electrodes' spatial resolution (Fig. 4.01).

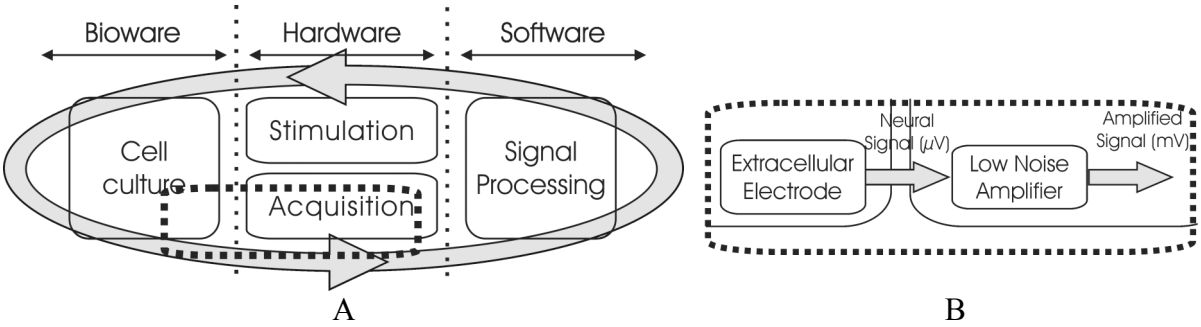

Figure 4.01. Location of the preamplifier. A. The closed-loop architecture from the previous chapter, with its Bioware, Hardware, and Software parts (Figs. 2.07 and 3.01). B. Detail of the amplifier input/output: inputs are microvolt signals from the extracellular electrodes; outputs are in the millivolt range.

I fully designed and tested this preamplifier, as an upgrade to the system presented in (Imfeld08b) with improvements on different items: schematic, layout, technology, etc.

I. Design

This section discusses the design of a low noise preamplifier ASIC for a large-scale high-density MEA (MultiElectrode Array). We define: the input signals, the characteristics of MEAs and the APS (Active Pixel Sensor) approach, the Operational Amplifier (OPA) (high cutoff frequency and stability, low cutoff frequency and feedback circuit), and the power consumption and layout. We will discuss noise issues related to each of the previous items. We end this section with the post-fabrication specifications of our device.

A. Input Signal

The signal applied to the input of the amplifier is composed of: (a) EAP – extracellular action potentials; (b) LFP – local field potentials; (c) EEI – electrode electrolyte interface potentials; and (d) SA – stimuli artifacts.

EAP appear mostly in the frequency range from 0.1 kHz to 10 kHz. LFP appear in the range from 1 Hz to 100 Hz. EAP and LFP come from the activity of the electrogenic cells (Harrison08) and carry the meaningful information in the signal. EEI create a near-to-DC potential difference between the solid electrode and the electrolyte solution. This potential varies spatially, from electrode to electrode, and temporally (Robinson 68). For example, in a gold recording site in buffered saline solution, the offset voltage can be as high as ± 50 mV (Wise75). This is extremely large compared to EAP signals in the range of 100 μV or LFP signals in the range of 1 mV (Harrison07a).

SA depend on the external application of stimulation signals. Commonly used stimuli are in the range of the 1 V, which represents the largest signal range processed by the amplifier. After a stimulus, the EEI take several milliseconds to evacuate the accumulated charge (Merrill05, Wagenaar04).

EEI and SA appear in low frequency bands (<< 0.1 Hz) and its harmonics may hide the information (EAP and LFP). The amplifier must take this into account.

In an MEA a reference electrode imposes the reference voltage, as illustrated in Fig. 4.02.A. This electrode has a large area and low resistance (Jochum09).

B. MultiElectrode Arrays (MEAs) with Active Pixel Sensors (APSs)

Between 1970 and 1980, the first Multielectrode arrays (MEAs) (Thomas72, Pine80) were developed providing a new tool for investigating cellular networks. MEAs proved their usefulness in studies for: pharmacology (Sttet03, Chiappalone03, Guenther06), propagation in cardiac cells (Rohr04), population coding (Puchalla05), activity patterning (Jimbo99, Wagenaar06b, Chiappalone06), and plasticity and learning (Wagenaar06a, Stegenga09, Ide2010).

An MEA is a bidimensional matrix of metallic electrodes engraved over a biocompatible substrate; on which cells are deposited or cultured over the MEA surface. A schematic representation is shown in Fig. 4.02.A (inspired from (Pine06)). Fig. 2B shows a picture of a commercial MEA device.

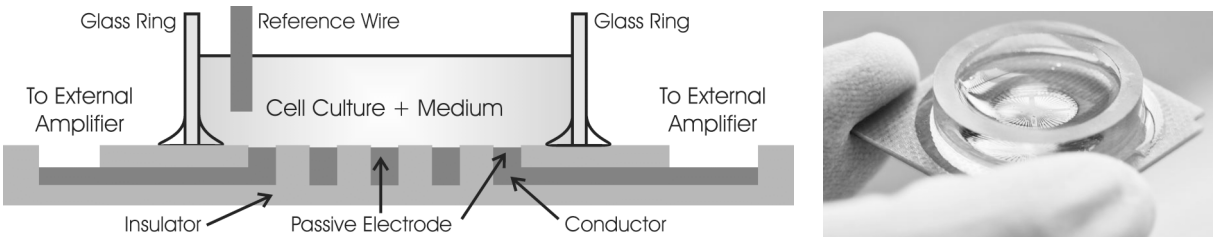

Figure 4.02. A Passive MEA. A. Schematic representation of the main elements. The glass ring keeps the medium and the cell culture on the passive electrodes. The medium contains nutrients to keep the culture alive. The signal measured by the external amplifier is an extracellular potential with an extremely low amplitude. A reference wire provides a reference potential for external use. B. Picture of an MEA60 from Ayanda™ Biosystems SA. It has 60 electrodes, each with an area of 40x40 µm2 and an inter-electrode distance of 200µm.

Classical MEAs, such as the one in Fig. 4.02, are passive. They convey the signal from each electrode to an external amplifier. They include typically 30-160 electrodes with an inter-electrode spacing of 100-500 µm (Multichannel Systems, Panasonic, Ayanda). The signal amplitude is too low for direct multiplexing. Connectivity from the electrode to the amplifier is therefore a main issue.

The Active Pixel Sensor (APS) is an approach to reduce the distance between the measurement electrode (pixel) and the preamplifier (Fossum93). This technique originates from image sensing devices (Willemin01). When adapting this technique to MEAs (Berdondini05, Imfeld08b), we obtain active electrodes (or pixels), as Fig. 4.03 shows. The APS solution moves the limiting factor for electrode density, from the connectivity to the amplifier's size. In other words, reducing the amplifier area per channel increases the density of electrodes.

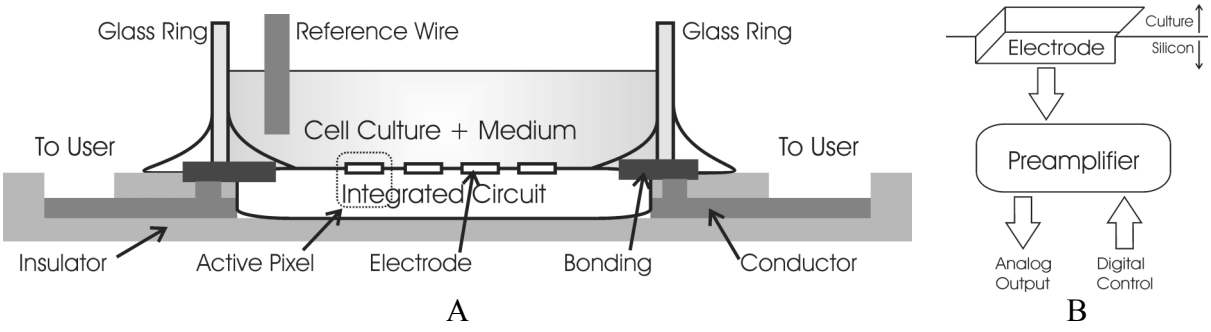

Figure 4.03. An MEA with the APS (Active Pixel Sensor) approach. A. MEA schematic: the signal is amplified as close as possible to the culture, and is delivered to the user with an optimal signal to noise ratio. The integrated circuit is reported or engraved on the MEA's substrate and the bounding must be protected from the medium. B. Active pixel schematic: this element is specific to each electrode. The preamplifier is as close as possible to the culture, as well as its analog outputs and digital control inputs.

C. Operational Amplifier (OPA), High cutoff frequency and stability

The low amplitude of cellular signals is resolved by the implementation of an amplifier with a large gain. For this propose we design an Operational Amplifier (OPA) using a standard and low cost CMOS (Complementary Metal-Oxide-Semiconductor) process.

(Bontorin07b) establishes a simple rule of thumb from the literature: the gain for a neural amplifier should be in the range of 1000 V/V for off-chip processing, and 100 V/V for on-chip processing (see Appendix I for the complete publication). This work also presents a first simulation study of circuit elements that strongly inspired the design of the current OPA.

The OPA gain is defined by its components' arrangements and sizing. Some well-known solutions are incompatible with a high density MEA, including: (a) the use of external components (Obeid03); (b) the ratio of integrated passive components (resistances (Patterson04, Mohseni04, Haidong04) or capacitors (Olsson02)); (c) the product of a transistor transconductance and a resistance (Dabrowski04, Lee06, Sacristan07); and (d) the ratio of transistor transconductances (Holleman07, Eversmann03, Gosselin03, Irazoqui03).

A solution compatible with multichannel integration is to base the gain on the product of a transistor's transconductance and a transistor's drain-source resistance. The transistor's polarization can be in the subthreshold (Uranga04, Harrison03a) or in the conducting region (Berdondini05, Parthasarathy06). We chose the second, due to the robustness for mismatching and for technological dispersion inherent to the CMOS fabrication process.

This classical operational amplifier architecture, as shown in Fig. 4.04, is composed of two stages. The first stage is a differential pair and the second stage a common-source, both with active charges. This ensures a gain of over 100 V/V.

We note that mismatch and dispersion effects are limited in over-threshold configurations. However, the use layout techniques, such as common centroïd and dummy transistors for the sensitive differential pair, reduce the effects to acceptable values (Okada00).

A Miller's capacitor is placed between the outputs of both stages. It creates a dominant pole with two functions: (a) to ensure a good phase margin and (b) to determine the high cutoff frequency. To ensure the stability of the closed-loop amplifier, we chose a minimal phase margin of 60 degrees for all the OPA configurations. For the low pass filter there is a compromise: a lower high cutoff frequency will reduce the noise and signal's bandwidth. For simple threshold detection of neural spikes, a frequency band in the range of 0-3 kHz

(Henze00) is enough. But more complex detection or clustering functions require processing higher frequencies, *e.g.* (Nemadic05). We chose to set the high cut-off frequency to at least 10 kHz.

We chose not to insert a third stage, as classically implemented in an OPA, in order to reduce area and power consumption. This stage usually ensures a high slew rate and a good current gain, but introduces harmonic distortion. As our amplifier will be used with a high impedance load (multiplexer, activity detector), this third stage is unnecessary (Bontorin07b, Palmisano01). All stages in the OPA work in class A in order to provide a good linearity, particularly important for LFP processing (Jochum09).

In the circuit, the OPA provides the gain and the high cutoff frequency. The feedback circuit provides the low cutoff frequency and input impedance.

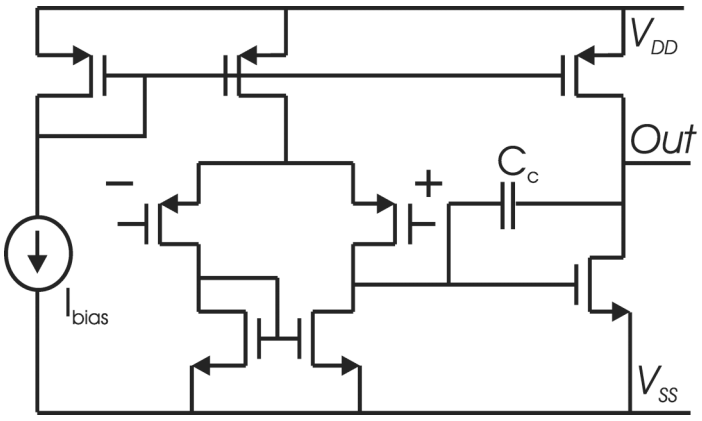

Figure 4.04: Schematic of the operational amplifier (OPA). We use a two-stages OPA, with a current source (Ibias) and a Miller's capacitor (Cc). Differential inputs (+ and -) are amplified through the single-ended output (Out).

D. Low cutoff frequency

EEI and SA have amplitudes much larger than the information signals (EAP and LFP). They can saturate the amplifier or, at the very least, hide EAP and LFP. They must be filtered before or in the amplifying stage. Fortunately, EEI and SA have lower frequencies than LFP and EAP.

A quick solution is to filter the signal using a high-pass filter. There are essentially two different ways to build a high pass filter: (a) blocking (Demosthenous05, Aziz05, Harrison03a, Olsson02) or (b) subtracting (Perelman05, Parthasarathy06, Jochum06, Gosselin07b) the low frequency. (a) requires large capacitors, that degrade the input impedance and then the signal quality. The use of an active subtraction in (b) can reduce to some

extent the area of the total amplifier (Jochum06, Gosselin07b), but not enough for our specifications.

A second solution is to design an amplifier with a low gain at low frequencies (Irazoqui03, Berdondini05). The simplest example of this solution is actually our OPA. Without more circuitry, it presents already a low gain at low frequencies. However, high amplitude EEI or SA potentials can saturate the OPA, especially when its power supply voltage is set low to insure low power.

A third solution, sometimes called stabilization, consists of scattering low frequency currents through a resistance (Chandran99, Dabrowski04, Mohseni04). This resistance must have a high value at EAP and LFP frequencies.

A fourth solution is chopper modulation (Nielsen04, Denison07, Gosselin04). This consists of modulating the signal to higher frequencies, *e.g.* 200kHz. There are two advantages in handling higher frequencies: (a) the CMOS's 1/f noise is lower; (b) a filter needs smaller time constants. Once amplified, the signal is demodulated. The architecture is quite complex and synchronization can be an issue. The additional elements (modulator, demodulator, …) increase the silicon area, thus decreasing the density.

A fifth solution is to adapt some classical offset canceling techniques (Enz96). Some examples of this are: the correlated double sampling (CDS) (Aziz05, Wey90), auto-zeroing (AZ) (Chan07), and digitally controlled DC voltage (DCDV) (Perelman05, Mojarradi03). In classical offset canceling techniques, the output of the signal is sampled and a feedback response cancels the offset. In CDS, the offset is sampled and reduced for each signal samples. In AZ, the offset is sampled in a calibration phase, stored in a capacitor, and subtracted in continuous mode. In DCDV the offset is computed from the already digitalized data.

This latter solution is a very good compromise between high integration and low frequency filtering. Therefore, we chose to adapt this latter solution in our feedback circuitry (Fig. 4.05).

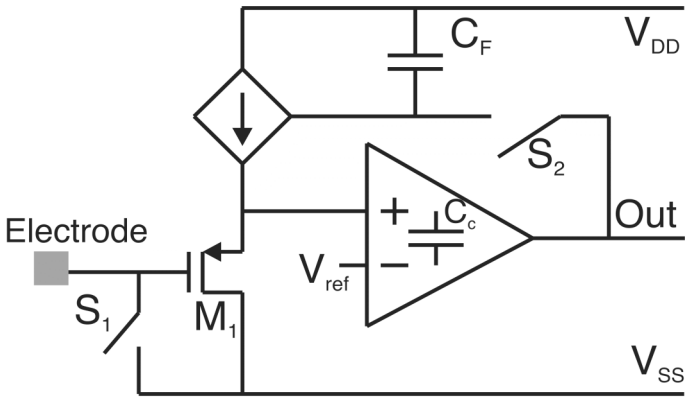

Figure 4.05. The OPA and its feedback circuit. The OPA detailed in the previous figure is inserted into the feedback circuit. In the amplifying operation, S1 and S2 are open. The Output signal is the amplification of the electrode's voltage. In the calibration phase, S2 is closed. Both of the OPA's inputs are set to Vref (0.5 x Vdd), reducing OPA's offset and EEI (electrolyte-electrode interface) effects. Cf stores the circuit's operating point for the amplification mode. The switch S1 is closed in the event of a stimulus on a nearby pixel.

The switch S1 is closed in the event of a stimulation in the neighborhood of the pixel. This grounds the input of the amplifier, which can help in two ways: (a) by providing a low impedance path for the SA, reducing the electrode's discharging (or recovering) time (Potter06); (b) by reducing the interference of the stimulus in the acquisition chain. (Jimbo03) uses a more sophisticated process of sampling and holding the EEI before and after the stimulus. This is useful for the stimulus efficiency but not for the recording (Grumet00).

The switch S2 sets the state of the amplifier. In the calibration phase, it is closed. The closed-loop drives both OPA inputs to the same potential, Vref ± the amplifier's offset. In the amplification phase, S2 is open. The feedback capacitor stores this polarization point from the calibration phase.

The transistor M1 acts as a DC level shifter between the amplifier and the OPA inputs. It cancels the effect of the EEI potential, which is of the order of ±100 mV according to (Harrison08). The calibration phase is repeated (every 20 s) to resample the EEI potential and refresh the capacitor's voltage.

E. Noise considerations

The most important characteristic of the preamplifier is its performance regarding noise. In this section we consider applying a low noise constraints to the design. In particular, we describe the influence of low noise constraints on the points already presented in sections A to D, as well as on some new points.

1) Input Signal: It has very low amplitude, *e.g.* EAP and LFP are in the range of hundreds of microvolts. It is therefore very sensitive to all noise sources. The EEI potential depends on the concentration of ions on the surface of the electrode, which may change over time.

2) Between the EEI and the amplifier input there is a conductor material. This no-null resistance generates noise. This path is also an antenna and induces interference with the environment. The APS approach reduces the effect of these noise sources by reducing the electrode-amplifier distance.

3) Setting a high gain for the OPA is useful because: the noise influence of further stages is reduced (Friis formula) and, once the signal is high enough, it is more robust to noise coupling. Another way to reduce the global noise is to limit the signal bandwidth, without loosing EAP and LFP information.

4) The transistor M1's size has been chosen in order to obtain a good compromise between area, input impedance, and gain (see Fig. 4.05). Alternative methods are: (a) optical coupling (Bontorin07a); (b) using a fully differential circuit; (c) capacitor coupling (Harrison03). (a) We have no information on the use of optical coupling in an integrated amplifier for our application field. (b) A fully differential amplifier occupies the double area of a single ended amplifier. Therefore, (a) and (b) are area consuming and do not directly resolve the low cutoff frequency. (c) may solve the low cutoff frequency issue, but will also deteriorate the input impedance. High input impedance is helpful in two ways: (i) reducing the signal deterioration by impedance division (Heer04, Berdondini05); and (ii) reducing the influence of fluctuations in the EEI impedance and potential (Robinson68).

Other design aspects that have a strong influence on noise performance are: power supply noise, power consumption and silicon area.

5) The power supply is a noise source that interferes with signals over the entire circuit. The most sensitive point is the OPA, or, more precisely its second stage: the common source (Steyaert90). A special effort is require in layout design at this point, for reducing power supply noise's influence (Ott88). The feedback and the first stage of the OPA are more robust. In the first stage, the supply noise affects simultaneously both branches of the differential pair, cancelling or reducing its effects. A similar phenomenon occurs between the sampling capacitor and the current source in the feedback.

6) Noise performance may be improved at the cost of increasing power and silicon area. Higher biasing current and/or larger transistors reduce thermal and flicker noise. Some design techniques, *e.g.* reducing parasitic resistance or coupling, increase noise performances as well as the silicon area (Ott88, Jimmin94).

Finally, we designed a preamplifier compatible with the APS architecture (see schematic in Fig. 4.05), in a pixel with a maximum area of 40x40 μm^2. This area is a good compromise between electronics performance and acquisition density. The amplifier's gain is at least 100 V/V, with a high cutoff frequency of about 10 kHz. EEI potential rejection is at least ± 100 mV. The power budget is 30 µA from a 1.8 V voltage source.

II - Measurements

A prototype Integrated Circuit (IC) was fabricated in UMC (United Microelectronics Corp, subcontracted foundry at IMT Neuchâtel) 0.18 µm CMOS technology, using Cadence CAD (Computer Aided Design) tools in full-custom mode. Fig. 4.06 shows A. the layout fabrication masks and B. a picture of the test board. The IC contains three different versions of the amplifier. We show in this section the detailed performances of the best one, *alpha*. The IC also includes mini-arrays designed for the study of coupling phenomena between the channels, in wet and dry measurements. They are the subject of further analysis, not presented in this thesis.

Three experimental protocols were considered for the measurements: (a) dry measurements, which characterize the amplifier, (b) dry measurements simulating wet measurements (with a biologically realistic artificial input), and (c) wet measurements (with a real biological input) for the final validation.

A. Dry measurements

The main characteristic of an amplifier is its gain. Fig. 4.07 shows the gain and phase, with both switches (S1 and S2) open. They are representative of a low-pass filter, non-inverting amplifier, with the cutoff frequency (- 3 dB and 45 degrees) at 10kHz.

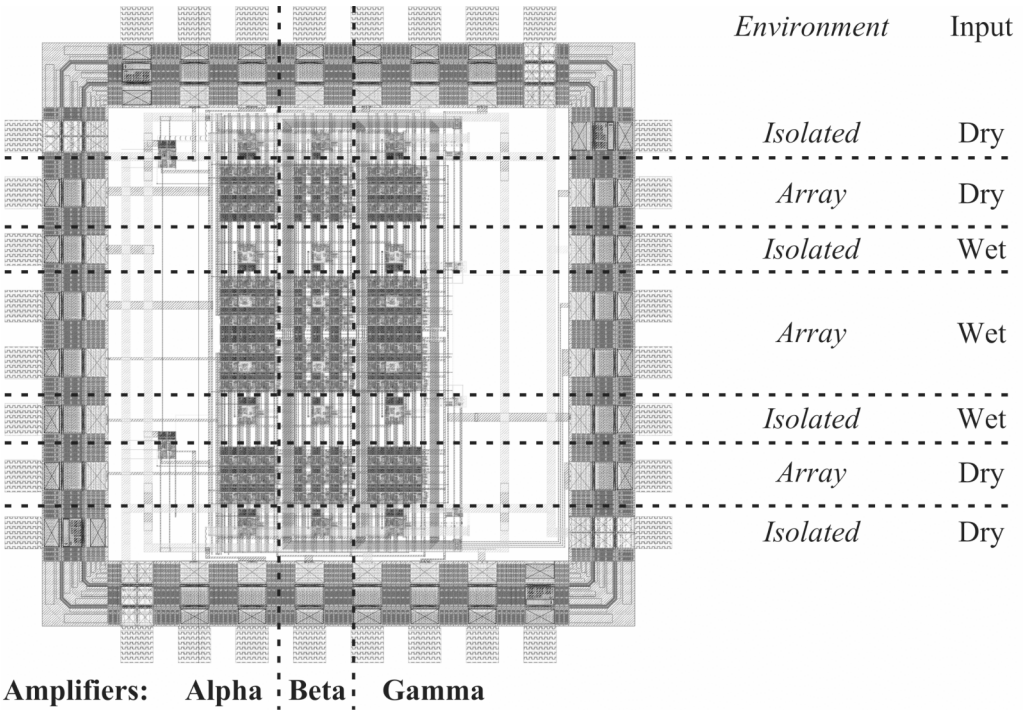

A

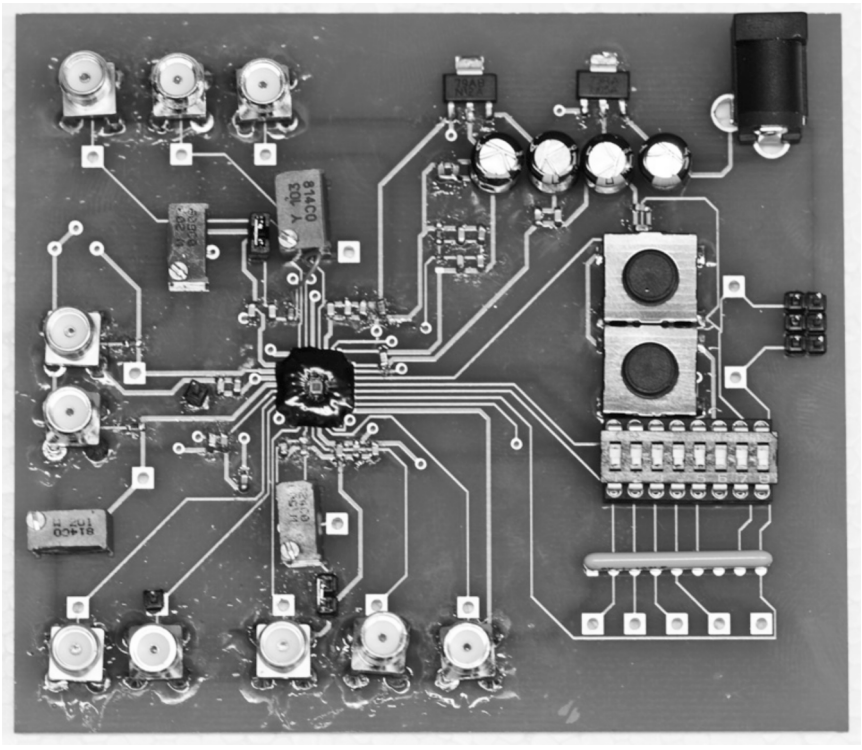

B

Figure 4.06. The Integrated Circuits (IC) design. A. The layout for mask fabrication. The IC integrates 3 preamplifier's versions: alpha, beta, and gamma. Each of the three preamplifiers is arranged in four different configurations, according to the amplifier environment and its input. Regarding its environment, the amplifier can be: isolated (for detailed electrical analysis) or in arrays (for studying the channel's coupling). For the input, the amplifier can have: an electrical pin (for dry measurements) or an electrode on the top layer of the circuit (for wet measurements). B. A picture of the Printed Circuit Board (PCB) specifically designed to test our IC. It presents analog and digital inputs and outputs to investigate all the IC's functionalities and characteristics.

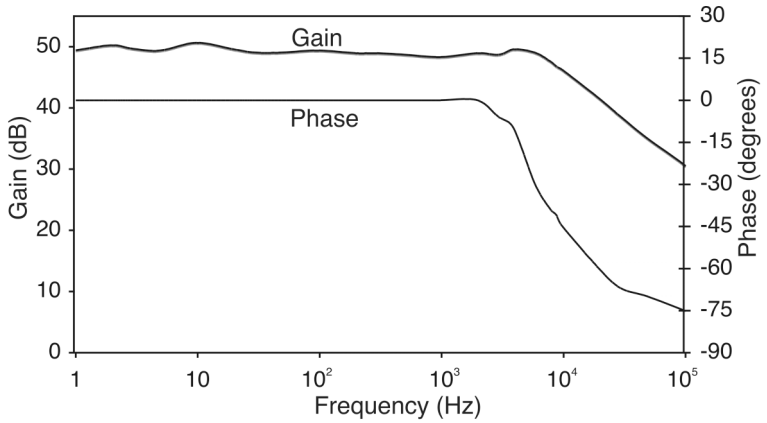

Figure 4.07. Characteristics of the alpha preamplifier: gain and phase. This non-inverting active low-pass filter has a cutoff frequency of 10kHz; its gain is 50 dB in the bandwidth.

The amplifier's equivalent input noise is 10 μV_{rms}, in the 1 Hz–10 kHz band. The power noise rejection is 40 dB at 1 kHz. This validates the low-noise feature of our amplifier. Its slew-rate is high, even without the third current amplifier of a classical OPA. The output load is a raw amplifier and an activity detector (ref detector), with a total equivalent load of 50 pF. The input impedance is very large (over a teraohm at 1 kHz). This increases the robustness of the preamplifier against EEI noise and variations. Table 4.1 summarizes the electrical characteristics of the best amplifier (*alpha*) among the 3 versions implemented.

Table 4.1 Main electrical characteristics of the alpha *amplifier.*

Characteristic	Measurement
Gain	300 V/V (49 dB)
Equivalent Input Noise	10 μV_{rms} (1 - 10kHz)
DC rejection @ input	± 430 mV
High Cutoff frequency	10 kHz
Slew Rate	1 V/µs
Total Harmonic Distortion	< - 30dB (1 kHz, 300 μV_{rms})
Power supply noise rejection	> 40dB
Input impedance	> 1 TΩ (f < 100 kHz)
Consumption	45 µW mean
Surface	1300 μm^2

Table 4.2 shows the main differences between the three versions of amplifier we implemented. They have different feedback circuitry, on the current source and on the capacitor. We can observe changes in the gain, bandwidth, surface, and DC rejection. Other electrical characteristics are equivalent.

The design of the *Beta* amplifier mainly reduces the gain of the feedback current source. This reduces DC input rejection, slightly increases the area and does not present any real advantage. The *Gamma*'s design mainly reduces the feedback capacitor and its total area. This widens the amplifiers' bandwidth and, consequently, increases the equivalent input noise. This design illustrates the consequences of capacitor reduction on amplifier's performance and justifies our choice of *alpha* as the most performant amplifier.

Table 4.2 Comparison of Alpha, Beta and Gamma amplifiers characteristics.

Amplifier	Gain (V/V)	High Cutoff Frequency (kHz)	Surface (μm^2)	DC rejection (mV)
Alpha	300	10	1300	430
Beta	150	17	1400	340
Gamma	250	30	1000	430

Lastly, Table 4.3 compares the main performances of the three amplifiers to others in the literature. Some amplifiers present a better noise performance, but a larger silicon area. This reduces the acquisition density, which is not relevant for our application. Other amplifiers have lower power consumption, which is crucial for implanted devices in medical applications. In our case, MEAs' power budget is more generous.

Table 4.3 Comparison of characteristics for Alpha, Beta, Gamma and literature amplifiers.

Reference	Technology (µm)	Gain (V/V)	Bandwidth (Hz)	Noise (μV_{rms})	Power (µW)	Area (μm^2)
Harrison 2003a	1.5 CMOS	100	0.025 - 7.2k	2.2	80	160 000
Rieger 2003	0.8 BiCMOS	100	dc -15k	0.3	1300	300 000
Ananth 2004	BiCMOS	100	10 - 10k	9.7	122	125 000
Mohseni 2004	1.5 CMOS	100	50 - 9k	8	115	107 000
Patterson 2004	1.5 CMOS	200	10 - 7.3k	9	52	160 000
Heer 2005	0.6 CMOS	10	5 - 5k	6	160	18 000
Olsson 2005	3 CMOS	100	100 - 9.9k	9	68	177 000
Ananth 2006	0.5 CMOS	1200	10 - 7k	5.6	33	3 200 000
Chua-Chin 2006	0.35 CMOS	7000	100 -7k	7	1500	151 000
Gosselin 2006	0.18 CMOS	450	100 - 9.2k	5	8.4	64 000
Blum2007	0.35 CMOS	50	30-3k	4.77	100	32 000
Holleman 2007	0.5 BiCMOS	60	0.3 - 7.5k	3.6	0.8	46 000
Ming 2007	1.5 CMOS	100	0.01- 4k	3.6	27.2	201 000
Samsukha 2007	0.5 CMOS	80	25 - 15k	1	160	130 000
Imfeld 2008b	0.35 CMOS	100	dc - 12k	11	83	1 600
MooSung 2008	0.35 CMOS	50	dc - 11k	5.5	170	120 000
Bottino 2009	0.35 CMOS	100	0.25 - 2.6k	5.7	4.5	130 000
Gamma 2010	0.18 CMOS	250	dc - 30k	12	45	1 000
Beta 2010	0.18 CMOS	150	dc - 17k	10	45	1 400
Alpha 2010	0.18 CMOS	300	dc - 10k	10	45	1 300

B. Dry measurements simulating wet measurements

This section presents the performance of our amplifier with predefined (simulated) input signals. An MEA-SG (Signal Generator), from MultiChannel Systems™ (MCS), produces signals simulating neural activity (MEA-Signal Generator ref.08). The signal is firstly amplified by the MEA-1060 from MCS and then attenuated by a resistive divider on the electronic test-bench board, to simulate non-amplified neural signals applied to our amplifier (Fig. 4.08). In this experiment, the module MEA-160 only connects our amplifier to the Signal Generator MEA-SG (or to the MEA200-30 in the case of the next section C. Wet measurements).

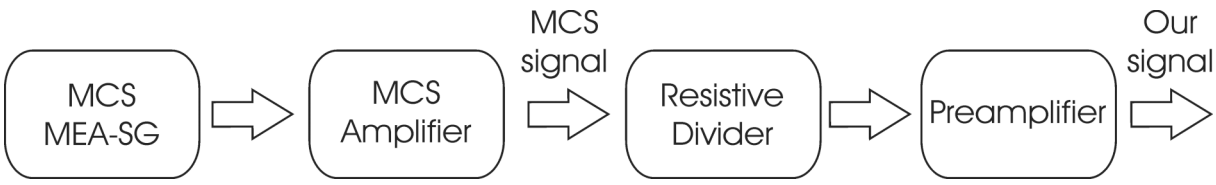

Figure 4.08. Schematic of the experiment for dry simulating wet measurements. An MEA-SG (Signal Generator), from MultiChannel Systems™ (MCS), generated signals that simulate neural activity (MEA-Signal Generator ref.08). The signal is firstly amplified by the MEA-1060 from MCS and afterwards attenuated by a resistive divider on the electronic test-bench board, to simulate non-amplified neural signals being applied to our amplifier (MEA User System Manual ref.06). The "MCS signal" label indicates where the signal "MCS" (see examples in Fig. 4.09) is measured. The label "Our signal" indicates the point where the signal "Our Amplifier" (Fig. 4.09) is measured.

Fig. 4.09.A shows examples of amplifier outputs, for input spikes in the EAP frequency range. Fig. 4.09.B shows the amplifier output of a mainly-LFP range signal, the ERG (ElectroRetinoGraphy). In both figures we compare the amplification of a signal with the MCS acquisition chain and the amplification with our amplifier.

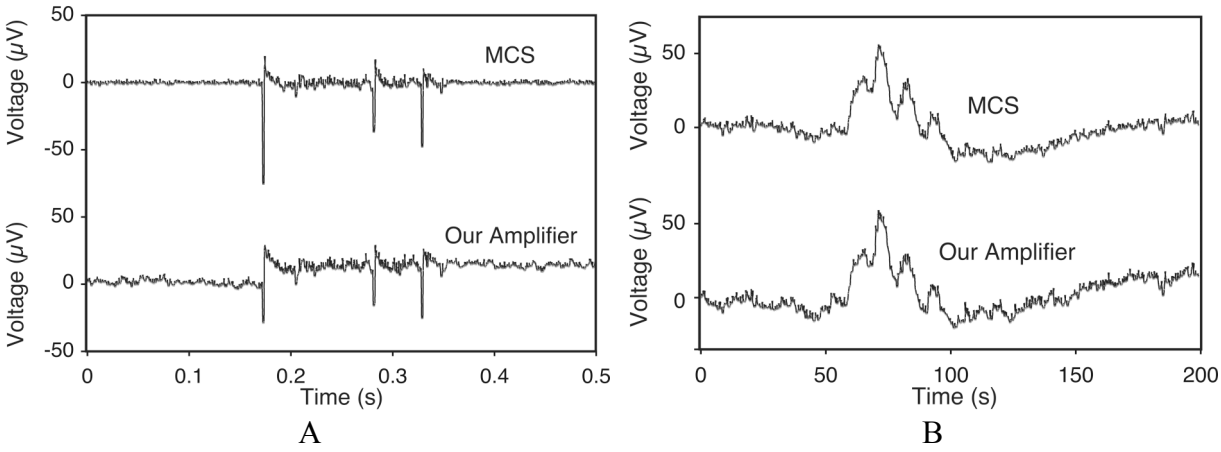

Figure 4.09. Comparison between the signals amplified with the MCS chain and our amplifier, as described in Fig. 4.08. Top plot: MCS amplifier output; Bottom plot: Our amplifier output. A. Artificial EAP. The reduction of the first spike amplitude in the bottom plot comes from the double filtering in high frequencies (10 kHz) by the processing chain. B. Artificial LFP. Plots are similar. In the graphs, the voltage axis is the output signal divided by the gain of each chain. Therefore, both signal are shown at a level equivalent to the input of amplifier.

C. Wet measurements

The last test of the amplifier is with a real biological signal. In pancreatic cells, changes in the spiking activity reveal a changing glucose concentration; the system acts as a glucose sensor. We use rat pancreatic ß-cells (INS-1E) from an insulinoma cell line cultivated on MEA (Merglen04). All experiments were conducted between passages 67 and 82. INS-1E cells were seeded at 200'000 to 300'000 cells/MEA with a complete medium containing 11 mM of glucose and were maintained at 37°C and 95 % O2 in an incubator for 5-7 days. The medium was replaced 24 to 48 h before recordings by a medium containing 5.5 mM of glu-

cose. Fig. 4.10 presents the schematic data flow for the wet measurements. The MEA-SG from the dry simulating wet measurement is replaced by the cell culture and the MEA200-30 from MCS (electrodes diameter 30 µm; inter-electrode distance 200 µm). The recordings (Fig. 4.11) show the spontaneous activity (without external stimuli) of the cells in a hyperglycemic medium (15 mM).

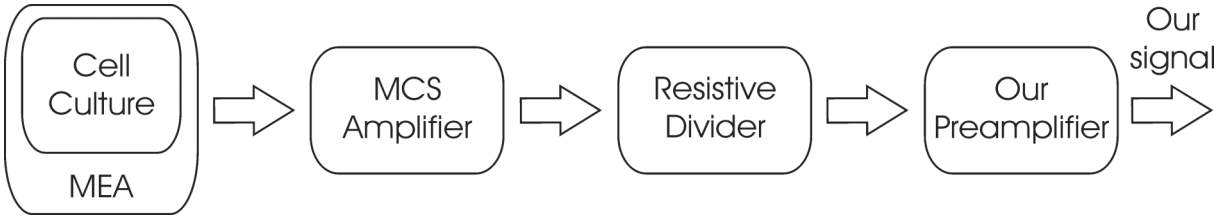

Figure 4.10. Schematic data flow for wet measurements. The cell culture is plated on a multielectrode array, MEA200-30 from MultiChannelsSystems (MCS). The signal is firstly amplified by the MEA-1060 from MCS and afterwards attenuated by a resistive divider on the electronic board, to simulate non-amplified neural signals applied to our amplifier (MEA System User Manual ref.06). The label "Our signal" indicates the point where the signal "Our Amplifier" (Fig. 4.11) is measured.

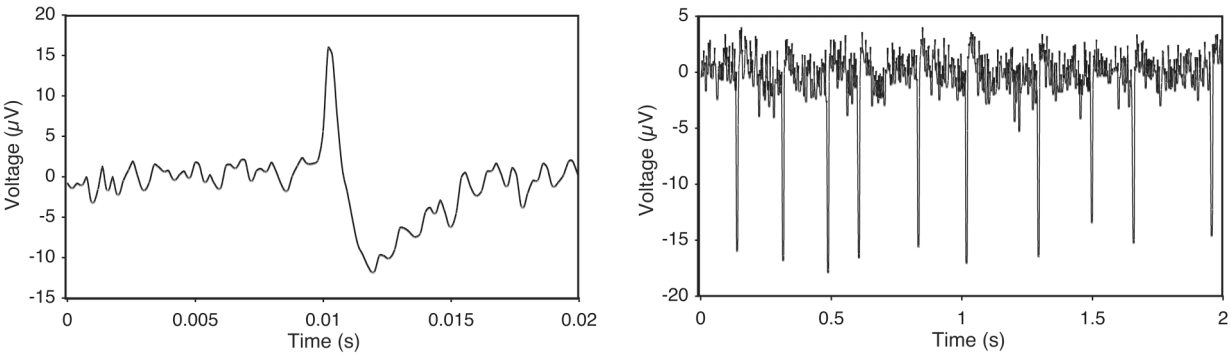

Figure 4.11. Recordings of pancreatic ß-cells activity in a hyperglycemic (15 mM) medium. In the graphs, the voltage axis is the output signal divided by the gain of each chain. Therefore, signals are shown at a level equivalent to the one at the amplifier's input. All signals presents a high quality amplification, with an acceptable noise lovel. A. Zoom on a single spike. B. Another recording with a different time scale and a regular spiking activity.

III. Discussion

We designed an amplifier that will be integrated into an acquisition system based on an APS (active pixel sensor) MEA. Such a device is chosen to increase the density of acquisition channels. In this case, the limiting factor is traditionally the connectivity of passive MEA (conductors and signal degradation) is replaced by the amplifier performances (noise and silicon area). Comparing to the system described in (Imfeld08b), our new amplifier decreases the pitch of each electrode from 40 µm to 36 µm, increases the gain (from 100 to 300), and reduces the power consumption per pixel (almost by a factor of 2, as the power supply voltage

passes from 3.3 to 1.8 V). The noise performance is slightly better, but is difficult to characterize, as the difference between the noise mean values is smaller than the measurement error.

If we compare our amplifier to others in the literature (Table III), some of them present a better noise performance, but with a larger silicon area. The great advantage of our amplifier is its high integration level, which increases the acquisition density.

Still comparing with the literature, other amplifiers have much lower power consumption, which is essential for long-term implanted devices. Large power consumption has three consequences for such devices: heat and damage on living tissue, larger batteries are required, and a lower implantation lifetime. In our case, MEAs are flexible. Firstly, *in vitro* cells require often an external heating (temperature regulation), which consumes more power than the amplifiers. Secondly, the power supply is usually external, which is more powerful than battery-based systems. Thirdly, long-term experiments *in vitro* last at most for months (Potter06 and Merglen04), and the cells' death determines the end of the experiment.

Compared to the passive MEA approach, the APS method provides a much higher density. For example, the MEA60 from Ayanda (Fig.4.02) (AyandaSystems ref.) has a pitch of 240 µm. Our amplifier has a pitch of 36 µm. This increases by almost 45 times the acquisition density (from 240x240 µm2 to 36x36 µm2).

It is worth mentioning that the technique for eliminating the DC level can be extrapolated to reduce also the LFP signals, providing to the user only EAP (spikes). This requires a careful study and modeling, which is currently ongoing in our group.

Considering high frequencies, the use of the Miller capacitor for the high cutoff frequency may also be extrapolated to reduce the EAP frequencies, keeping only the LFP components. This method may increase the amplifier surface, deteriorate the power supply noise rejection, reduce slew-rate, and increase power consumption. However, by working on the schematic and on the layout, we can reduce these drawbacks.

Finally, increasing the density and the scale of the system is useful in many applications, as already illustrated in the Introduction section. But this also increases the amount of data. In many applications, such as *Hynet*s (previous chapter), brain-machine interfaces (Nicolelis09), or motor rehabilitation systems (Loeb01), the data must imperatively be processed in real-time, which becomes an issue with large data flows. A solution is to detect activity on-line and discard useless data from the raw signal, as presented in the next chapter.

CHAPTER 5
DETECTOR

"I consider that a man's brain originally is like a little empty attic, and you have to stock it with such furniture as you choose. A fool takes in all the lumber of every sort that he comes across, so that the knowledge, which might be useful to him, gets crowded out, or at best is jumbled up with a lot of other things, so that he has a difficulty in laying his hands upon it."

Sherlock Holmes, fictional British detective,

Conan Doyle (1859-1930) Scottish physician and writer.

In "A Study in Scarlet".

The *Hynet* presented in chapter 3 (Hynet) has spatial performances limited by the use of commercial MEAs (MultiElectrode Array). Combining the APS (Active Pixel Sensor) approach and our new preamplifier, presented in chapter 4 (Preamplifier), potentially increases the channel density for the acquisition of biological signals. However, it also increases the amount of data to be processed. In order to maintain real-time operation, the processing performances of the system must progress at least proportionally.

With this in mind, I present the implementation of an "*Intelligent Pixel*" (*iP*) in this chapter. Such a pixel includes 3 items: electrode, preamplifier, and spike detector. One *iP* (Fig 5.01) replaces one acquisition channel as presented in the previous *Hynet* (system developed at the IMS laboratory). It will be used also in the system developed in IMT to perform real-time spike detection while keeping its large-scale and high-density features. The *iP* is designed in order to improve signal quality, acquisition density, and real-time data processing.

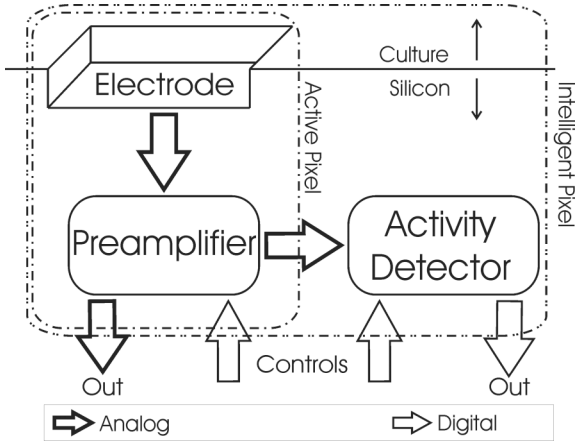

Figure 5.01. The Intelligent Pixel (iP) schematic. It integrates an Electrode, a Preamplifier, and an Activity Detector for each acquisition channel. Electronics parts are integrated under the electrode, as close as possible to the culture, in an Active Pixel Sensor (APS) approach. The preamplifier amplifies the analog biological signal. The active pixel provides the amplified biological output to the user and to the detector. The *iP* includes the active pixel and the activity detector. The activity detector generates a digital output that indicates the detected information timing. Digital signals control the *Intelligent Pixel*.

I. Design

The important specifications for our spike detector are: robustness under the variations in the biological signal, an area and power consumption that are compatible with high-density and large-scale implementation, and, as mentioned earlier, real-time data processing for a closed-loop integration. Section A provides information about the variability of the signal. Section B comments on the existing detection methods and their performances. Finally, section C shows the schematic of our detection circuit.

A. Signal

In the previous chapter, we presented some characteristics of biological signals. In this section, we detail some points that are more specific to spike detection.

Electrogenic cells have different spike waveforms. Differences can be found even in the same cell species. For example, a neuron can present different activity patterns, or even different spiking waveforms, depending on spatial location, or the afferent and efferent cells. Patterns also change over time (Fee96).

The EEI (Electrolyte-Electrode Interface) presents spontaneous current and voltage fluctuations. They originate from energy dissipation on conductors and electrochemical interactions. This noise is associated with white, 1/f and $1/f^2$ noise for, respectively, thermal noise in conductors, mass transfer process dominated by diffusion, and mass transfer dominated by electrical fields (Hassibi04).

Variations and noise complicate the development of an activity detector based on pattern, filtering or frequency-time components.

On the other hand, most of the signal variability for spike sorting is located near to its peaks, either positive or negative, in a time segment of about 0.5 ms. Longer acquisitions of one single spike increase slightly the spike sorting performance. For example, a 1.3 ms segment increases the mutual entropy of the recording by one bit (out of ten) if compared with the 0.5 ms (Fee96). These are the main characteristics that guided us to choose the processing methodology for our spike detector.

B. Detection method

We can sort all the existing methods for spike detection (reviewed *e.g.* in (Lewicki94) or (Bashashati07)) by looking at their constitutive blocks. The first one is the pre-processing block, which either accentuates the activity or attenuates the noise. The second one is the decision block, which decides the "information moment" by comparison with a threshold or by clustering. The third one is the adaptation block (also called calibration or learning). It takes into account the variations of the biological signal and adapts the processing parameters of the two previous blocks for an optimal performance (Fig. 5.02). We will see that the second block is the most sensitive in the detection process. Table I reviews the characteristics of state-of-the-art detection circuits.

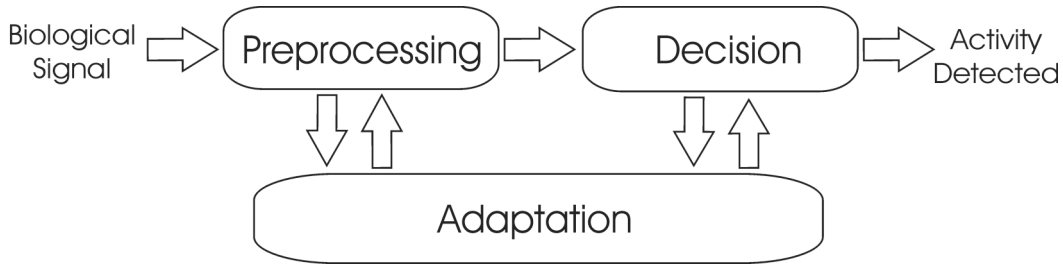

Figure 5.02. The activity detection circuit and its constituting blocks. The Biological Signal is applied to the Preprocessing block, which either accentuates the activity or attenuates the noise; the Decision block decides the "information moment"; the Adaptation block adapts the parameters of the two previous blocks for an optimal performance and outputs the Activity Detected.

Table 5.1. Activity detectors from the literature.

Reference	Blocks			Signal	Costs (/ch)	
	Preprocessing	Decision	Adaptation		Size (mm^2)	Power (µW)
Rogers 2005	Wavelet	Th.	None	Analog	0.056	1
Oweiss 2007	Wavelet *a*	Th.	None	Digital	0.117	0.71
	Wavelet *b*	Th.	None	Digital	0.040	0.87
Imfeld 2008a	Wavelet	Th.	Coeff	Digital	N/A	N/A
Zviagintsev 20006	PC	Cl.	Vector	Digital	N/A	N/A
Haas 2007	TM	Th.	None	Analog	N/A	N/A
Gosselin 2009	NEO	Th.	None	Analog	0.07	0.78
Moo Sung 2009	NEO	Th.	None	Digital	N/A	1000 *c*
Olsson 2005	None	Th.	None	Digital	0.078	75
Sodagar 2007	None	Th.	None	Digital	N/A	197
Horiuchi 2004	None	Th.	None	Analog	0.091	0.8
Harrison 2003a	None	Th.	SD	Analog	0.094	57 *d*
This	None	Th.	SD	Analog	0.0035 *e*	100

We identify in each reference the preprocessing, decision, and adaptation methods, the signal representation, and costs per channel (/ch). Preprocessing methods include: wavelet, PC (Principal Components), TM (Template Matching), NEO (Nonlinear Energy Operator), or no preprocessing. The decision is necessary and is normally by threshold (Th), but PC uses clustering (Cl) to divide the multidimensional space. The adaptation block is not mandatory. In the case of Wavelets, the filter coefficients can be updated. In the case of PC, the vectors may be computed to optimize clustering. The threshold can be adapted with an online estimation of the Standard Deviation (SD) of noise in the signal. In each of the detectors, the signal can be represented in analog or digital mode. Caption: *a* pipeline implementation; *b* sequential implementation; *c* consumption without the spike sorting; *d* consumption without the peak detector; *e* area without the capacitor, as its value is set according to the experiment.

In the literature, we find the following **preprocessing** techniques: wavelet transform, principal components analysis, template matching, energy-based transform, and no preprocessing other than the analog pre-amplification.

Wavelet transform (WT) is based on the convolution of the signal with a family of curves. This family is derived from the scaling and the translation operations applied to a predefined waveform, the mother wavelet. The performance of this preprocessing relies on the choice of the "*mother wavelet*". Currently, no wavelet seems to be adapted to all biological signals (Wenshan09). **Principal Components Analysis** (PCA) is based on the decomposition of the signal in an ordered set of orthogonal basis vectors. These vectors must be chosen to reveal the largest variation on the spike waveform (Zumsteg05, Donoho94). **Template matching** (TM) is based on the measurement of dissimilarity with waveforms used as references. However, the dissimilarity measurement is still a controversial method for detection (Thakur07).

These three methods demand highly complex computing for the convolution, for the clustering phase or for the dissimilarity measurement. They are efficient only if the spike waveform is known *a priori* and is mostly constant, which is rarely the case (Fee96, Wood04). They are very well adapted to offline software preprocessing, where real-time performances are not relevant by definition. They can barely be adapted for real-time applications while maintaining high-density performances on a complete system, taking also into account the fact that each pixel must have its own preprocessing block.

Energy-based systems estimate the instantaneous signal square. The most commonly used algorithm is the Non-Linear Operator (NEO), first presented by (Kaiser90), which is less complex than previously presented algorithms (Gosselin09). Nevertheless, (Obeid04) compares its performances to other methods, and concludes that a simple absolute operation on the signal before the detection is as efficient as Energy-based preprocessing.

Finally, we consider **no preprocessing**. This simple technique is used for example in (Harrison03a, Olsson02). It is obviously the option with the least processing complexity and can be highly integrated. We chose this method for our spike detection. A double thresholding (positive and negative) can substitute the absolute operation used on other preprocessing techniques, and achieve performances comparable to NEO (Obeid04).

The second block is the **decision**. It is the core of the detector, as it discriminates the activity. For multiple signals (multidimensional) preprocessing, *e.g.* PCA, the most adapted

method is clustering, as it defines regions into the mathematical space where there is activity. In the case of one-dimensional signals, the threshold technique is normally sufficient, the "activity" being found when the signal exceeds a threshold value. In this case, the most critical point for the detector performance is the choice of the threshold values. For a raw (not preprocessed) spiking signal, the optimal threshold value seems to be between 3 and 5 times the standard deviation of the signal (*N*SD*). Into this range [3:5], high values for *N* reduce the false positive error (detection of non-existing spikes) and low values reduce the false negative one (non-detection of existing spikes) (Garenne10). Depending on the application, the user defines the relative tolerance to theses errors and set precisely *N*.

A dynamic threshold is optimal for taking into account noise and signal variations over time (along the experiment) and over the space (from one channel to an other). This is the role of the third block, the **adaptation** one. PCA detectors must use this block to define the vector basis and optimal clustering. We use this block to compute in real-time an estimation of the standard deviation of the signal and dynamically update the detection threshold.

Finally, the signal can be processed, digitally or analogically. Both solutions are present in the literature (Table 5.01). The digital implementation has the advantage of a shorter development time. However, it requires the conversion of an Analog to Digital Converter (ADC). In this case: (a) the resolution is fixed by the number of bits; (b) the commutation time of logic gates limits the time resolution, and, of course, (c) these two characteristics are strongly linked to the area and power consumption factors (Walden99).

The analog processing does not require such a conversion. The data processing is naturally both continuous and in real-time, as the microelectronic component's kinetics are speeder than the signal's kinetics. The signal is also conveyed in one single wire and the resolution is limited by the signal to noise (S/N) ratio. A careful design of analog ICs allow us for obtaining high resolution in both: time and value, even when the silicon area is very limited.

To summarize, considering again Fig. 5.02, we made the following choices for our detector: no preprocessing (first block). The detection of the second block is based on thresholding of the raw signal from the preamplifier. The third block estimates the standard deviation (SD) of the raw signal and computes the adapted threshold level *N*SD*. All data processing is analog, configurable using either digital or analogical parameters. Thanks to the adaptation block, the system is able to deal with the signal variation. These choices privilege the

integration scale and the processing speed, *i.e.*, the spatiotemporal performances of the *Intelligent Pixel*.

C. The Circuit

From the specifications presented in the last section, we obtain the detector schematic as presented Fig. 5.03. The thresholding element executes the detection, and is specific for each channel. The raw signal from the amplifier is compared with the adapted threshold from the adaptation element, which is more complex and therefore more area consuming than the detector. In order to increase the acquisition density, this circuit can be deported from the pixel. To reduce even more the consumption and total silicon area, it can be shared among neighboring pixels. However this last solution has the consequence that the threshold adaptation will no large be related to a single pixel, but to a group of pixels.

Simple voltage comparators compose the thresholding circuit, as shown in Fig. 5.04. The output is a digital signal stating the presence or absence of activity; one bit is reserved for the positive threshold exceeding and one bit for the negative one.

The adaptation circuit estimates the standard deviation (SD) of the signal noise. Experimental tests in (Fee96) confirm that the biological noise is white, which means that the probability of the signal being higher than its standard deviation is 16 %. In a recording that is considerably long compared to the desired event, this probability can be extrapolated as the percentage of time that the signal is higher than its standard deviation. This principle is also used by (Harrison03a). Using this mathematical approach, the signal is higher than its – SD 84 % of the time (Fig. 5.05.A).

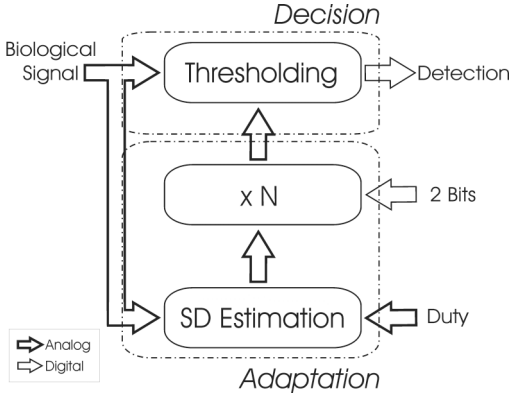

Figure 5.03. The activity detector. The analog biological signal is thresholded by the decision block. The result is a one-bit digital signal detecting the presence or absence of activity. The threshold is computed based on the estimated Standard Deviation (SD) of the biological signal multiplied by N. N is a digital input set by the user. The adaptation block uses also an analog voltage (Duty) as an input to

compute SD. The decision part is specific to each pixel but the adaptation may be deported and/or shared, respectively, to increase the acquisition density and/or to reduce area and power consumption.

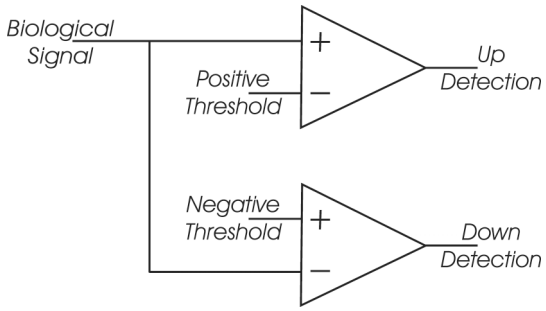

Figure 5.04. The decision circuit. The biological signal is compared to two different thresholds. One comparator identifies the signals above the Positive Threshold and gives an output as Up Detection. The comparator identifies the signals below the Negative Threshold and gives an output as Down Detection. Together, these two comparators perform the mathematical absolute operator.

Fig. 5.05.B shows the block diagram of the SD computing component. The first comparator creates a digital image of the periods when the input signal is higher than + SD (or – SD for the negative threshold). The duty cycle is then computed and compared with the requested level, 16 % for + SD and 84 % for – SD. The output of the block is N*SD that will be used as a positive or a negative threshold by the decision module.

Fig. 5.05.C details the schematic of the electronics circuit of Fig. 5.05.B. The same non-latched electronics comparator of the decision block makes the first comparison between the raw signal and the estimated sigma. A low pass filter computes the duty cycle and a differential pair compares the actual duty cycle with the target voltage value.

The detector's inputs are: the analog raw signal from the preamplifier Vin, two analog references Vduty and Vref, and the digital code for N, in order to set the threshold to N*SD. Vduty comes along with +SD or -SD. Vduty is 0.84 x Vdd or 0.16 x Vdd for, respectively, + SD or – SD. Vref is set to 0.5 x Vdd. In our test chip, these parameters are applied on input pins. N is an integer encoded on two bits and defines the thresholding factor, in the range [1:5]. The N value is used to multiplex the corresponding N*SD tension value from the resistive bridge to the threshold output.

The detector also includes switches to stop the adaptation in the case where the input signal is interrupted, *e.g.* in a calibration phase of the preamplifier. In such a case, S1 is closed and S2 is open. In normal use, S1 is open and S2 is closed.

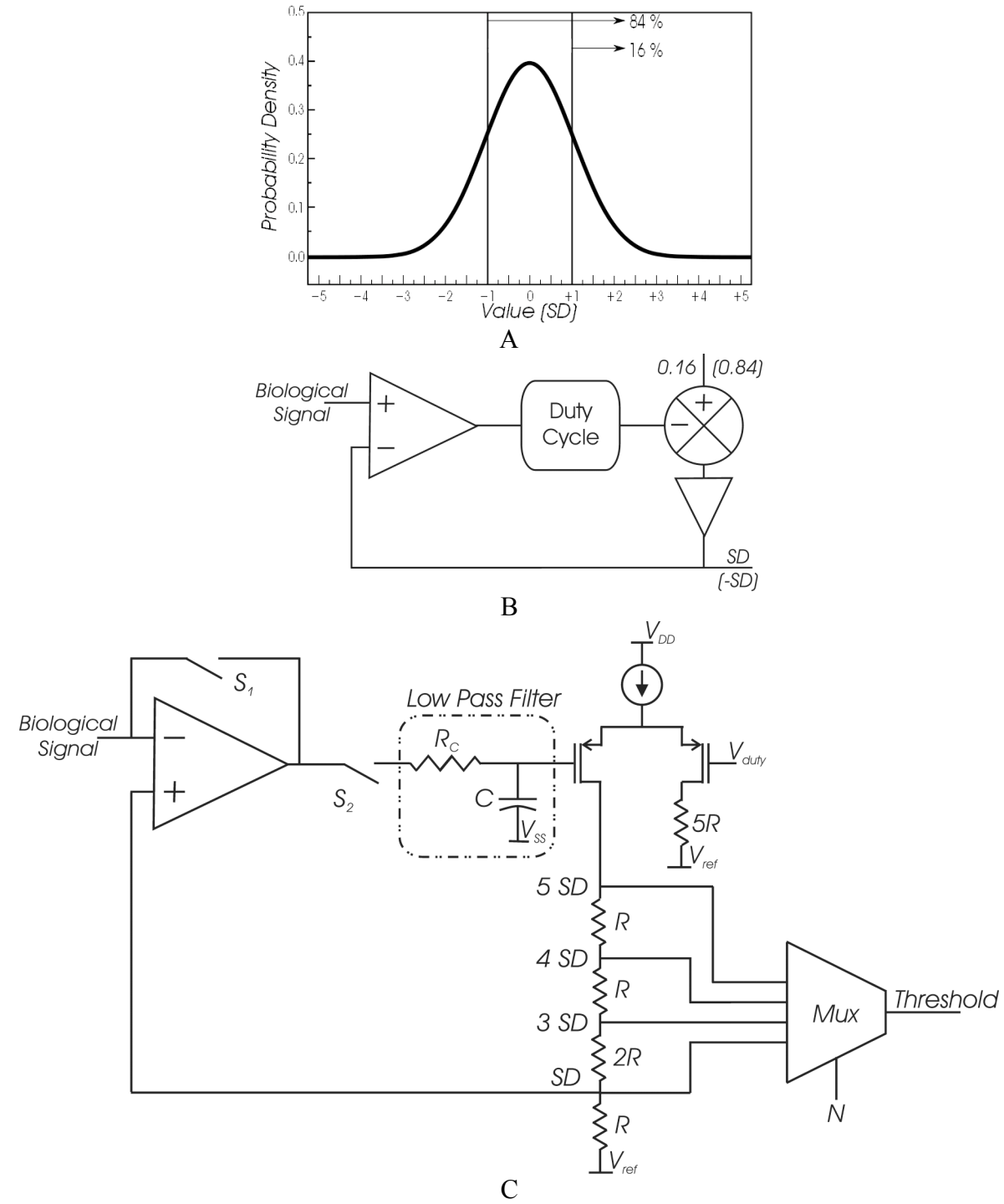

Figure 5.05 The adaptation block. A. The mathematical illustration of the Standard Deviation (SD) estimation. The probability for a white noise to be over its positive SD is 16 %, and 84 % for its negative SD. B. The Block diagram. The SD is dynamically estimated in a closed-loop. The Biological Signal is compared to the estimated SD. The duty cycle of the resulting signal is computed and the SD is updated according to the deviation from the target: the positive SD has a target of 0.16 for the duty cycle, while the negative SD has a target of 0.84. C. Schematic of the adapted positive threshold (N*SD) circuit. A simple comparator compares the biological signal and the estimated SD. A passive low pass filter (C and Rc) computes the duty cycle. A differential pair compares the duty cycle to the target (Vduty). The differential pair's load provides multiple threshold values. Finally, controlled by the digital value N, a multiplexer defines N*SD. S1 and S2 switches can stop the adaptation if the

input signal is unavailable. In such a case, S1 is closed and S2 is open. In normal use, S1 is open and S2 is closed.

The last parameter depends on the targeted application. EAP and LFP are different in their frequency spectrum and thus require a different time constant (TC) for the low pass filter. For EAP detection, TC must be in the range of some milliseconds. LFP requires some hundreds (or even thousands) of milliseconds. Our architecture is compatible, in theory, with both, by changing the filtering cutoff frequency (Rc and C).

In the literature, (Harrison03a) presents a close detector's architecture, as it uses also an estimated SD to adapt the threshold. However, our system has two major advantages. The first is the use of a double thresholding in the decision block, which improves the detection and further sorting of spikes (see figure 5.11.B below). The second is the tunability of the adaptation block, with the possibility of choosing the factor N (see Fig. 5.11.B below) and the time constant of the low pass filter (see Fig. 5.09.B).

II. Measurements

A prototype Integrated Circuit (IC) was fabricated in UMC (United Microelectronics Corp, subcontracted foundry at IMT Neuchâtel) 0.18 μm CMOS technology, using Cadence CAD (Computer Aided Design) tools in full-custom mode. Figure 5.06 shows A. the layout fabrication masks and B. a picture of the test board. The IC includes three versions of the detector associated with three versions of the preamplifier, resulting in 9 different versions of the "intelligent" pixel. The three amplifiers are as described in the previous chapter (4. Preamplifier): alpha, beta and gamma. The three detectors differ on the adaptation circuit. Positive and Negative compute the positive and negative thresholds, respectively. Kappa has the same architecture as Positive, except for the resistances on the resistor bridge, which are smaller; as is the surface of the whole detector. At the end, Kappa has a larger power consumption (almost 10 times higher) for a limited reduction in area (15 %). This solution was discarded.

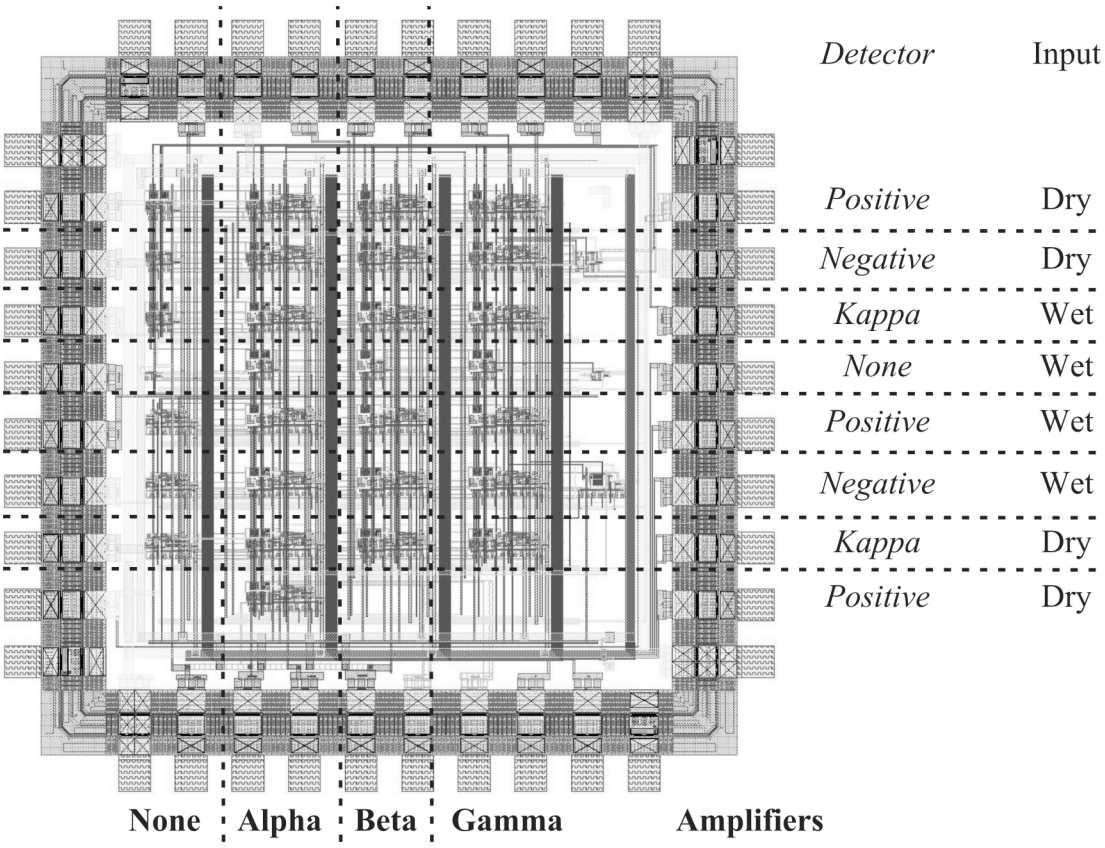

A

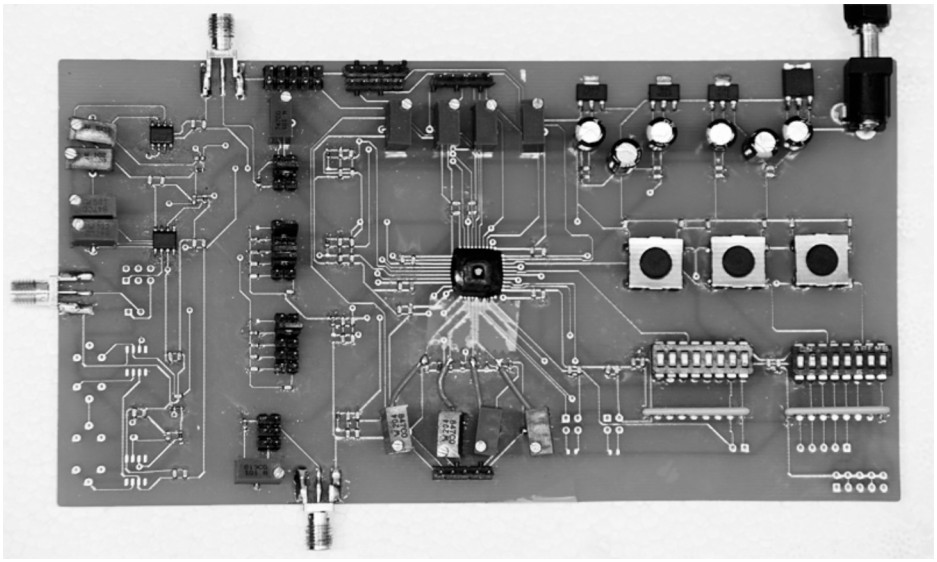

B

Figure 5.06. The IC design. A. The layout drawing. The IC presents three different detectors: positive, negative, and kappa. They are all complete, each one with its own decision and adaptation blocks. The positive and the negative detectors are identical except for the multiplier sign. The Kappa detector has the same architecture as the positive one, but a different multiplier. Each version of the detector is associated with three versions of the preamplifier (alpha, beta, and gamma). Lastly, the IC presents five different configurations. Three of them have dry inputs, *i.e.* electrical pins. They are: a preamplifier alone, a detector alone, and an *Intelligent Pixel* (preamplifier + detector) with adaptation. The other two have wet inputs, *i.e.*, a top electrode in contact with the culture. They are: a preamplifier alone and an *Intelligent Pixel* with the adaptation. B. The electrical test bench. This presents analog and digital inputs and outputs to access all the IC's functionalities.

Three experimental protocols were considered for the measurements: (a) dry measurements, which characterize the detector circuitry, (b) dry measurements simulating wet measurement (with biologically-realistic computed inputs), and (c) wet measurements (with biological signal inputs) for the final validation.

In the prototype version of the detector, the low pass filter capacitor is not integrated, to allow us adapt the cut-off frequency to the input signal. Further studies will define the optimum cutoff frequency and the corresponding capacitor for each activity (spike, burst, or LFP) of each cell (neuron, beta-cell, or etc.).

Table 5.2 Characteristics of the detector.

Characteristic	Measurement
Comparator	
Input offset	< 450 µV
Frequency	> 2 MHz
Delay	< 0.2 µs
Area	150 μm^2
Power	27 µW
Decision	
Area	300 μm^2
Power	54 µW
Adaptation	
Area	3200 μm^2 *a*
Power	45 µW
Intelligent Pixel	
Area	1600 μm^2
Power	100 µW
Intelligent Pixel + Adaptation	
Area	4800 μm^2 *a*
Power	145 µW

a area without the capacitor. Its value is set according to the experiment.

A. Dry measurements

Table 5.2 shows the results of the dry measurement of the detector's performances. We separated the results for the 3 parts: comparator, decision, and adaptation; and for 2 configurations of the *Intelligent Pixel*: with or without integrated adaptation.

As described previously, the decision sub-circuit is composed of two comparators. The adaptation sub-circuit has one comparator, a multiplier, and a low pass filter. Comparators are therefore key elements for the circuit and we measured their characteristics such as the input offset, the input impedance, the output slew rate, and the maximal commutation frequency.

In order to test the adaptation module, we use as an input a sine wave (1 kHz) with a 3-Hz amplitude modulation. This modulation is reflected by the dynamic change of + 5*SD (Fig. 5.07).

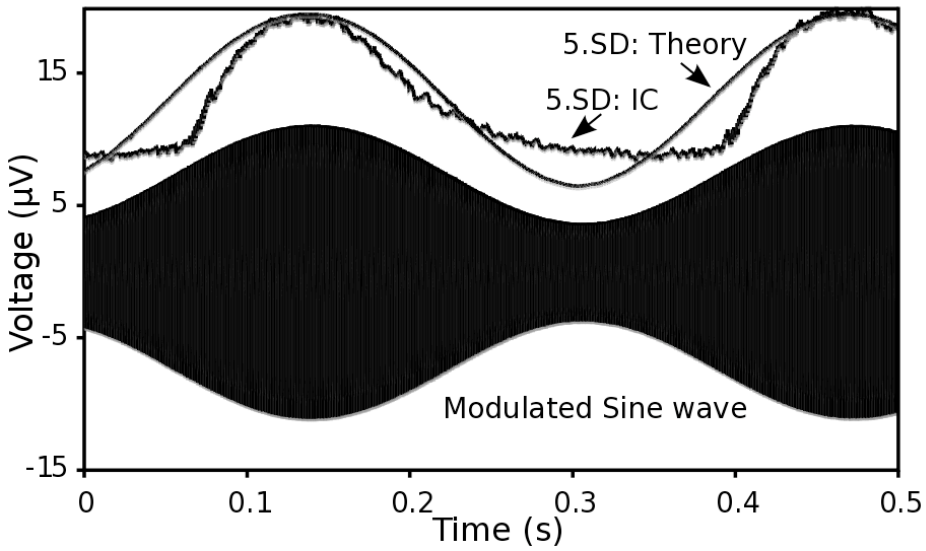

Figure 5.07. Test of the adaptation. The input signal is a sine wave with an amplitude modulation. This is an easy way to simulate evolution of the noise in the signal. The N*SD threshold (here N=5) adapts to the "noisy" signal. The adaptation must be slow to prevent false adaptations in the case of many consecutives spikes.

B. Dry simulating wet measurements

This section presents the performance of our amplifier with predefined (simulated) input signals. We use an MEA-SG (Signal Generator), from MultiChannel Systems (MCS), to generate signals that simulatie neural spikes (MEA-Signal Generator ref.08). The signal is pre-amplified by the MEA-1060 from MCS and then attenuated by a resistive divider on the electronic test-bench board, to simulate non-amplified neural signals applied to our amplifier

(previous chapter). The amplified signal is then applied to the detector (Fig. 5.08). In this experiment, the module MEA-160 only connects our amplifier to the Signal Generator MEA-SG (or to the MEA200-30 in the case of the next section C. Wet measurements).

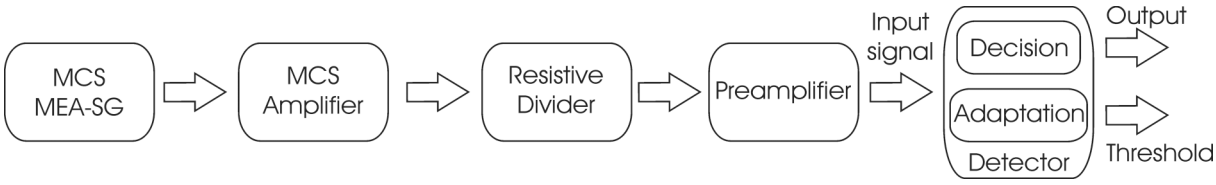

Figure 5.08. Schematic of the experiment for dry simulating wet measurements. MEA-SG (Signal Generator), from MultiChannel Systems™ (MCS), generates signals that simulate neural activity (ref MEA-Siganal Generator ref.08). The signal is firstly amplified by the MEA-1060 from MCS (MEA System User Manual ref.06) and secondly attenuated by a resistive divider on the electronic board, to simulate non-amplified neural signals applied to our amplifier. The preamplifier's output is presented as the biological signal (label Input Signal) to the detector. The detector's output is a 1-bit signal indicates the presence of activity. The threshold is also an output of the detector.

Fig. 5.09 shows the measurement of artificial spikes (EAP frequency range) amplified and detected. Fig. 5.09.A presents a down detection (– SD) of three spikes in a noisy signal. The threshold remains almost unchanged, as expected. Fig. 5.09.B presents an easy to detect signal with a high signal to noise ratio. The threshold presents small changes, detecting the beginning of a LFP signal. This adaptation would be interesting if the spikes were superimposed on the LFP signal. As the LFP signal is short, the threshold returns to the previous value, as expected.

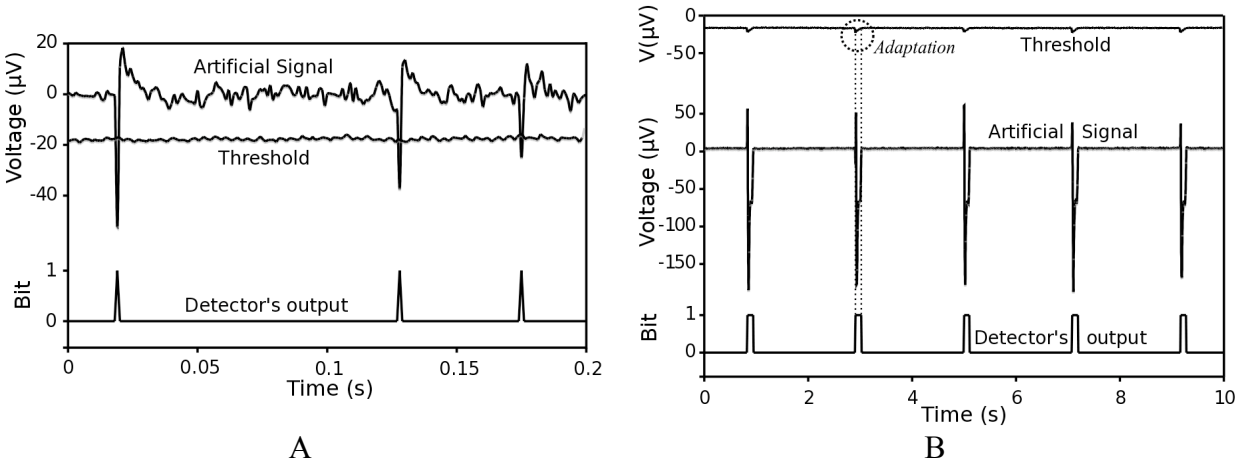

Figure 5.09. Test of the detector with dry simulating wet signals. In the graphs, the voltage axis is the output signal divided by the gain of each chain. Therefore, signals are shown at a level equivalent to the output of MEA-SG. We plotted the input (Artificial Signal), the dynamic threshold (Threshold) and the detector's output. A. A noisy signal. The down detector detects three spikes. In the presence of a constant energy noise, the threshold has an almost constant value. B. A low noise signal, with easy decision. The threshold is dynamically modified following the LFP length.

C. Wet measurements

The last test of the amplifier is with a real biological signal. We use rat pancreatic ß-cells (INS-1E) from an insulinoma cell line cultivated on the MEA (Merglen04). All experiments were conducted between passages 67 and 82. INS-1E cells were seeded at 200'000 to 300'000 cells/MEA with a complete medium containing 11 mM of glucose and were maintained at 37°C and 95 % O2 in an incubator for 5-7 days. The medium was replaced 24 to 48 h before recordings by a medium containing 5.5 mM of glucose. Fig. 5.10 presents the schematic data flow for the measurements. The MEA-SG from the dry simulating wet measurement is substituted by the cell culture and the MEA200-30 from MCS (diameter 30µm; inter-electrode distance is 200µm). The recordings (Fig.11) show the spontaneous activity (without external stimuli) of the cells in a hyperglycemic medium (15 mM).

Table 5.3 summarizes the detector's configuration for the measurements presented in the previous sections (Fig. 5.07, 5.09, and 5.11): positive or negative detection (SD, – SD), the factor N, and the time constant of the low pass filter in the adaptation block.

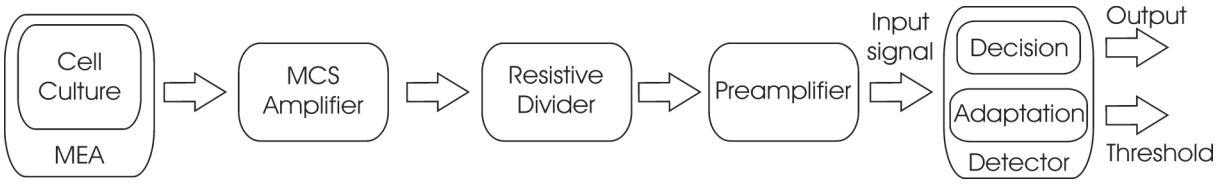

Figure 5.10. Schematic of the experiment for wet measurements. The experiment set-up is identical to Fig. 5.08 except that the inputs that are real biological signals.

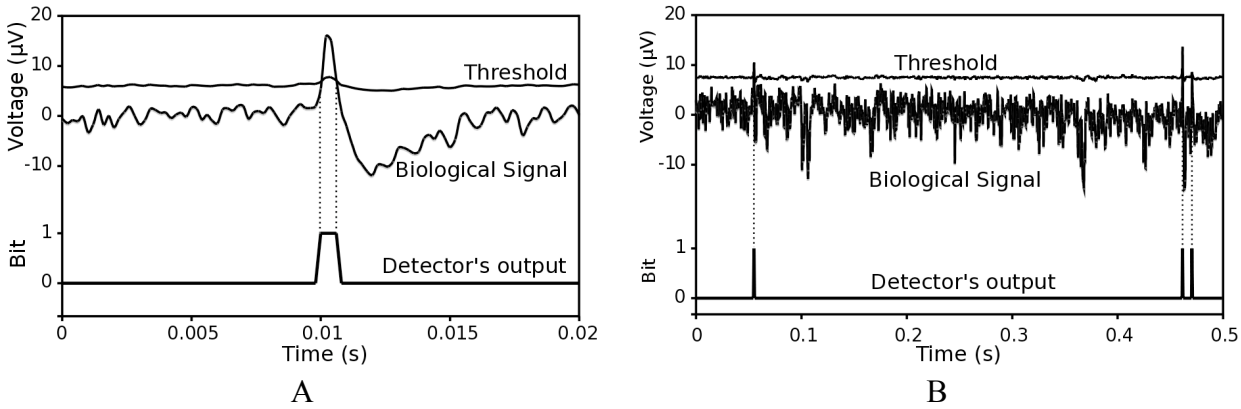

Figure 5.11. Recordings of pancreatic ß-cell activity in a hyperglycemic (15 mM) medium. In the above graphs, the voltage axis is the output signal divided by the gain of each chain. Therefore, both signals are shown at a level equivalent to the one at the amplifier's input. A. A Zoom on the detection of a single spike. As the peak of the spike is above the threshold, the up output of the detector is activated. The noise energy of the signal is constant, and so is the threshold. B. Another recording with a larger recording window. The signal looks noisier, but this is due to the time window. The threshold is almost constant, as is the noise energy. In this case, if N were to be set to 5, the last spike would not be detected. The choice of N = 4 is well adapted for such a signal.

Table 5.3 Detector's settings for each series of measurements.

Figure	Detection	Factor N	Time Constant (ms)
7	Positive	5	1
9A	Negative	4	0.5
9B	Negative	3	0.3
11A	Positive	4	0.5
11B	Positive	3	0.5

For Fig. 5.07, the detector's low pass filter's Time Constant (TC) was chosen to have a higher value than in other measurements. This value is still the lowest value that allows the computation of the variations in such an input signal. Indeed, this figure shows the worst-case scenario for the adaptor. N is chosen to be high purely to show the variations. In Fig. 5.09, N has an arbitrary value. In Fig. 5.09.B, the TC is intentionally lower than in the other cases to present a visible threshold variation. Of course, if this behavior were unpleasant, the chosen TC would be as high as others. Fig. 5.11 A presents arbitrary values. Fig. 5.11.B presents a low N and an up detection. It highlights two advantages. First, thanks to the tunability of N, the lower spike can be detected. Second, as the up threshold detects only half of the activity, this experiment illustrates the importance of the double detection, as the single up detection detects only half of the activity.

III. Discussion

The measurements we presented validate the functionality of the spike detector. It is easier to go deeper into its performances, if we consider separately: (a) the decision module, (b) the adaptation module, and (c) the detector usage.

A. The decision module

The comparator remains the critical element of the decision module. The lack of latches avoids any clocking and associated noise, which could compromise the quality of the whole pixel, as well as disturb the analog signal directly on the amplifier's output. The great disadvantage of a non-latched comparator is its reduced working frequency, which is not an issue in our application.

The input offset is the most sensitive characteristic for the comparator: any mismatch between the two inputs of the comparator can result in a wrong decision and induce detection errors. Even if a careful design can reduce the offset (Enz96), this problem concerns both analog and digital implementations. Actually, in digital devices, the offset problem does not occurs directly in the detector, but it is indirectly presented in the previous step, the analog to digital converter.

To really quantify this error, we need to analyze its equivalent input value. Our comparator has an input offset lower than 0.5 mVpp. As the signal presented at its input is amplified with a 300 gain (alpha preamplifier, from previous chapter), it results in a maximum equivalent input offset error of around 1 µV. Such an error is admissible, since it is much lower than the preamplifier's one.

B. Adaptation module

Regarding the adaptation module, one key point is the low pass filter. This module allows the user to define a time constant by choosing a capacitor. The particular case of a signal presenting both LFP and EAP is particularly interesting. Two points of view can be considered: first, the LFP signal (lower frequencies) can be considered as "noise" that disturbs the spike detection. In this case, the LFP can be subtracted from the global signal. In our system this is done by two elements. The first element is the preamplifier (previous chapter), which is able to filter the LFP low frequencies. The second is the adaptation block, which can adapt the threshold by following the LFP frequencies. The Figure 9B is a short example.

The second point of view concerns applications in which the LFP signal must be detected. Even if the detection principle remains the same for the LFP, such a signal is composed of lower frequencies and the meaningful signal is longer in time. Therefore, the bandwidth reduction is not as significant as it is in the case of spike detection. Our detector is not previewed for LFP. Such a detection as the data compression is insufficient and a low cutoff frequency would require more consumption in power and surface, which is not coherent with our initial specifications.

C. The Detector

We intend our detector to be as close as possible to the electrode and to be able to determine the timing of useful information. The spike detection enables the transmission of only

active data, discarding the inter-spike signal early in the processing chain. To illustrate quantitatively this, we propose two examples.

A neural signal has a maximum spiking rate of 100 Hz and its spike waveform covers around 2 ms per spike (Moxon00, Zviagintsev06). Considering these numbers, the data is useless for over 80 % of the time. For a high precision spike sorting, the use of this detector can reduce the amount of transmission by a factor of 5, simply by discarding useless data. In a more radical approach, (Fee96) found out that only about 0.5 ms would be necessary for spike sorting. If we consider this approximation, the useful information can be found 5 % of the time and our detector would reduce the signal bandwidth by a factor of 20.

We can also consider applications where only spike stamping is important, such as in AER (Address-Event Representation) neuromorphic devices (Indiveri06). In this particular case, the real-time transmitted event can be coded using only one bit.

We conclude that, even in extreme configurations, our detector can optimize systems with a large number of parallel channels in order to guarantee real-time performance.

More than the time performance, the tunable performance of our detector allows multiple experiments. The N parameter, which multiplies the standard deviation (SD) to determine the threshold, is an integer. If necessary, the circuit can be modified to compute rational multiples of SD (N*SD/K), by simply changing the Vduty to the equivalent of SD/K, and leaving N as an integer. In this case, the Vduty is used as a fine setting for the threshold computing.

We are also working on a procedure to define the optimal time constant depending on the application. Our goal is to propose a software interface listing a choice of cells (neuron, beta-cells, myocardium…) and of activities (spikes, EAP, LFP, burst + spikes) , and have the system automatically tune the time constant for the low pass filter by selecting one capacitor among a pre-implemented bank of capacitors.

Another alternative is to use the estimation of SD as the estimation of the instantaneous energy of the signal, by choosing a small time constant for the low pass filter.

CHAPTER 6
CONCLUSION

"An expert is a man who has made all the mistakes which can be made in a very narrow field."

Niels Bohr (1885-1962), Danish physicist.

We have essentially presented in this thesis two elements I designed. The first one is a real-time closed-loop hybrid system (or *Hynet*). The second one is a device that will improve the spatiotemporal performances in systems in charge of the acquisition of the biological electrical signal. Both are promising tools to help the evolution of bioelectronics systems, for investigations in biology or applications in medical science.

I. The Hynet

The *Hynet* carries out a bidirectional communication between a cell culture and an artificial system. The artificial system eventually mimics biological networks, using for example neuromimetic circuits as developed in our group (Renaud10), but such a configuration was not considered during this thesis. Communication in the *Hynet* is possible through multiple parallel channels, using the multielectrode interface. The transmission delay in the closed-loop is low enough to allow a 10 kHz sampling rate and still leave time for processing reaction stimuli, whilst ensuring real-time. The Graphical User Interface (GUI) provides a friendly and portable interface.

The *Hynet* system design is intended to be highly tunable. Different types of experiments are currently being conducted using the *Hynet*: we are investigating plasticity mechanisms in cortical neural networks (Bontorin07a), we are studying cultured neural networks exposed to electromagnetic waves (PEPS08), and we are exploring the dependence to glucose of the electrical activity of pancreatic beta-cells (Raoux10).

In studies on plasticity in neural networks, the role of the artificial part is to evaluate the relationship between the evolution of the network dynamics and a “consistent” feedback. By consistent feedback, we mean that the biological network is informed in real-time about the actual sensory consequences of its activity, just like an “unprogrammed” living organism embedded into the real world. In this “brain-in-a-box” paradigm, the biological brain is in communication with the “outside body”. Two essential features are necessary for the experimental set-up in this project: (i) real-time biological signal processing and real-time communication (already functional in *Hynet*); and (ii) feedback functions to drive a dissociated network to adapt its evoked responses to stimuli in a learning-like process. Thus, we can use the *Hynet* to invest bioinspired learning and plasticity functions at the network and at the cellular level.

The second series of experiments using the *Hynet* system aims to study the influence of electromagnetic fields on neural networks. Cultured cortical preparations are exposed to repetitive and controlled fields (using a custom exposition system in which an MEA is embedded) that reproduce Bluetooth or other GSM microwaves. For such an experiment, the artificial part (presently computed by software) is a network of conductance-based neurons. The *Hynet* helps us to investigate the evolution of activity and connectivity of biological cells, while the artificial neural network has inhibitory or excitatory actions to control or cancel this evolution. It may also be useful for investigating therapeutic usage of electromagnetic waves, although this is not its primary goal.

The third series of experiments, a study of electrical activity of beta-cells of the pancreas, could be useful in providing give a key to a better life for diabetics. The fundamental study on the behavior of such cells shows that the firing rate represents the glucose concentration and is modulated by agents such as the GLP–1 (Glucagon-like Peptide-1). This new model will help us to develop our understanding of the electrical code used by these cells to translate glucose/nutrient/hormone signals into precisely adapted secretion of insulin. A glucose sensor that reacts in real time, which is capable of taking hormones and other nutrients into account and of detecting hypo/hyperglycemia, represents an important need and challenge for life expectancy, life quality and medical costs of a growing number of diabetic.

Even though this system is operational and useful, it is of great interest to increase the number and the density of acquisition channels in order to increase the details of the information or simply for parallel computing performances. For example, we proposed in a recent project the development a screening device to measure on a single device and on multiple channels the insulin demand of pancreatic islets (by characterizing its electrical activity as shown in chapter 5 – Detector). We intend, however, to maintain the closed-loop real-time feature essentially for experiments that address the investigation of hybrid (living-artificial) neural networks.

Thus, we proposed, developed and tested the *Intelligent Pixel*.

II. The Intelligent Pixel

The spatiotemporal performances of the *Hynet* systems are limited by two factors: the commercial MEA performance and the software data processing of raw signals.

Considering spatial density, we proposed a new preamplifier, inspired by the Active Pixel Sensor (APS) approach. In this approach, the preamplifier is as close as possible to the sensor, which minimizes noise interference in connections and in wires; the preamplifier gain is high enough for the signal to be processed on-chip or to be multiplexed to the device outputs. Integration density is also a key feature for these multi-channel devices.

The integration of this new preamplifier into the previous system developed by the University of Neuchâtel (Imfeld08b) had the following advantages: it decreased the pitch of each electrode from 40 µm to 36 µm; it increased the gain (from 100 to 300); it reduced the power consumption per pixel (almost by a factor of 2, as the power supply voltage passes from 3.3 to 1.8 V); the noise figure is equivalent.

Considering timing performances the new detector presents a simple and integrated way to process an increasing amount of data while respecting real-time constraints. The detector discards "non-informative" signals for each electrode, which is the case 80 % of the time (Moxon00, Zviagintsev06). If we consider the approximation of (Fee96), useful information can be found 5 % of the time. The detector can therefore reduce the amount of transmitted data by a factor of 5 or even 20, without losing information on the spikes' occurrence.

Considering the closed-loop implementation (Bontorin07a), integrating the preamplifier and detector means that transmitted data is compressed from 12 bits (digital conversion of the analog signal) to 1 bit for each channel. If we combine this gain by the supposed factor of 5 on time compression, we can envisage a gain of 60 in terms of compared performance with commercial MEAs. In parallel, we showed that the delay to spike detection decreases from 25 µs for less than 1 µs. If we create a "spatiotemporal" index this new pixel would improve the first *Hynet* system by a factor of 1500.

The intelligent electrode was specifically designed to be tunable. The preamplifier low cut-off frequency can be tuned depending on the biological signal characteristics (LFP or EAP for example), as well as the detector parameters (N and Vduty), to define a compromise between false positive and negative detection errors. We can envisage the use of this *Intelligent Pixel* to characterize cells variability and behavior, either individually or in networks.

We expect the intensive use of intelligent MEAs to contribute to experiment databases. We are developing a software user interface to help the user (usually a biologist) to optimize the pixels' parameters for his own experiment by proposing predefined configurations adapted to classical experimental protocols: type of cell (neuron, beta-cells, myocar-

dium…) and of preparation (acute, culture), activity to be considered (EAP, LFP, …), requested confidence level for the detection, etc…

Finally, this co-supervised thesis project resulted in more than an association of the strong points of each participating research group: it resulted in a global improvement. The results for both teams and the perspective for future work are highly promising. Several thousands of *Intelligent Pixels* will compose the future Intelligent MultiElectrode Array (iMEA) while the use of a novel *Hynet* with *Intelligent Pixels* is part of different projects in the Bordeaux group. These developments contribute to the expansion of Bioelectronics as a specific research field, as discussed in our conclusion section.

Table 6.1 Review of major improvements provided to the research groups by this thesis project.

Characteristic	Place	Before	After
Hynet			
Closing Loop	FR	No	GUI
Active Pixel			
Pitch (µm)	SW	40	35
Gain (V/V)	SW	100	300
Power (µW)	SW	83	45
Technology	SW	CMOS 0.35 µm	CMOS 0.18 µm
	FR	Discrete	
Detection			
Computing	FR	Software	Hardware
	SW	Digital (FPGA)	Analog & Chip
	SW	Offline	Online
Delay (µs)	FR	25	< 1

III. Bioelectronics

"A Framework for Bioelectronics" (Walker09) describes the outline of Bioelectronics, its past success and future issues. Regarding history, we find:

"The study of biology also has been transformed by electronics. In the late 1940s and early 1950s, understanding the molecular basis of nerve and muscle function was achieved with the use of high-impedance amplifiers. Those studies led to a new era of quantitative biology and practical clinical neuroscience. The patch clamp, which allowed research-

ers to measure the ionic current through single ion channels gave further insight into nerve action. These studies led directly to three Nobel Prizes and ultimately seven more. The electron microscope is also an example of applying electronics to biological problems. First demonstrated in the 1930s and developed over the next decade, the electron microscope allowed scientists to visualize the miniscule world of cells at an entirely new level of detail. Much of modern cell biology is built on information captured from these indispensable tools."

And, further in the text, (Walker09) presents areas where electronics has a real impact:

"The nascent field of systems biology – using systems engineering approaches to analyze cellular function – is driving the development of new technology that can monitor multiple aspects of cellular behavior over many time points. Systems biology embodies a new perspective from which to view biological systems and knowledge culled from its approaches could lead to advances in medicine and security. However, significant investment is needed to develop tools and associated standards and metrology that can characterize and continuously monitor the states of cells at subcellular resolutions."

This thesis project was conducted in the same philosophy described in this "Framework for Bioelectronics". We provided the basis for enhanced MEA-based platforms, with real time capability to access complex biological networks in a closed loop. Relying on microelectronics advanced (but standardized) technologies, the iMEA will present strong spatio-temporal performances for the accomplishment of the goals of Bioelectronics.

Being confident in the future of Bioelectronics, our final expectation is that, during this century, neo-Galvanis will provide new electronics systems worldwide. They will present characteristics such as high density, large scale, real time, closed loop, and hybridation. These devices may be: neural stimulators, brain stimulators, cochlear prostheses, neuromuscular reanimates, brain machine interfaces, visual prostheses, diabetics health control systems, cognitive prostheses, memory expansion keys, and others we cannot even imagine yet. All these are coming soon.

REFERENCES

Ananth R.S. and Lee E.K. (2004). "*Design of a low-power, implantable electromyogram amplifier"*. Circuits and Systems, 2004. ISCAS '04. Proceedings of the 2004 International Symposium on, IV-9-12 Vol.14.

Ananth R.S., Lee E.K., Taihu L. and Lam A. (2006). "*Low-power, implantable sensing system for signal detection from the central or peripheral nervous system"*. Circuits and Systems, 2006. ISCAS 2006. Proceedings. 2006 IEEE International Symposium on, 4 pp.-2576.

Aziz J.N.Y. and Genov R. (2005). "*Multi-channel integrated neural interfaces for distributed electro-chemical sensing"*. Circuits and Systems, 2005. 48th Midwest Symposium on, 1782-1785 Vol. 1782.

Bakkum D.J., Shkolnik A.C., Ben-Ary G., Gamblen P., DeMarse T.B. and Potter S.M. (2004). "*Removing Some 'A' from AI: Embodied Cultured Networks"*.in: Embodied Artificial Intelligence**:** 629-629.

Bashashati A., Fatourechi M., Ward R.K. and Birch G.E. (2007). "*A survey of signal processing algorithms in brain–computer interfaces based on electrical brain signals*." Journal of Neural Engineering **4**(2).

Berdondini L., van der Wal P.D., Guenat O., de Rooij N.F., Koudelka-Hep M., Seitz P., Kaufmann R., Metzler P., Blanc N. and Rohr S. (2005). "*High-density electrode array for imaging in vitro electrophysiological activity*." Biosensors and Bioelectronics **21**(1): 167-174.

Berger T.W., Ahuja A., Courellis S.H., Deadwyler S.A., Erinjippurath G., Gerhardt G.A., Gholmieh G., Granacki J.J., Hampson R., Min Chi H., Lacoss J., Marmarelis V.Z., Nasiatka P., Srinivasan V., Dong S., Tanguay A.R. and Wills J. (2005). "*Restoring lost cognitive function*." Engineering in Medicine and Biology Magazine, IEEE **24**(5): 30-44.

BioMEA ref. (2009). *BioMEA - BioLogic Science Instruments*. Claix, France.

Blum R.A., Ross J.D., Brown E.A. and DeWeerth S.P. (2007). "*An Integrated System for Simultaneous, Multichannel Neuronal Stimulation and Recording*." Circuits and Systems I: Regular Papers, IEEE Transactions on **54**(12): 2608-2618.

Bontorin G. (2006). *Bioelectronics closed-loop for hybrid neural networks: towards a fully integrated approach*, Master thesis, University Bordeaux 1.

Bontorin G., Renaud S., Garenne A., Alvado L., Le Masson G. and Tomas J. (2007a). "*A Real-Time Closed-Loop Setup for Hybrid Neural Networks"*. Engineering in Medicine and Biology Society, 2007. EMBS 2007. 29th Annual International Conference of the IEEE, 3004-3007.

Bontorin G., Tomas J. and Renaud S. (2007b). "*Low noise and low cost neural amplifiers"*. Electronics, Circuits and Systems, 2007. ICECS 2007. 14th IEEE International Conference on, 1324-1327.

Bontorin G., Lopez C., Bornat Y., Lewis N., Renaud S., Garenne A. and Le Masson G. (2008). "*A real-time setup for multisite signal recording and processing in living neural networks"*. Circuits and Systems, 2008. ISCAS 2008. IEEE International Symposium on, 2953-2956.

Bontorin G., Garenne A., Tomas J., Lopez C., Morin F.O. and Renaud S. (2009). "*A real-time system for multisite stimulation on living neural networks"*.in: 2009 Joint Ieee North-East Workshop on Circuits and Systems and Taisa Conference**:** 137-140.

Bontorin G., Imfeld K., Raoux M. and Renaud S. (2010a). "*A low noise, low area, low cost preamplifier for large scale, high resolution Multielectrode Array (MEA).*" submitted to IEEE Transactions in Neural System and Rehabilitation Engineering.

Bontorin G., Robert C., Raoux M. and Renaud S. (2010b). "*Smart Integrated Pixel for high-density MEA systems. .*" submitted to Journal of Neural Engineering (IOP).

Bontorin G., Garenne A., Lopez C., Le Masson G. and Renaud S. (2010c). "*Hybrid Systems in Real-time Closed-loop*." submitted to Frontiers in Neuroengineering.

Bornat Y. (2006). *Réseaux de neurones sur silicium : une approche mixte, analogique / numérique, pour l'étude des phénomènes d'adaptation, d'apprentissage et de plasticité*, Université Bordeaux I.

Bornat Y., Raoux M., Boutaib Y., Morin F., Charpentier G., Lang J. and Renaud S. (2010). "*Detection of Electrical Activity of Pancreatic Beta-cells Using Micro-electrode Arrays"*. IEEE Computer Society Washington, DC, USA, 233-236.

Bottino E., Massobrio P., Martinoia S., Pruzzo G. and Valle M. (2009). "*Low-noise low-power CMOS preamplifier for multisite extracellular neuronal recordings*." Microelectronics Journal **40**(12): 1779-1787.

Burns A. (1991). "*Scheduling hard real-time systems: a review*." Softw. Eng. J. **6**(3): 116-128.

Carmena J.M., Lebedev M.A., Crist R.E., O'Doherty J.E., Santucci D.M., Dimitrov D.F., Patil P.G., Henriquez C.S. and Nicolelis M.A.L. (2003). "*Learning to Control a Brain-Machine Interface for Reaching and Grasping by Primates*." PLoS Biol **1**(2): e42.

Chan C.-H., Wills J., LaCoss J., Granacki J.J. and Choma J. (2007). "*A Novel Variable-Gain Micro-Power Band-Pass Auto-Zeroing CMOS Amplifier"*. Circuits and Systems, 2007. ISCAS 2007. IEEE International Symposium on, 337-340.

Chandran A.P., Najafi K. and Wise K.D. (1999). "*A new dc baseline stabilization scheme for neural recording microprobes"*. BMES/EMBS Conference, 1999. Proceedings of the First Joint, 386 vol.381.

Chao Z.C., Bakkum D.J., Wagenaar D.A. and Potter S.M. (2005). "*Effects of random external background stimulation on network synaptic stability after tetanization - A modeling study*." Neuroinformatics **3**(3): 263 - 280.

Chapin J.K., Moxon K.A., Markowitz R.S. and Nicolelis M.A.L. (1999). "*Real-time control of a robot arm using simultaneously recorded neurons in the motor cortex*." Nature Neuroscience **2**: 664 - 670.

Chay T.R. (1997). "*Effects of extracellular calcium on electrical bursting and intracellular and luminal calcium oscillations in insulin secreting pancreatic beta-cells*." Biophysical Journal **73**(3): 1673-1688.

Chiappalone M., Vato A., Tedesco M., Marcoli M., Davide F. and Martinoia S. (2003). "*Networks of neurons coupled to microelectrode arrays: a neuronal sensory system for pharmacological applications*." Biosensors and Bioelectronics **18**(5-6): 627-634.

Chiappalone M., Bove M., Vato A., Tedesco M. and Martinoia S. (2006). "*Dissociated cortical networks show spontaneously correlated activity patterns during in vitro development*." Brain Research **1093**(1): 41-53.

Chua-Chin W., Chi-Chun H., Jian-Sing L. and Kuan-Wen F. (2006). "*A 140-dB CMRR Low-noise Instrumentation Amplifier for Neural Signal Sensing"*. Circuits and Systems, 2006. APCCAS 2006. IEEE Asia Pacific Conference on, 696-699.

Dabrowski W., Grybos P. and Fiutowski T. (2004). "*Design for good matching in multichannel low-noise amplifier for recording neuronal signals in modern neuroscience experiments*." Microelectronics Reliability **44**(2): 351-361.

Demosthenous A. and Triantis I.F. (2005). "*An adaptive ENG amplifier for tripolar cuff electrodes*." Solid-State Circuits, IEEE Journal of **40**(2): 412-421.

Denison T., Consoer K., Santa W., Avestruz A.T., Cooley J. and Kelly A. (2007). "*A 2uW 100 nV/rtHz Chopper-Stabilized Instrumentation Amplifier for Chronic Measurement of Neural Field Potentials*." Solid-State Circuits, IEEE Journal of **42**(12): 2934-2945.

Donoho D.L. and Johnstone I.M. (1994). "*Ideal denoising in an orthonormal basis chosen from a library of bases"*. Technical Reports, Stanford University.

Enz C.C. and Temes G.C. (1996). "*Circuit techniques for reducing the effects of op-amp imperfections: autozeroing, correlated double sampling, and chopper stabilization*." Proceedings of the IEEE **84**(11): 1584-1614.

Eversmann B., Jenkner M., Hofmann F., Paulus C., Brederlow R., Holzapfl B., Fromherz P., Merz M., Brenner M., Schreiter M., Gabl R., Plehnert K., Steinhauser M., Eckstein G., Schmitt-Landsiedel D. and Thewes R. (2003). "*A 128 × 128 CMOS biosensor array for extracellular recording of neural activity*." Solid-State Circuits, IEEE Journal of **38**(12): 2306-2317.

Fee M.S., Mitra P.P. and Kleinfeld D. (1996). "*Variability of extracellular spike waveforms of cortical neurons*." Journal of Neurophysiology **76**(6): 3823-3833.

Focaccia M. and Simili R. (2007). "*Luigi Galvani, Physician, Surgeon, Physicist: From Animal Electricity to Electro-Physiology"*.in: Brain, Mind and Medicine: Essays in Eighteenth-Century Neuroscience**:** 145-158.

Fossum E.R. (1993). "*Active pixel sensors: are CCDs dinosaurs?"* Charge-Coupled Devices and Solid State Optical Sensors III, San Jose, CA, USA, SPIE, 2-14.

Garenne A., Maillard A., Alvado L., Tomas J., Bontorin G., Nagy F., Renaud S. and Le Masson G. (2010). "*A real-time closed-loop setup allowing sensory feedback driven learning strategies*." submitted.

Gargour C., Gabrea M., Ramachandran V. and Lina J.M. (2009). "*A short introduction to wavelets and their applications*." Circuits and Systems Magazine, IEEE **9**(2): 57-68.

Georgopoulos A.P., Schwartz A.B. and Kettner R.E. (1986). "*Neuronal population coding of movement direction*." Science **233**(4771): 1416-1419.

Gerstner W. and Kistler W.M. (2002). "*Spiking neuron models: Single neurons, populations, plasticity"*. Cambridge.

Gosselin B., Simard V. and Sawan M. (2003). "*Low power programmable front-end for a multichannel neural recording interface"*. Electrical and Computer Engineering, 2003. IEEE CCECE 2003. Canadian Conference on, 911-914 vol.912.

Gosselin B., Simard V. and Sawan M. (2004). "*An ultra low-power chopper stabilized front-end for multichannel cortical signals recording"*. Electrical and Computer Engineering, 2004. Canadian Conference on, 2259-2262 Vol.2254.

Gosselin B., Ayoub A.E. and Sawan M. (2006). "*A low-power bioamplifier with a new active DC rejection scheme"*. Circuits and Systems, 2006. ISCAS 2006. Proceedings. 2006 IEEE International Symposium on, 4 pp.-2188.

Gosselin B., Ayoub A.E. and Sawan M. (2007a). "*A Mixed-Signal Multi-Chip Neural Recording Interface with Bandwidth Reduction"*. Biomedical Circuits and Systems Conference, 2007. BIOCAS 2007. IEEE, 49-52.

Gosselin B., Sawan M. and Chapman C.A. (2007b). "*A Low-Power Integrated Bioamplifier With Active Low-Frequency Suppression*." Biomedical Circuits and Systems, IEEE Transactions on **1**(3): 184-192.

Gosselin B. and Sawan M. (2009). "*An Ultra Low-Power CMOS Automatic Action Potential Detector*." Neural Systems and Rehabilitation Engineering, IEEE Transactions on **17**(4): 346-353.

Grumet A.E., Wyatt J.L. and Rizzo J.F. (2000). "*Multi-electrode stimulation and recording in the isolated retina*." Journal of Neuroscience Methods **101**(1): 31-42.

Guenther E., Herrmann T. and Stett A. (2006). "*The Retinasensor: An In Vitro Tool to Study Drug Effects on Retinal Signaling"*.in: Advances in Network Electrophysiology**:** 321-331.

Haas A.M., Cohen M.H. and Abshire P.A. (2007). "*Real-time variance based template matching spike sorting system"*. Life Science Systems and Applications Workshop, 2007. LISA 2007. IEEE/NIH, 104-107.

Haidong G., Champion C.L., Rector D.M. and La Rue G.S. (2004). "*A low-power low-noise sensor IC"*. Microelectronics and Electron Devices, 2004 IEEE Workshop on, 60-63.

Harrison R.R. and Charles C. (2003a). "*A low-power low-noise CMOS amplifier for neural recording applications*." Solid-State Circuits, IEEE Journal of **38**(6): 958-965.

Harrison R.R. (2003b). "*A low-power integrated circuit for adaptive detection of action potentials in noisy signals"*. Engineering in Medicine and Biology Society, 2003. Proceedings of the 25th Annual International Conference of the IEEE, 3325-3328 Vol.3324.

Harrison R.R., Watkins P.T., Kier R.J., Lovejoy R.O., Black D.J., Greger B. and Solzbacher F. (2007a). "*A Low-Power Integrated Circuit for a Wireless 100-Electrode Neural Recording System*." Solid-State Circuits, IEEE Journal of **42**(1): 123-133.

Harrison R.R. (2007b). "*A Versatile Integrated Circuit for the Acquisition of Biopotentials"*. Custom Integrated Circuits Conference, 2007. CICC '07. IEEE, 115-122.

Harrison R.R. (2008). "*The Design of Integrated Circuits to Observe Brain Activity*." Proceedings of the IEEE **96**(7): 1203-1216.

Hassibi A., Navid R., Dutton R.W. and Lee T.H. (2004). "*Comprehensive study of noise processes in electrode electrolyte interfaces*." Journal of Applied Physics **96**(2): 1074-1082.

Hebb D.O. (1949). "*The Organization of Behavior: A Neuropsychological Theory"*. New York, Wiley.

Heer F., Franks W., Blau A., Taschini S., Ziegler C., Hierlemann A. and Baltes H. (2004). "*CMOS microelectrode array for the monitoring of electrogenic cells*." Biosensors and Bioelectronics **20**(2): 358-366.

Heer F., Hafizovic S., Franks W., Ugniwenko T., Blau A., Ziegler C. and Hierlemann A. (2005). "*CMOS microelectrode array for bidirectional interaction with neuronal networks"*. Solid-State Circuits Conference, 2005. ESSCIRC 2005. Proceedings of the 31st European, 335-338.

Henze D.A., Borhegyi Z., Csicsvari J., Mamiya A., Harris K.D. and Buzsaki G. (2000). "*Intracellular features predicted by extracellular recordings in the hippocampus in vivo*." J Neurophysiol **84**(1): 390-400.

Holleman J. and Otis B. (2007). "*A Sub-Microwatt Low-Noise Amplifier for Neural Recording"*. Engineering in Medicine and Biology Society, 2007. EMBS 2007. 29th Annual International Conference of the IEEE, 3930-3933.

Horiuchi T., Swindell T., Sander D. and Abshier P. (2004). "*A low-power CMOS neural amplifier with amplitude measurements for spike sorting"*. Circuits and Systems, 2004. ISCAS '04. Proceedings of the 2004 International Symposium on, IV-29-32 Vol.24.

Ide N., Andruska A., Boehler M., Wheeler B.C. and Brewer G.J. (2010). "*Chronic network stimulation enhances evoked action potentials*." Journal of Neural Engineering **7**(1).

Imfeld K., Maccione A., Gandolfo M., Martinoia S., Farine P.A., Koudelka-Hep M. and Berdondini L. (2008a). "*Real-time signal processing for high-density microelectrode array systems*." International Journal of Adaptive Control and Signal Processing **23**(11): 983-998.

Imfeld K., Neukom S., Maccione A., Bornat Y., Martinoia S., Farine P.A., Koudelka-Hep M. and Berdondini L. (2008b). "*Large-Scale, High-Resolution Data Acquisition System for Extracellular Recording of Electrophysiological Activity*." Biomedical Engineering, IEEE Transactions on **55**(8): 2064-2073.

Indiveri G., Chicca E. and Douglas R. (2006). "*A VLSI array of low-power spiking neurons and bistable synapses with spike-timing dependent plasticity*." IEEE Transactions on Neural Networks **17**(1): 211-221.

Irazabal J.-M. and Blozis S. (2003). *Application note AN10216-0: I2C Manual*, Philips Semiconductors Inc.

Irazoqui-Pastor P., Mody I. and Judy J.W. (2003). "*In-vivo EEG recording using a wireless implantable neural transceiver"*. Neural Engineering, 2003. Conference Proceedings. First International IEEE EMBS Conference on, 622-625.

Jimbo Y., Tateno T. and Robinson H.P.C. (1999). "*Simultaneous induction of pathway-specific potentiation and depression in networks of cortical neurons*." Biophys J **76**(2): 670 - 678.

Jimbo Y., Kasai N., Torimitsu K., Tateno T. and Robinson H.P.C. (2003). "*A system for MEA-based multisite stimulation*." Biomedical Engineering, IEEE Transactions on **50**(2): 241-248.

Jimmin C., Abidi A.A. and Viswanathan C.R. (1994). "*Flicker noise in CMOS transistors from subthreshold to strong inversion at various temperatures*." Electron Devices, IEEE Transactions on **41**(11): 1965-1971.

Jochum T. and Wolf P. (2006). "*An integrated neural amplifier with positive-gain input configuration"*. BMES Ann.Fall Meet., Chicago, 335.

Jochum T., Denison T. and Wolf P. (2009). "*Integrated circuit amplifiers for multi-electrode intracortical recording*." Journal of Neural Engineering **6**(1).

Joseph M. and Goswami A. (1988). "*What's 'real' about real-time systems?"* Real-Time Systems Symposium, 1988., Proceedings., 78-85.

Jung R., Brauer E.J. and Abbas J.J. (2001). "*Real-time interaction between a neuromorphic electronic circuit and the spinal cord*." Neural Systems and Rehabilitation Engineering, IEEE Transactions on **9**(3): 319-326.

Kaiser J.F. (1990). "*On a simple algorithm to calculate the 'energy' of a signal"*. Acoustics, Speech, and Signal Processing, 1990. ICASSP-90., 1990 International Conference on, 381-384 vol.381.

Lee E.K.F., Matei E., Lam A. and Taihu L. (2006). "*A 1V 420uW 32-channel Cortical Signal Interface"*. Custom Integrated Circuits Conference, 2006. CICC '06. IEEE, 277-280.

Lewicki M.S. (1998). "*A review of methods for spike sorting: the detection and classification of neural action potentials*." Network: Computation in Neural Systems **9**(4): R53-R78.

Loeb G.E., Peck R.A., Moore W.H. and Hood K. (2001). "*BION(TM) system for distributed neural prosthetic interfaces*." Medical Engineering & Physics **23**(1): 9-18.

Loeb G.E. (2003). "*Cochlear Prosthetics*." Annual Review of Neuroscience **13**(1): 357-371.

Lu C., Stankovic J.A., Son S.H. and Tao G. (2002). "*Feedback Control Real-Time Scheduling: Framework, Modeling, and Algorithms**." Real-Time Systems **23**(1): 85-126.

Masson G.L., Renaud S., Debay D. and Bal T. (2002). "*Feedback inhibition controls spike transfer in hybrid thalamic circuits*." Nature **417**: 854-858.

Matthews E.K. and Sakamoto Y. (1975). "*Electrical characteristics of pancreatic islet cells*." The Journal of Physiology **246**(2): 421-437.

MEA System User Manual ref. (2006). *MEA System User Manual*. MultiChannel Systems. Reutlingen, Germany.

MEA-Signal Generator ref. (2008). *MEA - Signal Generator*. MultiChannel Systems. Reutlingen, Germany.

Merglen A., Theander S., Rubi B., Chaffard G., Wollheim C.B. and Maechler P. (2004). "*Glucose Sensitivity and Metabolism-Secretion Coupling Studied during Two-Year Continuous Culture in INS-1E Insulinoma Cells*." Endocrinology **145**(2): 667-678.

Merrill D.R., Bikson M. and Jefferys J.G.R. (2005). "*Electrical stimulation of excitable tissue: design of efficacious and safe protocols*." Journal of Neuroscience Methods **141**(2): 171-198.

Ming Y. and Ghovanloo M. (2007). "*A Low-Noise Preamplifier with Adjustable Gain and Bandwidth for Biopotential Recording Applications"*. Circuits and Systems, 2007. ISCAS 2007. IEEE International Symposium on, 321-324.

Mohseni P. and Najafi K. (2004). "*A fully integrated neural recording amplifier with DC input stabilization*." Biomedical Engineering, IEEE Transactions on **51**(5): 832-837.

Mojarradi M., Binkley D., Blalock B., Andersen R., Ulshoefer N., Johnson T. and Del Castillo L. (2003). "*A miniaturized neuroprosthesis suitable for implantation into the brain*." Neural Systems and Rehabilitation Engineering, IEEE Transactions on **11**(1): 38-42.

Moo Sung C., Wentai L. and Sivaprakasam M. (2008). "*Design Optimization for Integrated Neural Recording Systems*." Solid-State Circuits, IEEE Journal of **43**(9): 1931-1939.

Moo Sung C., Zhi Y., Yuce M.R., Linh H. and Liu W. (2009). "*A 128-Channel 6 mW Wireless Neural Recording IC With Spike Feature Extraction and UWB Transmitter*." Neural Systems and Rehabilitation Engineering, IEEE Transactions on **17**(4): 312-321.

Morin F.O., Takamura Y. and Tamiya E. (2005). "*Investigating neuronal activity with planar microelectrode arrays: achievements and new perspectives*." J Biosci Bioeng **100**: 131 - 143.

Mortimer J.T. and Bhadra N. (2004). "*Peripheral Nerve and Muscle Stimulation"*.in: Neuroprosthetics: Theory and Practice. Kenneth W Horch and G.S. Dhillon, World Scientific.

Moxon K.A., Morizio J., Chapin J.K., Nicolelis M.A. and Wolf P. (2000). "*Designing a brain-machine interface for neuroprosthetic control"*.in: Neural Prostheses for Restoration of Sensory and Motor Function. J.K. Chapin and K.A. Moxon, Boca Raton, FL: CRC Press**:** 179-220.

Nenadic Z. and Burdick J.W. (2005). "*Spike detection using the continuous wavelet transform*." Biomedical Engineering, IEEE Transactions on **52**(1): 74-87.

Nicolelis M.A.L. (2001). "*Actions from thoughts*." Nature **409**(6818): 403-407.

Nicolelis M.A.L. and Lebedev M.A. (2009). "*Principles of neural ensemble physiology underlying the operation of brain-machine interfaces*." Nat Rev Neurosci **10**(7): 530-540.

Nielsen J.H. and Bruun E. (2004). "*A CMOS Low-Noise Instrumentation Amplifier Using Chopper Modulation*." Analog Integrated Circuits and Signal Processing **42**(1): 65-76.

Novellino A., Angelo P.D., Cozzi L., Chiappalone M., Sanguineti V. and Martinoia S. (2007). "*Connecting neurons to a mobile robot: an in vitro bidirectional neural interface*." Intell. Neuroscience **2007**: 2-2.

Nowotny T., Zhigulin V.P., Selverston A.I., Abarbanel H.D.I. and Rabinovich M.I. (2003). "*Enhancement of Synchronization in a Hybrid Neural Circuit by Spike-Timing Dependent Plasticity*." J. Neurosci. **23**(30): 9776-9785.

Nsanze F. (2005). *ICT Implants in the Human Body - A Review*. The European Group on Ethics in Science and New Technologies to the European Commission.

Obeid I., Morizio J.C., Moxon K.A., Nicolelis M.A.L. and Wolf P.D. (2003). "*Two multichannel integrated circuits for neural recording and signal processing*." Biomedical Engineering, IEEE Transactions on **50**(2): 255-258.

Obeid I. and Wolf P.D. (2004). "*Evaluation of spike-detection algorithms fora brain-machine interface application*." Biomedical Engineering, IEEE Transactions on **51**(6): 905-911.

Okada K., Onodera H. and Tamaru K. (2000). "*Layout Dependent Matching Analysis of CMOS Circuits*." Analog Integrated Circuits and Signal Processing **25**(3): 309-318.

Olsson R.H., III, Gulari M.N. and Wise K.D. (2002). "*Silicon neural recording arrays with on-chip electronics for in-vivo data acquisition"*. Microtechnologies in Medicine & Biology 2nd Annual International IEEE-EMB Special Topic Conference on, 237-240.

Olsson R.H., III and Wise K.D. (2005). "*A three-dimensional neural recording microsystem with implantable data compression circuitry*." Solid-State Circuits, IEEE Journal of **40**(12): 2796-2804.

Oprisan S.A., Prinz A.A. and Canavier C.C. (2004). "*Phase Resetting and Phase Locking in Hybrid Circuits of One Model and One Biological Neuron*." Biophysical Journal **87**(4): 2283-2298.

Ott H.W. (1988). "*Noise reduction techniques in electronic systems"*. New York, Wiley.

Oweiss K.G., Mason A., Suhail Y., Kamboh A.M. and Thomson K.E. (2007). "*A scalable wavelet transform VLSI architecture for real-time signal processing in high-density intra-cortical implants*." IEEE Transactions on Circuits and Systems I: Regular Papers **54**(6): 1266-1278.

Palmisano G., Palumbo G. and Pennisi S. (2001). "*Design Procedure for Two-Stage CMOS Transconductance Operational Amplifiers: A Tutorial*." Analog Integrated Circuits and Signal Processing **27**(3): 177-187.

Palti Y., David G.B., Lachov E., Mida Y.H. and Schatzberger R. (1996). "*Islets of Langerhans generate wavelike electric activity modulated by glucose concentration*." Diabetes **45**(5): 595-601.

Parthasarathy J., Erdman A.G., Redish A.D. and Ziaie B. (2006). "*An Integrated CMOS Bio-potential Amplifier with a Feed-Forward DC Cancellation Topology"*. Engineering in Medicine and Biology Society, 2006. EMBS '06. 28th Annual International Conference of the IEEE, 2974-2977.

Patterson W.R., Yoon-Kyu S., Bull C.W., Ozden I., Deangellis A.P., Lay C., McKay J.L., Nurmikko A.V., Donoghue J.D. and Connors B.W. (2004). "*A microelectrode/microelectronic hybrid device for brain implantable neuroprosthesis applications*." Biomedical Engineering, IEEE Transactions on **51**(10): 1845-1853.

Peps (2008). "*Electrophysiologie de cultures neuronales exposées aux micro-ondes*." Groupe Bioélectronique - Laboratoire IMS.

Perelman Y. and Ginosar R. (2005). "*An Integrated System for Multichannel Neuronal Recording with Spike / LFP Separation and Digital Output"*. Neural Engineering, 2005. Conference Proceedings. 2nd International IEEE EMBS Conference on, 377-380.

Pine J. (1980). "*Recording action potentials from cultured neurons with extracellular microcircuit electrodes.*" J Neurosci Methods **2**(1): 19-31.

Pine J. (2006). "*A History of MEA Development"*.in: Advances in Network Electrophysiology**:** 3-23.

Potter S.M. and DeMarse T.B. (2001). "*A new approach to neural cell culture for long-term studies*." Journal of Neuroscience Methods **110**(1-2): 17-24.

Potter S.M., Wagenaar D. and DeMarse T. (2006). "*Closing the Loop: Stimulation Feedback Systems for Embodied MEA Cultures"*.in: Advances in Network Electrophysiology**:** 215-242.

Puchalla J.L., Schneidman E., Harris R.A. and Berry M.J. (2005). "*Redundancy in the Population Code of the Retina*." Neuron **46**(3): 493-504.

Raoux M., Bontorin G., Bornat Y., Lang J. and Renaud S. (2010). "*Bioelectronic sensing of insulin demand"*.in: Biohybrid Systems. R. Jung. Weinheim, Wiley-Vch, to be published.

Reger B.D., Fleming K.M., Sanguineti V., Alford S. and Mussa-Ivaldi F.A. (2000). "*Connecting Brains to Robots: The Development of a Hybrid System for the Study of Learning in Neural Tissues"*. Proc. of the VIIth Intl. Conf. on Artificial Life, Springer-Verlag, 263-272.

Renaud S., Tomas J., Lewis N., Bornat Y., Daouzli A., Rudolph M., Destexhe A. and Saighi S. (2010). "*PAX : A Mixed Hardware/Software Simulation Platform for Spiking to be published on Neural Networks*." Neural Networks: to be published.

Rieger R., Taylor J., Demosthenous A., Donaldson N. and Langlois P.J. (2003). "*Design of a low-noise preamplifier for nerve cuff electrode recording*." Solid-State Circuits, IEEE Journal of **38**(8): 1373-1379.

Rivera F. and Herve T. (2002). "*Extracellular electrical activity recording of pancreatic islet"*. Microtechnologies in Medicine & Biology 2nd Annual International IEEE-EMB Special Topic Conference on, 490-495.

Robert J.C. (2009). "*Deep Brain Stimulation Devices: A Brief Technical History and Review*." Artificial Organs **33**(3): 208-220.

Robinson D.A. (1968). "*The electrical properties of metal microelectrodes*." Proceedings of the IEEE **56**(6): 1065-1071.

Rogers C.L., Harris J.G., Principe J.C. and Sanchez J.C. (2005). "*An analog VLSI implementation of a multi-scale spike detection algorithm for extracellular neural recordings"*. Neural Engineering, 2005. Conference Proceedings. 2nd International IEEE EMBS Conference on, 213-216.

Rohr S. (2004). *Role of gap junctions in the propagation of the cardiac action potential*, Oxford University Press.

Sacristan-Riquelme J. and Osés M.T. (2007). "*Implantable stimulator and recording device for artificial prosthesis control*." Microelectronics Journal **38**(12): 1135-1149.

Saighi S. (2004). *Circuits et Systèmes de Modélisation Analogique de Réseaux de Neurones Biologiques : Application au Développement d'outils pour les Neurosciences Computationnelles*, Université Bordeaux I.

Samsukha P. and Garverick S.L. (2007). "*A Monolithic Bandpass Amplifier for Neural Signal Processing with 25-Hz Low-Frequency Cutoff"*. Custom Integrated Circuits Conference, 2007. CICC '07. IEEE, 177-180.

Shannon C.E. (1949). "*Communication in the Presence of Noise*." Proceedings of the IRE **37**(1): 10-21.

Sodagar A.M., Wise K.D. and Najafi K. (2007). "*A Fully Integrated Mixed-Signal Neural Processor for Implantable Multichannel Cortical Recording*." Biomedical Engineering, IEEE Transactions on **54**(6): 1075-1088.

Stegenga J., Feber le J., Marani E. and Rutten W.L.C. (2009). "*The Effect of Learning on Bursting*." IEEE Transactions on Biomedical Engineering **56**(4): 1220-1227.

Stett A., Egert U., Guenther E., Hofmann F., Meyer T., Nisch W. and Haemmerle H. (2003). "*Biological application of microelectrode arrays in drug discovery and basic research*." Analytical and Bioanalytical Chemistry **377**(3): 486-495.

Steyaert M.S.J. and Sansen W.M.C. (1990). "*Power supply rejection ratio in operational transconductance amplifiers*." Circuits and Systems, IEEE Transactions on **37**(9): 1077-1084.

Streit J., Tscherter A. and Darbon P. (2006a). "*Rhythm generation in spinal cultures: Is it the neuron or the network?"*in: Advances in network electrophysiology using multi electrode arrays. M. Taketani and M. Baudry, Springer**:** 377-408.

Streit J., Tscherter A. and Darbon P. (2006b). "*Rhythm Generation in Spinal Cultures: Is It the Neuron or the Network?"*in: Advances in Network Electrophysiology**:** 377-408.

Thakur P.H., Lu H., Hsiao S.S. and Johnson K.O. (2007). "*Automated optimal detection and classification of neural action potentials in extra-cellular recordings*." Journal of Neuroscience Methods **162**(1-2): 364-376.

Thomas C.A., Springer P.A., Loeb G.E., Berwald-Netter Y. and Okun L.M. (1972). "*A miniature microelectrode array to monitor the bioelectric activity of cultured cells*." Experimental Cell Research **74**(1): 61-66.

Uranga A., Navarro X. and Barniol N. (2004). "*Integrated CMOS amplifier for ENG signal recording*." Biomedical Engineering, IEEE Transactions on **51**(12): 2188-2194.

Wagenaar D.A., Pine J. and Potter S.M. (2004). "*Effective parameters for stimulation of dissociated cultures using multi-electrode arrays*." Journal of Neuroscience Methods **138**(1-2): 27-37.

Wagenaar D.A., Pine J. and Potter S. (2006a). "*Searching for plasticity in dissociated cortical cultures on multi-electrode arrays*." Journal of Negative Results in BioMedicine **5**(1): 16.

Wagenaar D.A., Pine J. and Potter S. (2006b). "*An extremely rich repertoire of bursting patterns during the development of cortical cultures*." BMC Neuroscience **7**(1): 11.

Walden R.H. (1999). "*Analog-to-digital converter survey and analysis*." Selected Areas in Communications, IEEE Journal on **17**(4): 539-550.

Walker G.M., Ramsey J.M., Cavin III R.K., Herr D.J.C., Merzbacher C.I. and Zhirnov V. (2009). *A Framework for Bioelectronics: Discovery and Innovation*. The National Institute of Standards and Technology (NIST).

Weiland J.D. and Humayun M.S. (2005). "*A biomimetic retinal stimulating array*." Engineering in Medicine and Biology Magazine, IEEE **24**(5): 14-21.

Wenshan Z., Yichuang S., Xi Z. and Yigang H. (2009). "*A multiple loop feedback Gm-C bandpass filter for wavelet transform implementation"*. Circuits and Systems, 2009. MWSCAS '09. 52nd IEEE International Midwest Symposium on, 106-109.

Wey H.M. and Guggenbuhl W. (1990). "*An improved correlated double sampling circuit for low noise charge coupled devices*." Circuits and Systems, IEEE Transactions on **37**(12): 1559-1565.

Whittington R.H., Giovangrandi L. and Kovacs G.T.A. (2005). "*A closed-loop electrical stimulation system for cardiac cell cultures*." Biomedical Engineering, IEEE Transactions on **52**(7): 1261-1270.

Willemin M., Blanc N., Lang G.K., Lauxtermann S., Schwider P., Seitz P. and W‰ny M. (2001). "*Optical characterization methods for solid-state image sensors*." Optics and Lasers in Engineering **36**(2): 185-194.

Wise K.D. and Angell J.B. (1975). "*A Low-Capacitance Multielectrode Probe for Use in Extracellular Neurophysiology*." Biomedical Engineering, IEEE Transactions on **BME-22**(3): 212-219.

Wood F., Black M.J., Vargas-Irwin C., Fellows M. and Donoghue J.P. (2004). "*On the variability of manual spike sorting*." Biomedical Engineering, IEEE Transactions on **51**(6): 912-918.

Zumsteg Z.S., Kemere C., O'Driscoll S., Santhanam G., Ahmed R.E., Shenoy K.V. and Meng T.H. (2005). "*Power feasibility of implantable digital spike sorting circuits for neural prosthetic systems*." Neural Systems and Rehabilitation Engineering, IEEE Transactions on **13**(3): 272-279.

Zviagintsev A., Perelman Y. and Ginosar R. (2006). "*Algorithms and architectures for low power spike detection and alignment*." Journal of Neural Engineering **3**: 35-42.

APPENDIXES

"- Do you think he is still alive?

- Of course, my son. None, no one in the entire world, could ham the joker."

Jostein Gaarder (1952 –), Norwegian writer.

In "The Solitaire Mystery".

I. The first generations of preamplifiers

The work presented in chapter 4 (Preamplifier) is the last generation of preamplifiers I have designed. In this appendix, I present a copy of an article describing the first generation. The work presented is, of course, strongly based on this first generation. These results are put apart only to clarity the presentation.

Low noise and low cost neural amplifiers

Guilherme Bontorin, *Student Member IEEE,* Jean Tomas, and Sylvie Renaud
Neuromorphic Systems Engineering
IMS laboratory – ENSEIRB – University of Bordeaux 1
Bordeaux – France
guilherme.bontorin@ims-bordeaux.fr

***Abstract*—Extracellular neural signal acquisition requires low noise, high gain, low power, and low cost amplifiers. This paper presents amplifiers with a simple architecture that ensures a good compromise among these characteristics. We present three amplifiers based on the same architecture, in which the first stage is a differential pair, respectively based on HBT, NMOS or PMOS transistors. The HBT-based solution presents the lowest intrinsic noise, followed by the NMOS solution. We use Monte Carlo simulation to validate the robustness of amplifiers' characteristics of technological dispersions.**

I. Introduction

Biomedical applications imply specific constraints on the design of electronic circuits. For integrated circuits, these constraints are not always in phase with the design rules in standard signal processing applications. We focus in this paper on emerging applications that necessitate the real-time acquisition of individual neurons' electrical activity. We can mention among these applications the insulin control relying on beta-cells activity [1], the brain-machine interfaces [2], or the closed-loop systems for hybrid (living-artificial) neural networks [3-6].

All these applications use arrays of extracellular electrodes integrated on discrete probes or on chips. The advantages of this kind of interface, compared to the intracellular electrode solution, are make easier the multisite access and increase the living cells' lifetime. But using extracellular electrodes also implies dealing with two issues: the low amplitude of acquired neural signal (10-100µV) and its high noise level (millivolts at low frequencies). A low noise, high gain, and filtering electronic amplifier is then necessary to process each signal. But, a low consumption and a small silicon area are also crucial constraints. With such an amplifier, a system will be able to process in parallel many neural channels, either when the density of electrodes is high or when their arrangement is complex. Fig. 1.a. presents the architecture such a system organized in a closed-loop where living neurons in *in vitro* cultures communicate in real-time with an artificial unit, through an electronic interface. In Fig. 1.b., we identify the amplifying electronics on the acquisition channels.

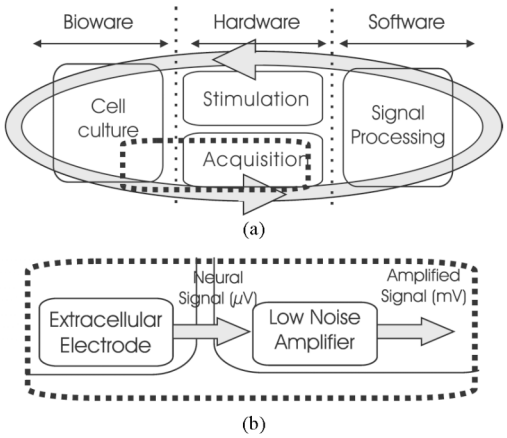

Figure 1. (a) A hybrid (living-artificial) closed-loop system, like in [3-6] (b) The low noise amplifier localisation in a such system.

This paper compares the characteristics of three "neural" amplifiers designed for processing neural signals. The amplifiers differ by their first stage based on a differential pair of: HBTs, NMOS transistors, PMOS transistors. Section II details the design of architecture and the resulting schematic chosen to optimize the performances. Section III shows the simulation results and performances of three configurations.

II. Amplifier Design

In neural amplifiers, the classical compromise in IC design between performances and cost becomes a key issue. Table I summarizes information on neural amplifiers described in the literature. Optimized component consumption and silicon area will limit the global cost (for fabrication and use). The technological process is also taken into account: choosing a BiCMOS process increases the fabrication cost. Performance features mentioned here are the equivalent input noise and the intrinsic gain; but the cutoff frequency, the slew rate, and the rejection of power supply noise are also important and will be specified in the presentation of our amplifiers.

This work was supported by Égide and the French Minister of Foreign Affairs.

TABLE I. SOME NEURAL AMPLIFIERS

Ref.	Gain (dB)	Noise[a] (µVrms)	Consumption (W)	Area (mm²)
[7]	36	9	98µ	0.35
[8]	38.9	9.2	68µ	0.177
[9]	39.3	7.8	115µ	0.107
[10]	40	15	330µ	0.076[b]
[11][c]	40	0.3	1.3m	0.3
[12]	40	2.2	80µ	0.16
[13]	51	3	775µ	0.52
[14]	60	3	1.7m	0.35
[15]	61	0.8	20m	Discrete
[16]	60 – 80	3.1	3m	-
[17]	70 – 94	1	130m	Discrete

a. Input equivalent noise, in the bandwidth between 100 Hz and 10 kHz.

b. Without the feedback circuit.

c. BiCMOS technology.

The neural amplifiers are intended to be part of a highly integrated closed-loop hybrid system [4], which simplified schematic is shown in Fig. 1. In such a system, extracellular electrodes are integrated on a Multi-Electrode Array (MEA) device [18], on which are placed cell cultures (dissociated cultures of rat embryonic cells). It processes in parallel 60 acquisition and stimulation channels. The amplifiers are optimized to be integrated as close as possible to the MEA, to limit external noise injection. We plan for a short term prospective to integrate the amplifiers directly on the MEA die. Their design considerations are:

A. *Gain and intrinsic noise*

These two factors are linked by the Friis formula, as expressed below:

$$F = F_1 + \frac{F_2 - 1}{G_1} + \ldots + \frac{F_m - 1}{\prod_{i=1}^{m-1} G_i}, \xrightarrow{G_1 \to +\infty} F = F_1 \qquad (1)$$

Where F_n and G_n are the noise factor and the gain of n^{th} stage.

A high first stage gain (G_1) reduces the influences of other stages. As observed in the literature, two solutions exist for setting the amplifier gain: in systems where the signal processing functions and the neural amplifier are embedded on the same die [7-13], G_1 is around 40 dB; in systems where the signal post-processing is separated from the amplification, G_1 is fixed around 60 dB or even higher [14-17]. We chose the second solution, which is less selective, in order to have the possibility to choose whether to integrate the post-processing functions together with the amplifiers or not.

Due to the biophysical specificities of neural activity, the information is contained in the range [100 Hz; 10 kHz]; experiments showed also that first order cut-off frequencies are efficient enough to discriminate this band width [7-17]. We implement a first order band-pass filter between 100 Hz and 10 kHz to eliminate the high level noise (some millivolts) existing at low frequencies and the environment noise at high frequencies. With this filter, the neuron activity (spike) can be discerned from noise, in an extracellular acquisition [19].

For our application, we fix the polarization of first and the second stages to, respectively, 10 µA and 5 µA. Each amplifier active area is limited to 1000 µm2; this constraint is imposed by the BiCMOS configuration die area.

B. *Operating frequencies and slew rate*

These two characteristics are secondary in our application. First, the signal's bandwidth is quite low, as explained in II.A. Second, the amplifier load is the post-processing unit and is custom designed. It is so well-controlled and has high input impedance. At this point, the costs limitations are privileged, in two ways: (a) the classical third stage, with high current gain, is not implemented. This case is well explained in [20]; (b) the Miller capacitor is used both: for setting the high cutoff frequency (about 10 kHz) and for the classical phase compensation. The resulting phase margins for the three amplifiers are around 45 degrees.

C. *Power supply noise*

Another important noise source in an amplifier is the power supply noise. We test three alternatives for the first stage: (a) a cascoded first stage [21], (b) a passive equilibrated load for the first stage, and (c) a classical simple differential pair with active load. The additional area and consumption costs to achieve (a) and (b) are prohibitive. The classical architecture (c) provides a good compromise between performance and cost, and is finally chosen.

D. *Neural amplifier schematic*

The schematic resulting from the technical choices described in the previous paragraphs is shown in Fig. 2, in the HBT configuration. It includes two stages; the first stage is based on a simple differential amplifier of HBTs, NMOS or PMOS transistors with an active load; the second is a common source with an active load. The Miller phase compensation circuit provides the high cutoff frequency and a good stability.

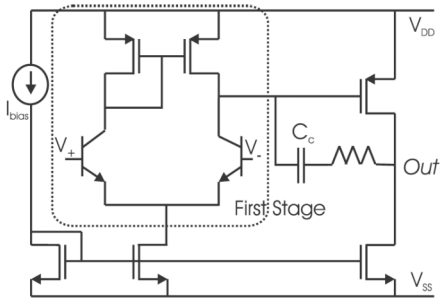

Figure 2. The HBT based amplifier's architecture

III. RESULTS AND DISCUSSION

A. *Amplifiers active part*

The three configurations of amplifier are designed to fit the application's constraints. The chosen technology is the 0.35µm HBT-BiCMOS technology from *austriamicrosys-*

tems™, and the design and simulation tools are from the *Cadence*™ suite. Table II summarizes the performances of HBT, NMOS and PMOS versions, simulated in open-loop. To estimate the effects of mismatch and process variations, we run Monte Carlo simulations.

A first statement from Table II is that the HBT-based amplifier presents the best noise figure. This result was expected, as the bipolar transistor is based on a volume current displacement, while the MOS transistors has a current displacement predominant in surface [22]. This good result is compensated by the high fabrication cost of a BiCMOS process compared to a CMOS process.

Analyzing the differences between two others solutions, the preconception that PMOS differential pairs are better in noise than NMOS ones falls down. This affirmation is based on the comparison between NMOS and PMOS transistors with an identical transconductance (g_m). Some well-known and efficient methods to design amplifiers (e.g. [20]) are based on the evaluation of g_m necessary to reach predetermined performance (equivalent noise, slew rate …). For an equivalent g_m, a PMOS transistor occupies a largest silicon area than a NMOS transistor (for the selected process the electron and the hole mobility are, respectively, 370 and 126 cm²/V.s). As a larger area goes together with a smaller charge carry density, and as the noise level increases with the carry density, a PMOS-based amplifier presents a lower noise characteristic than the NMOS-based (for an equivalent g_m).

However, as our comparison rule is to keep constant the area and the consumption (see II.A), and not g_m, our conclusion is different. With the same biasing and area, the NMOS-based amplifier presents a higher g_m. As the carry density is lower in the NMOS-based amplifier, the noise figure is better.

Considering the power supply noise rejection, the three amplifiers present equivalent characteristics. The transfer function shows a maximal gain value under 0.4. In the signal bandwidth, it is reduced to 0.2 at worst (Fig. 3).

To summarize, the best noise and gain figures are obtained with the HBT-based amplifier. When considering also the fabrication cost, a NMOS-based amplifier implemented using a simple CMOS technology is also a solution. Finally, the power supply noise rejection is strongly linked to the architecture, and is not a discriminatory criterion.

TABLE II. PERFORMANCES OF THREE VERSIONS OF NEURAL AMPLIFIER

Config.	Gain[a] (dB)	Noise[a,b](µVRMS)	Ft(MHz)
HBT	110±1	1.65±0.05	15
NMOS	98±1	3.8±0.1	11
PMOS	95±1	4.5±0.1	10

a. Gain and Noise are shown as (mean ± standard deviation), obtained from a 400-trial Monte Carlo simulation, considering mismatch and fabrication variations.

b. Input equivalent noise, in the bandwidth [100Hz; 10 kHz].

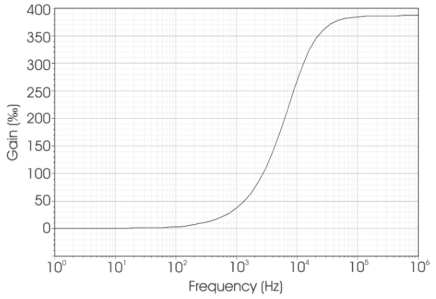

Figure 3. Power supply noise rejection

B. *Amplifier with filter*

We consider now the circuit including the filtering circuitry (Fig. 4). The feedback resistance R2 sets the gain and with the capacitor Cc, defines the high cutoff frequency. The frequency response curves are superimposed for the three configurations, and respect the specifications. We present in Fig. 5 and Table III simulation results from a Monte Carlo simulation with 400 trials, considering mismatch and process variations.

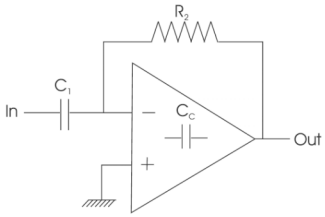

Figure 4. Amplifier with filter

The low cutoff frequency is around 100 Hz. It is important to mention that this parameter depends on the output impedance of extracellular electrodes. More precise simulations should take in to account the electrode model, which is difficult to established, due to the high variability of experimental environment (electrodes and biological medium). However, if we consider standard models [23], the cutoff frequency stays in the 100Hz range.

Finally, the noise figures for the amplifiers with filter stay unchanged. The HBT-based amplifier is still the most performing solution, followed by the NMOS-based one.

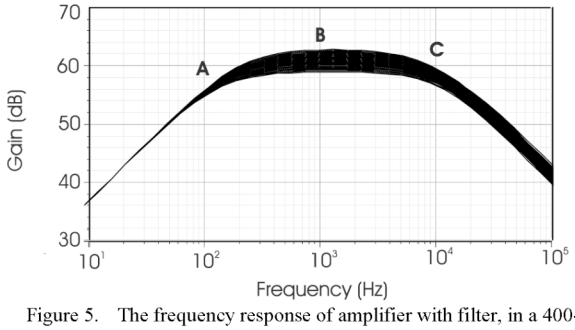

Figure 5. The frequency response of amplifier with filter, in a 400-trial Monte Carlo simulation.

TABLE III. GAIN VALUES AT 3 FREQUENCIES, FROM FIG. 4.

Label	F (Hz)	Gain (dB)		
		Min.	*Mean*	*Max.*
A	100	54	55	56
B	1000	59	61	63
C	10 000	57	58	59

IV. CONCLUSION

This paper compares three integrated amplifiers dedicated to the processing of neural electrical activity measured using extracellular electrodes. The three versions differ by their first stage, designed, respectively, with a HBT, a NMOS, and a PMOS differential pair. After defining the specifications, we discussed the amplifiers characteristics: intrinsic noise, gain, operating frequencies, slew rate, and rejection of power supply noise. We also discussed costs issues, characterized by power consumption and silicon area. From these considerations, we defined a common architecture for the three amplifiers. Simulations using Monte Carlo technique for the chosen process showed us that all amplifiers present the requested frequency response. If we take into account the other characteristics, the HBT-based solution is optimal, except for the fabrication cost. If a CMOS technology is mandatory, the NMOS-based solution is the best one. Both HBT and CMOS versions will be implemented on prototype chips, and connected to a MEA device to measure the activity of cultured cortical cells. This circuitry will be included in a integrated closed-loop platform running hybrid neural networks [4]. The platform currently uses commercial neural amplifiers based on discrete components [6, 15]. The integrated solution will strongly increase the precision and the reliability on the cultured neurons' activity measurement.

REFERENCES

[1] B. Catargi et al., "Delivrer : In vivo feedback control of insulin delivery (or, in french, DELivrance d'Insuline in Vivo Régulée et Rétrocontrôlée)," Aquitaine Region Project, 2007-2010.

[2] J.M. Carmena et al., "Learning to control a brain-machine interface for reaching and grasping by primates," PLoS Biol, vol. 1, p. E42, 2003.

[3] B. D. Reger et al., "Connecting brains to robots: an artificial body for studying the computational properties of neural tissues," Artif Life, vol. 6, pp. 307-324, 2000.

[4] G. Bontorin, "Bioelectronics closed-loop for hybrid neural networks: towards a fully integrated approach," Master thesis, University Bordeaux 1, 2006.

[5] F. Heer et al., "Single-chip microelectronic system to interface with living cells," Biosens Bioelectron, vol. 22, pp. 2546-2553, 2007.

[6] G. Bontorin et al., "A real-time closed-loop setup for hybrid neural networks," in Medicine and Biology Society (EMBC 2007), 29th Annual International Conference of the IEEE Engineering on, Lyon, 2007, pp. 3004-3007.

[7] J. Wu, W. F. Feng, and W. C. Tang, "A multi-channel low-power circuit for implantable auditory neural recording microsystems," unpublished work.

[8] R. H. III Olsson et al., "Band-tunable and multiplexed integrated circuits for simultaneous recording and stimulation with microelectrode arrays," Biomedical Engineering, IEEE Transactions on, vol. 52, pp. 1303-1311, 2005.

[9] P. Mohseni, K. Najafi, S. J. Eliades, and X. Wang, "Wireless multichannel biopotential recording using an integrated FM telemetry circuit," Neural Systems and Rehabilitation Engineering, IEEE Transactions on, vol. 13, pp. 263-271, 2005.

[10] Q. Bai and K. D. Wise, "Single-unit neural recording with active microelectrode arrays," Biomedical Engineering, IEEE Transactions on, vol. 48, pp. 911-920, 2001.

[11] R. Rieger et al., "Design of a low-noise preamplifier for nerve cuff electrode recording," Solid-State Circuits, IEEE Journal of, vol. 38, pp. 1373-1379, 2003.

[12] R. R. Harrison and C. Charles, "A low-power low-noise CMOS amplifier for neural recording applications," Solid-State Circuits, IEEE Journal of, vol. 38, pp. 958-965, 2003.

[13] Y. Hu and M. Sawan, "CMOS front-end amplifier dedicated to monitor very low amplitude signal from implantable sensors," Analog Integrated Circuits and Signal Processing, vol. 33, pp. 29–41, 2002.

[14] W. Dabrowski, P. Grybos, and A. M. Litke, "A low noise multichannel integrated circuit for recording neuronal signals using microelectrode arrays," Biosensors and Bioelectronics, vol. 19, pp. 749–76, 2004.

[15] "MEA Amplifier with Blanking Circuit for Upright Microscopes — User Manual," Multi Channel Systems MCS, 2006.

[16] Y. Perelman and R. Ginosar, "Analog frontend for multichannel neuronal recording system with spike and LFP separation," J Neurosci Methods, vol. 153, pp. 21-26, 2006.

[17] I. Obeid and P. D. Wolf, "Evaluation of spike-detection algorithms fora brain-machine interface application," Biomedical Engineering, IEEE Transactions on, vol. 51, pp. 905-911, 2004.

[18] L. Berdondini et al., "High-density microelectrode arrays for electrophysiological activity imaging of neuronal networks," in Electronics, Circuits and Systems, The 8th IEEE International Conference on (ICECS 2001), 2001, pp. 1239-1242.

[19] D. A. Henze et al., "Intracellular features predicted by extracellular recordings in the hippocampus in vivo," J Neurophysiol, vol. 84, pp. 390-400, 2000.

[20] G. Palmisano, G. Palumbo, and S. Pennisi, "Design Procedure for Two-Stage CMOS Transconductance Operational Amplifiers: A Tutorial," Analog Integrated Circuits and Signal Processing, vol. 27, pp. 179–189, 2001.

[21] M. S. J. Steyaert and W. M. C. Sansen, "Power supply rejection ratio in operational transconductance amplifiers," Circuits and Systems, IEEE Transactions on, vol. 37, pp. 1077-1084, 1990.

[22] P. Cazenave, Integrated bipolar transistors modeling I: silicon devices (french book: Modélisation du transistor bipolaire intégré 1 : dispositifs au silicium) vol. 1: Paris , Hermès science publ. , Lavoisier 2004.

[23] S. Martinoia, P. Massobrio, M. Bove, and G. Massobrio, "Cultured neurons coupled to microelectrode arrays: circuit models, simulations and experimental data," Biomedical Engineering, IEEE Transactions on, vol. 51, pp. 859-863, 2004.

II. List of Author's publications

Chapters in books

Raoux M., **Bontorin G**., Bornat Y., Lang J. and Renaud S. (2010). "*Bioelectronic sensing of insulin demand*".in: Biohybrid Systems. R. Jung. Weinheim, Wiley-Vch, to be published.

Papers in Peer-reviewed International Journals

Bontorin G., Imfeld K., Raoux M. and Renaud S. (2010a). "*A low noise, low area, low cost preamplifier for large scale, high resolution Multielectrode Array (MEA).*" submitted to IEEE Transactions in Neural System and Rehabilitation Engineering.

Bontorin G., Robert C., Raoux M. and Renaud S. (2010b). "*Smart Integrated Pixel for high-density MEA systems. .*" submitted to Journal of Neural Engineering (IOP).

Bontorin G., Garenne A., Lopez C., Le Masson G. and Renaud S. (2010c). "*Hybrid Systems in Real-time Closed-loop*." submitted to Frontiers in Neuroengineering.

Garenne A., Maillard A., Alvado L., Tomas J., **Bontorin G.**, Nagy F., Renaud S. and Le Masson G. (2010). "*A real-time closed-loop setup allowing sensory feedback driven learning strategies*." submitted to Frontiers in Neurorobotics.

Papers in Peer-reviewed International Conference Proceedings

Bontorin G., Renaud S., Garenne A., Alvado L., Le Masson G. and Tomas J. (2007a). "*A Real-Time Closed-Loop Setup for Hybrid Neural Networks*". Engineering in Medicine and Biology Society, 2007. EMBS 2007. 29th Annual International Conference of the IEEE, 3004-3007.

Bontorin G., Tomas J. and Renaud S. (2007b). "*Low noise and low cost neural amplifiers*". Electronics, Circuits and Systems, 2007. ICECS 2007. 14th IEEE International Conference on, 1324-1327.

Bontorin G., Lopez C., Bornat Y., Lewis N., Renaud A S., Garenne M.C. and Le Masson G. (2008). "*A real-time setup for multisite signal recording and processing in living neural networks*". Circuits and Systems, 2008. ISCAS 2008. IEEE International Symposium on, 2953-2956.

Bontorin G., Garenne A., Tomas J., Lopez C., Morin F.O. and Renaud S. (2009). "*A real-time system for multisite stimulation on living neural networks*".in: 2009 Joint Ieee North-East Workshop on Circuits and Systems and Taisa Conference**:** 137-140.

Master Thesis

Bontorin G. (2006). "*Bioelectronics closed-loop for hybrid neural networks: towards a fully integrated approach*", Master thesis, University Bordeaux 1.

III. Résumé en Français

Les travaux décrits dans cette thèse ont été menés au Laboratoire de l'Intégration du Matériau au Système (IMS) à Bordeaux et à l'Institut de MicroTechnique (IMT) à Neuchâtel sur une période allant d'octobre 2006 à septembre 2010.

Mes travaux portent sur le développement et l'amélioration des performances spatio-temporelles d'un système hybride (vivant - artificiel) appelé « Réseau Hybride » ou « *Hynet* » dans la version anglaise.

A. Hynet

« *Hynet* » est un système hybride bidirectionnel, à boucle fermée et à temps réel.

Comme son nom l'indique, ce système contient deux parties : une partie vivante et une partie artificielle. Par boucle fermée, on entend que ces deux parties communiquent entre elles d'une manière bidirectionnelle et interagissent de la sorte. Temps réel signifie que les communications mises en jeu sont assez rapides pour qu'il n'y ait pas de préjudice quant au déroulement du traitement de données (ni perte, ni retards d'informations).

Ainsi, le rôle de la partie de la partie artificielle (constituée par le matériel (Hardware) et le logiciel (Software)) est d'acquérir l'activité de la partie vivante (appelée Bioware), de traiter les données enregistrées et d'appliquer la réponse adéquate sur forme de stimulus, dans un délai suffisamment petit pour que cette boucle respecte le critère temps réel (Fig. F.01).

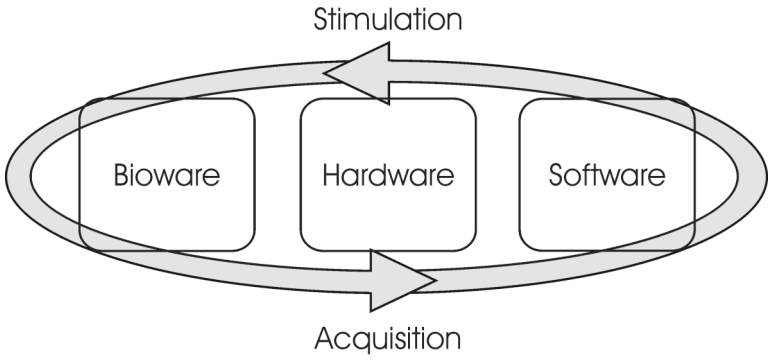

Figure F.01. La boucle Hynet. La communication bidirectionnelle entre le vivant (Bioware) et le logiciel (Software) passe par le matériel (Hardware).

La partie vivante peut, par exemple, être constituée par des neurones ou par des cellules pancréatiques. Le matériel fait le lien entre le logiciel et le vivant. Le logiciel, à son tour, communique l'activité de la partie vivante à l'utilisateur et, en respectant les consignes fixées par ce dernier, commande la fermeture de la boucle temps réel.

Dans notre premier système, la chaîne d'acquisition débute par un bloc commercial de MultiChannel Systems™ (MCS), avec 60 canaux analogiques. Les signaux sont amplifiés par les cartes ACQ et numérisés par les cartes DIGI. La carte PCI dirige les signaux numériques vers le logiciel. L'application temps réel (ReTA) traite les données et peut les envoyer à un port TCP/IP. La chaîne de stimulation commence dans le logiciel, soit dans ReTA, soit par un processus externe. La carte PCI envoie les commandes à la carte DIGI. Celle-ci les transmet aux cartes STT et STM qui génèrent à leur tour la stimulation analogique sur 30 canaux. (Fig F.02)

La configuration logicielle de la fermeture de boucle est composée de quatre étapes (Fig. F.03.A). La première est la définition des conditions d'acquisition, par le Condition Descriptor (Fig. F.03.B). La deuxième est la définition des stimuli de réponse, par le Pattern Descriptor (Fig. F.03.C). La troisième est l'association entre les éléments engendrés dans les deux premières étapes et chacun des canaux du MEA pelo Linker (Fig. F.03.D). Ces trois premiers logiciels (un pour chaque étape) fonctionnent sans les contraintes temps réel. La dernière étape est exécutée par ReTA, qui lit la configuration issue des trois premières étapes et l'exécute en temps réel.

Dans « *Hynet* », le facteur temps réel est strict : il implique qu'entre deux échantillons de l'acquisition, tout le traitement des données doit être effectué et la stimulation respective doit être générée. La période de boucle fermée est définie dans ce cas comme le temps utilisé par le système pour effectuer l'opération d'acquisition et l'opération de génération du stimulus. Cette période ne doit pas dépasser la période d'échantillonnage.

Fig. F.04 résume le temps moyen de propagation dans les modules de notre « *Hynet* ». Une fréquence d'échantillonnage adéquate est, par exemple, 10 kHz. Cela correspond à une période d'échantillonnage de 100 µs. Comme notre période de boucle fermée est de 46 µs, plus de 50 µs sont disponibles entre chaque échantillon, pour que le logiciel puisse fermer la boucle.

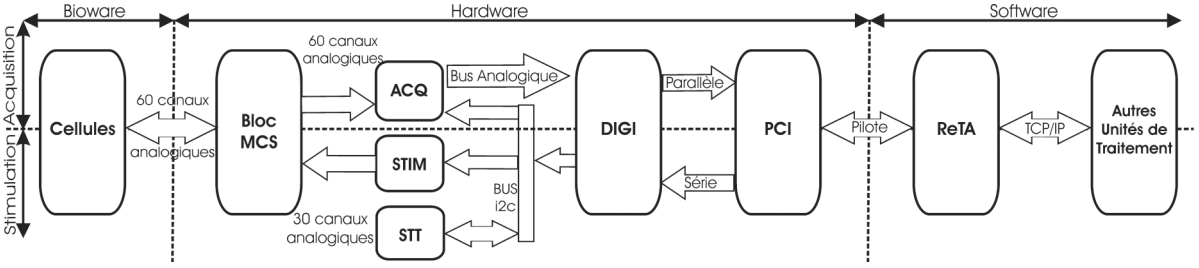

Figure F.02. Détails de la boucle fermée.

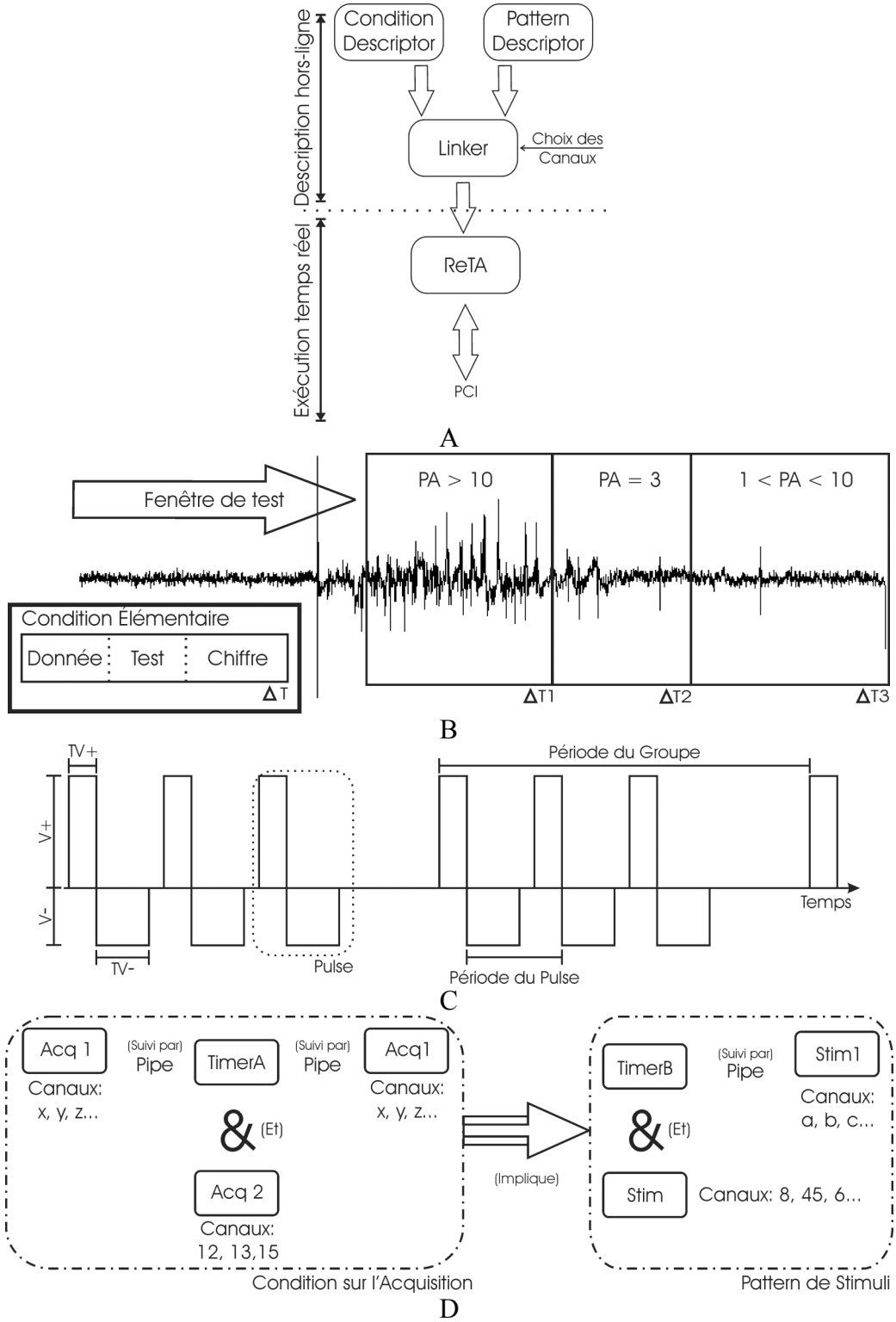

Figure F.03. Le logiciel de fermeture de boucle. A. Les étapes pour la configuration d'une expérience. B. Un exemple de condition, constitué par trois conditions élémentaires. PA = potentiel d'action. C. Un stimulus avec ses paramètres. D. Un exemple de lien pour la boucle fermée.

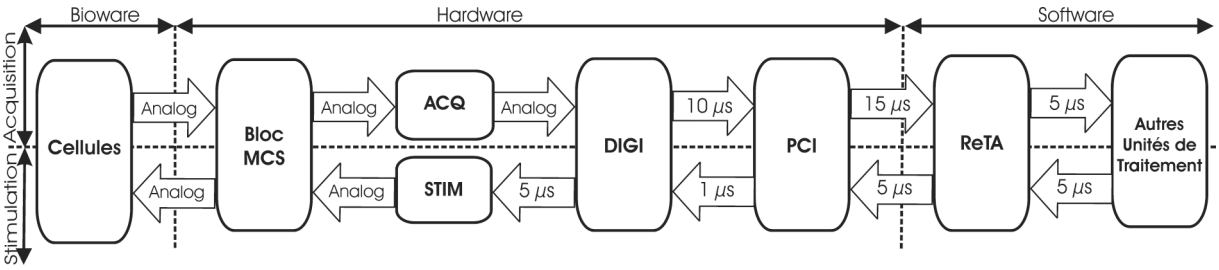

Figure F.04. Délais de propagations des modules du Hynet. Analog=Analogique.

B. Le Pixel Intelligent

Notre premier « *Hynet* » présente une interface conviviale avec l'utilisateur. Par contre, ses performances spatiotemporelles sont limitées par : (a) l'utilisation des éléments commerciaux de MCS dans la partie matérielle et (b) le traitement des données dans le logiciel. Notre solution pour dépasser ces limitations est la création d'un Pixel Intelligent (*iP*).

Ce pixel est introduit dans la chaîne d'acquisition de notre système, au plus proche de la culture. Plus précisément au-dessous de celle-ci, notre électronique se trouve incrustée à l'intérieur de la matrice d'électrodes (MEA) qui est à la fois le support mécanique et l'accès électrique à la culture. (Fig. F.05)

L'*iP* est constitué par : une électrode, un préamplificateur et un détecteur d'activité (Fig. F.06). Il est conçu pour améliorer la qualité du signal, la densité d'acquisition et le traitement des données en temps réel. En outre, il remplace un canal complet d'acquisition de notre « *Hynet* ».

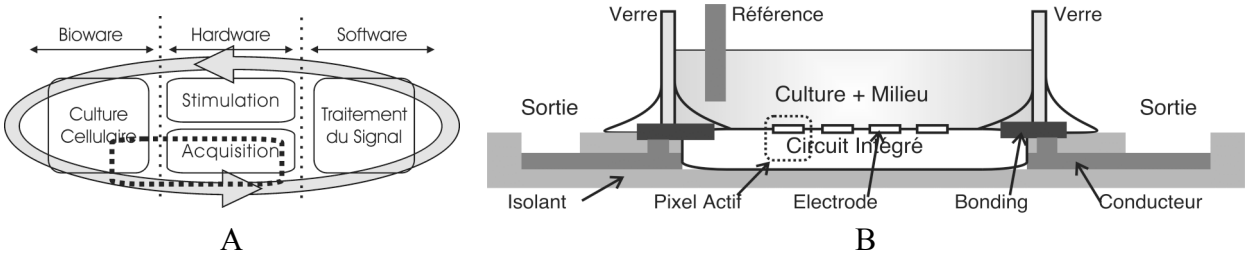

Figure F.05. Location du pixel intelligent. A. À l'intérieur de la boucle fermée. B. Dans la matrice d'électrodes.

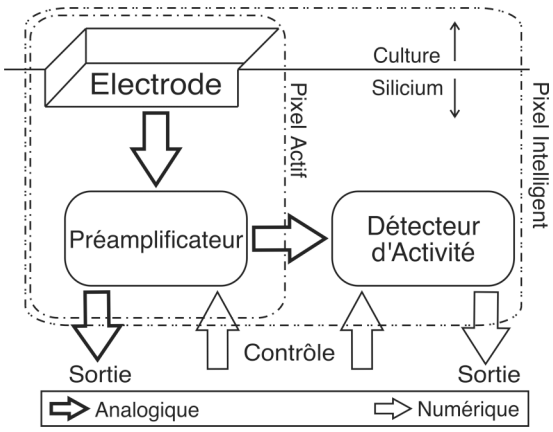

Figure F.06. Le pixel intelligent.

Le préamplificateur est conçu suivant l'approche des capteurs à pixel actif, laquelle conduit à réduire la distance entre l'électrode de capture et le traitement des données. Cette approche permet également d'augmenter le nombre et la densité des points d'acquisition, car le signal est suffisamment amplifié pour être multiplexé et/ou traité *in situ*.

Notre préamplificateur doit être capable d'amplifier un signal biologique très bruité par nature. Cela implique une conception soigneuse de l'étage amplification ainsi que du circuit de filtrage intégré à ce bloc. Au même temps, pour maintenir forte la densité d'électrodes, la surface de silicium doit demeurée très restreinte. Fig F.07 présente notre architecture compatible avec ces spécifications.

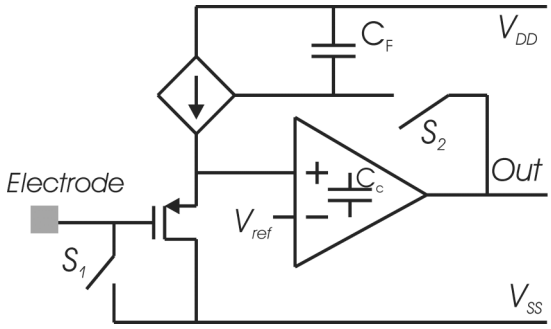

Figure F.07. Le schéma électrique du préamplificateur.

L'amplificateur opérationnel (OPA) contient un condensateur de Miller (Cc) qui est responsable de la fréquence de coupure haute. En mode amplification, les interrupteurs S1 et S2 sont ouverts. La sortie (Out) est l'image amplifiée de la tension présente sur l'électrode. Dans la phase de calibration, S2 est fermé. La tension de décalage de l'OPA et l'effet de l'interface électrolyte-électrode sont compensées ; ainsi, les deux entrées de l'OPA présentent la même tension Vref. Cf conserve le point de fonctionnement du circuit pour le mode amplification. S1 est fermé en cas de présence d'un stimulus sur une électrode voisine. Notre préamplificateur présente les caracteristiques suivantes (Table F.1).

Table F.1 Principales caractéristiques électriques du préamplificateur

Caractéristique	Mesure
Gain	300 V/V (49 dB)
Bruit équivalent en entrée	10 μV_{rms} (1 - 10kHz)
Rejection DC en entrée	± 430 mV
Fréquence de Coupure Haute	10 kHz
Vitesse de balayage	1 V/µs
Distorsion Harmonique Totale	< - 30dB (1 kHz, 300 μV_{rms})
Réjection au bruit de l'alimentation	> 40dB
Impédance d'entrée	> 1 TΩ (f < 100 kHz)
Consommation	45 µW moyenne
Surface	1300 μm^2

À fin de tester notre amplificateur, a été utilisé le MEA-SG (Génerateur de Signaux), de MCS. Ses signaux simulent l'activité neuronale. Le signal est premièrement amplifié par le MEA-1060 (produit MCS). Il est ensuite atténué par un pont résistif afin de simuler le signal non amplifié. L'étiquette "Signal MCS" (Figs. F.08.A) indique où le signal "MCS" (Figs. F.08.B et F.08.C) est mesuré. L'étiquette "Notre Signal" (Figs. F.08.A) indique où le signal "Notre Amplificateur" (Figs. F.08.B et F.08.C) est mesuré.

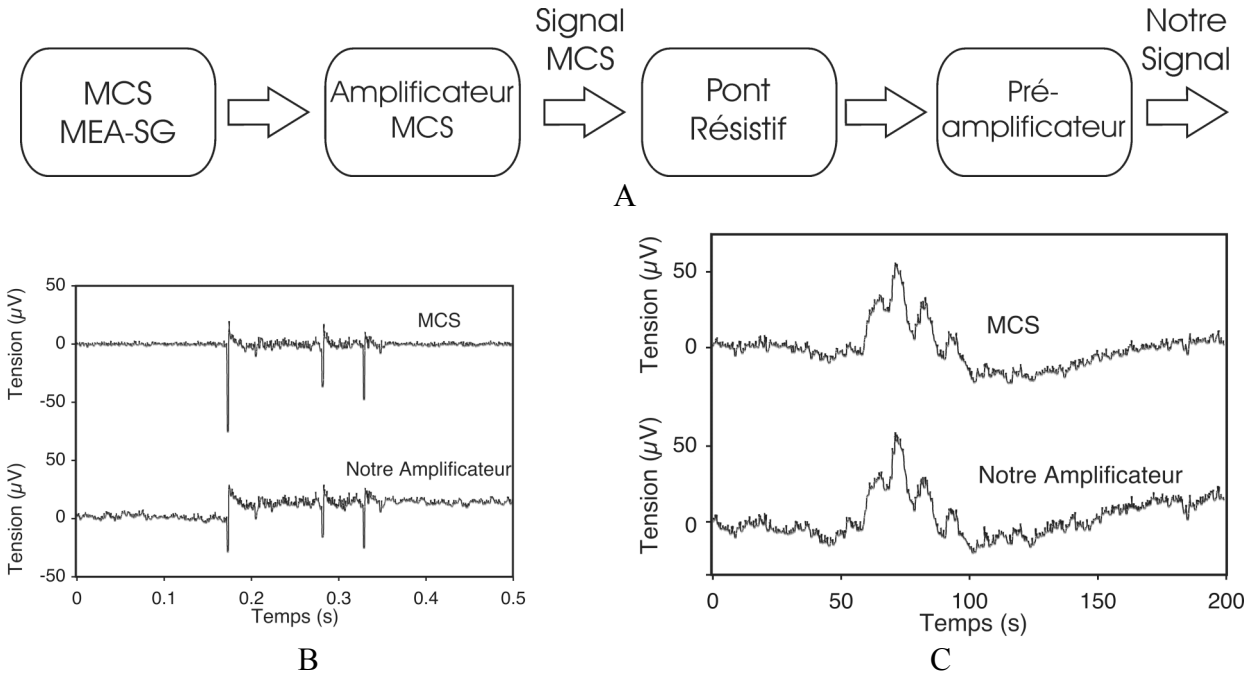

Figure F.08. Mesures avec des signaux neuronaux simulés. A. Schématique. B. Potentiel d'action extracellulaire artificiel. La réduction de l'amplitude du premier potentiel d'action est due au double filtrage des hautes fréquences. C. Potentiel des champs locaux. Les signaux de l'amplificateur MCS sont en haut et ceux de notre amplificateur sont en bas sur les figures B et C. Les signaux ont les amplitudes équivalentes à celles de l'entrée du préamplificateur.

Intégré dans un pixel actif, notre nouvel amplificateur a le potentiel d'augmenter la densité et le nombre de points d'acquisition. Pour maintenir le traitement temps réel, les performances temporelles du traitement de données doivent être améliorées en conséquence.

Notre solution est, bien évidement, l'usage du détecteur d'activité, présent dans l'*iP*. Comme le préamplificateur, il sera placé aussi proche de l'électrode que possible. Son rôle est de détecter les plages d'activité de la culture et, ainsi, d'ignorer les intervalles entre potentiels d'action. Le détecteur doit être robuste aux variations du signal biologique et avoir une surface et une consommation compatibles avec un grand nombre et une forte densité d'électrodes.

Le schéma électrique du circuit retenu est celui de la Fig. F.09. Un seuil est appliqué au signal biologique dans la partie décision. Le résultat est codé sur un bit confirmant le dépassement du seuil par le signal d'entrée. Ce seuil est défini comme un multiple (N) de l'écart type (SD) du signal biologique et est actualisé en permanence par le bloc d'adaptation.

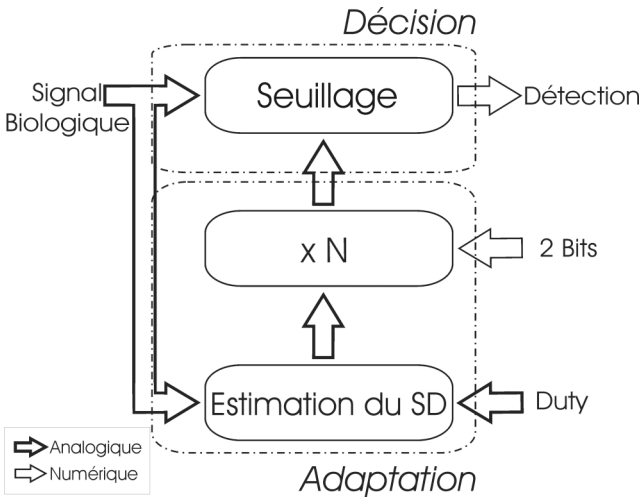

Figure F.09 Le schéma du detector

La partie de décision doit impérativement être propre à chacun des pixels, mais la partie d'adaptation peut être déportée et commune à plusieurs pixels et cela à fin d'augmenter la densité d'intégration et de réduire la surface et la consommation.

Finalement, la Table F.2 présente les caractéristiques du notre détecteur.

Table F.2 Caractéristiques du détecteur.

Caractéristique	Mesure
Comparateur	
Tension de décalage	< 450 µV
Fréquence	> 2 MHz
Retard	< 0.2 µs
Surface	150 μm^2
Consommation	27 µW
Décision	
Surface	300 μm^2
Consommation	54 µW
Adaptation	
Surface	3200 μm^2 *a*
Consommation	45 µW
Pixel Intelligent	
Surface	1600 μm^2
Consommation	100 µW
Pixel Intelligent + Adaptation	
Surface	4800 μm^2 *a*
Consommation	145 µW

a surface sans condensateur, car sa valeur est variable en fonction de l'expérience.

Le test de chaque partie du détecteur est fait séparément. Premièrement, l'adaptation du seuil est testée en utilisant en entrée une sinusoïde modulée (Fig. F.10). L'adaptation doit être lente pour éviter de considérer certains potentiels d'actions comme bruit.

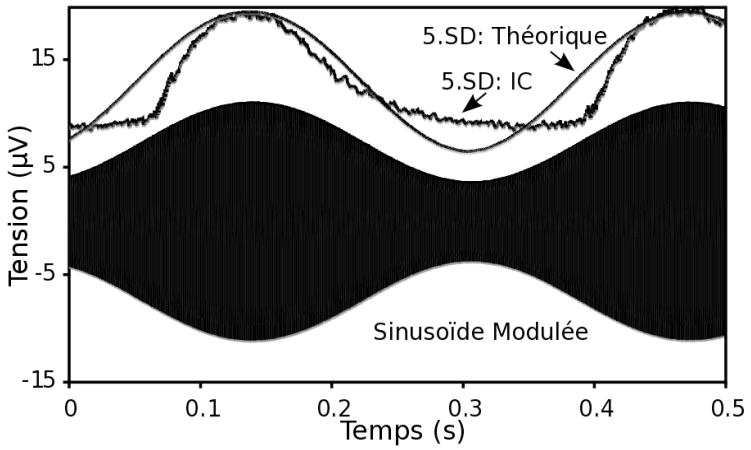

Figure F.10. Test de l'adaptation.

Deuxièmement, la décision est testée avec de vrais signaux biologiques issus de cellules Bêta du pancréas. L'activité spontanée des cellules Bêta est fonction de la concentration du glucose dans le milieu extracellulaire.

Un MEA contient la culture cellulaire dans un milieu hyperglycémique. L'activité est premièrement amplifiée par l'amplificateur MEA-1060 de MCS et, ensuite, atténuée par un pont résistif afin de simuler un signal non amplifié à l'entrée de notre préamplificateur. Le signal amplifié est transmis au détecteur qui renvoie la présence ou non d'activité, signa codé sur un bit (Fig. F.11 A).

Fig. F.11.B présente la détection d'un unique potentiel d'action. Quand ce dernier dépasse le seuil, la détection est effectuée. Fig. F.11.C montre un autre enregistrement. Si le seuil avait été choisi égal à 5 fois SD, le dernier potentiel d'action serait omis. Cette figure démontre l'intérêt de la double détection, positive et négative.

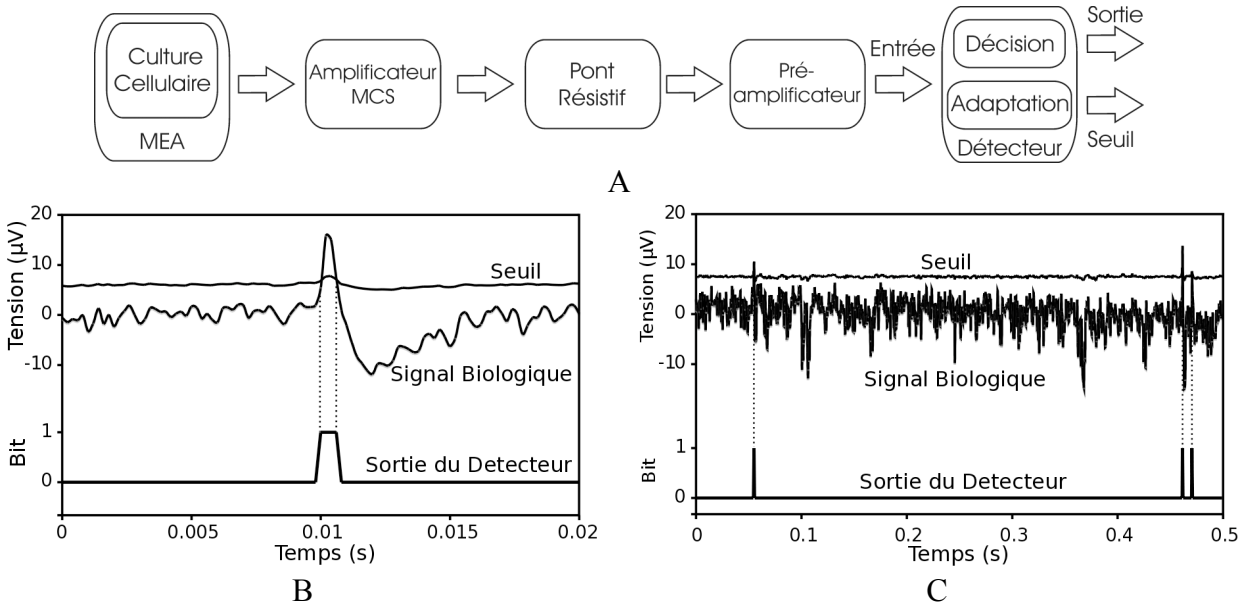

Figure F.11. L'enregistrement de l'activité des cellules Bêta du pancréas dans un milieu hyperglycémique. A. Le schéma électrique du banc de mesures. B. La détection d'un seul potentiel d'action. C. Un autre enregistrement avec plusieurs potentiels d'action.

C. Conclusion

La co-direction de cette thèse a une synergie qui, en dépassant la simple association des domaines d'expertise particuliers, a conduit à une amélioration sensible de toutes les performances du système (Table F.3). La réalisation d'une future matrice d'électrodes avec des milliers de pixels intelligents ainsi développés sera un moyen de faire avancer la recherche et les applications de la Bioélectronique, dans chacune des deux équipes et d'une manière globalisée.

Table F.3 Résumé des principales améliorations apportées par ce travail à chacune des équipes.

Caractéristique	Pays	Avant	Après
Hynet			
Fermeture de Boucle	FR	Natif	GUI
Pixel Actif			
Pitch (µm)	CH	40	35
Gain (V/V)	CH	100	300
Consommation (µW)	CH	83	45
Technologie	CH	CMOS 0.35 µm	CMOS 0.18 µm
	FR	Discrète	
Détection			
Traitement	FR	Logiciel	Matériel
	CH	Numérique (FPGA)	Analogique & Intégré
Retard (µs)	FR	25	< 1

IV. Resumo em português

O trabalho descrito neste manuscrito foi realizado no Laboratório da Integração do Material ao Sistema (IMS) em Bordeaux e no Instituto de Microtécnica (IMT) em Neuchâtel, de outubro de 2006 à setembro 2010.

Ele tinha por objetivo o desenvolvimento e o aperfeiçoamento do desempenho espaço-temporal de um sistema híbrido (vivo - artificial) chamado Rede Híbrida ou *Hynet*.

A. Hynet

Hynet é um sistema híbrido bidirecional, em laço fechado e tempo real. Como o seu nome indica, este sistema conta de duas partes: uma viva e uma artificial. Sendo um laço fechado, as duas partes se comunicam bidirecionalmente, ou seja, a entrada de uma é alimentada pela saída da outra. Enfim, o fator tempo real implica que as comunicações do sistema são suficientemente rápidas para que não haja degradação (por perda ou por atraso) do fluxo de dados.

Neste contexto, a função da parte artificial (constituída pelo Hardware e pelo Software) é a de adquirir a atividade elétrica da parte viva (também chamada Bioware), processar os dados coletados e aplicar a resposta adequada na forma de um estímulo elétrico. E isto num prazo de tempo suficientemente curto para que o laço funcione em tempo real (Fig. P.01).

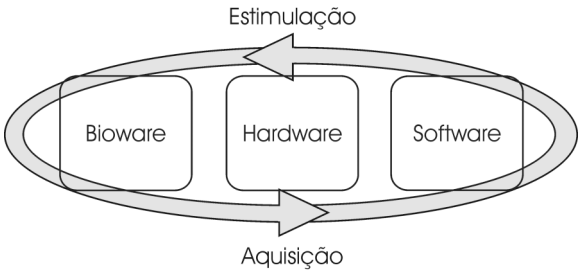

Figura P.01. O laço Hynet. A comunicação bidirecional entre o Bioware e o Software passa pelo Hardware.

O Bioware pode ser constituído, por exemplo, de neurônios ou de células pancreáticas. O Hardware estabelece a ligação entre o Bioware e o Software. Este último interage com o utilizador para que este configure o experimento e feche o laço em tempo real.

No primeiro sistema, a cadeia de aquisição começa por um bloco comercial de MCS (MultiChannel System™), com 60 canais analógicos. Os sinais provenientes da cultura são amplificados pela carta ACQ e digitalizados pelas cartas DIGI. A carta PCI envia os sinais digitais ao Software. O programa em tempo real (ReTA) processa os dados podendo envia-los

à uma porta TCP/IP. A cadeia de estimulação começa no Software, seja no ReTA, seja por um processo externo. A carta PCI envia comandos às cartas DIGI, que a seu turno transmitem-nas às carta STT e STM. Estas duas últimas se encarregam de gerar estimulações elétricas em 30 canais analógicos (Fig P.02).

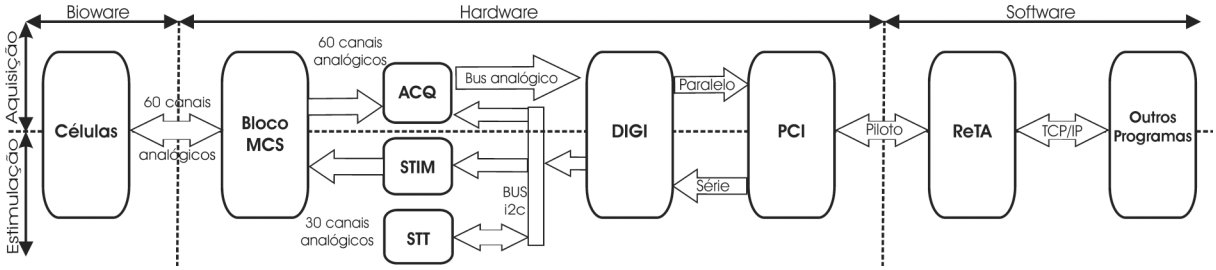

Figura P.02. Detalhes do laço fechado.

A configuração do Software de fechamento de laço é constituída de três etapas (Fig. P.03.A). A primeira é a definição das condições na aquisição com o Condition Descriptor (Fig. P.03.B). A segunda é a definição dos estímulos que serão enviados como resposta, pelo Pattern Descriptor (Fig. P.03.C). A terceira é a associação dos elementos descritos nas etapas precedentes entre elas e com os respectivos canais, pelo Linker (Fig. P.04 .C). Estes três programas (um para cada etapa) não precisam funcionar em tempo real. A última etapa é executada pelo ReTA, que lê a configuração descrita anteriormente e a executa em tempo real.

Em um *Hynet*, o fator tempo real é restrito: ele determina que, entre duas amostras da aquisição, todo o processamento de dados deve ser executado e a respectiva estimulação gerada. O período do laço fechado é definido como o tempo necessário para efetuar a aquisição e a estimulação. Este período não pode exceder o período de amostragem.

Fig. P.04 resume o tempo médio de propagação dentro dos módulos do nosso *Hynet*. Uma freqüência adequada é, por exemplo, 10 kHz. Ela corresponde à um período de 100 µs. Do fato que nosso período de laço fechado é de 46 µs, mais de 50 µs são disponíveis entre cada amostragem para que o programa possa fechar o laço.

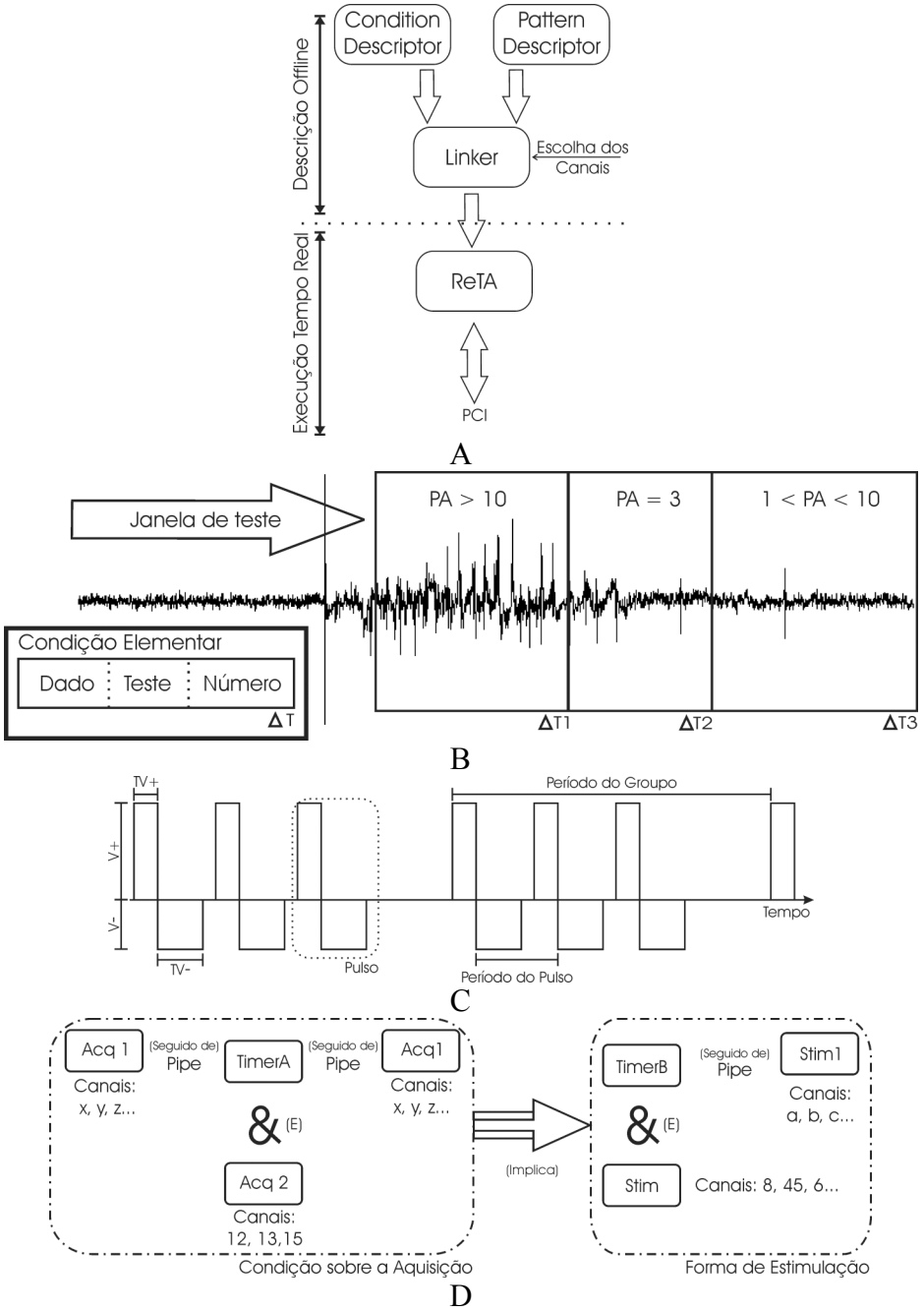

Figura P.03. O programa de fechamento de laço. A. As etapas de configuração de um experimento. B. Um exemplo de condição, constituído de três condições elementares. PA = Potencial de Ação. C. Um estímulo com seus parâmetros. D. Um exemplo de ligações para o laço fechado.

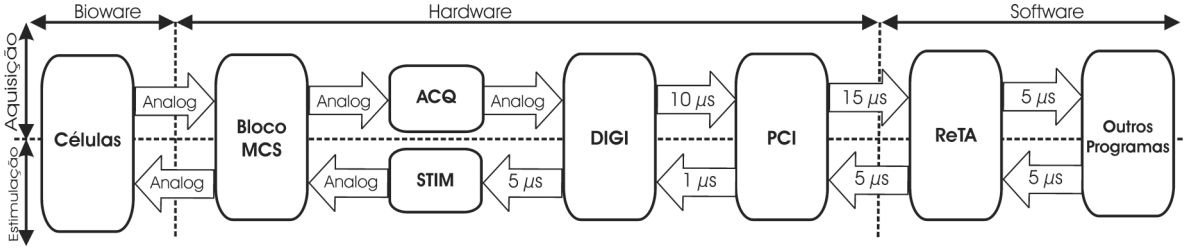

Figura P.04. Tempo de propagação dos módulos do Hynet. Analog=Analógico

B. Pixel Inteligente

O primeiro *Hynet* apresenta uma interface convivial para com o utilizador. No entanto, o desempenho espaço-temporal do sistema é limitada: primeiro pelo uso de elementos comerciais de MCS e segundo pelo processamento de dados pelo software. Nossa solução para transpor estes limites é o *Pixel Inteligente* (*iP*).

Este pixel é introduzido na cadeia de aquisição de nosso sistema, o mais próximo possível da cultura. Mais precisamente, embaixo desta. Nosso circuito eletrônico se encontra incrustado no interior da matriz de eletrodos. Esta atua como um suporte mecânico para o meio celular e como um acesso elétrico à cultura. (Fig. P.05).

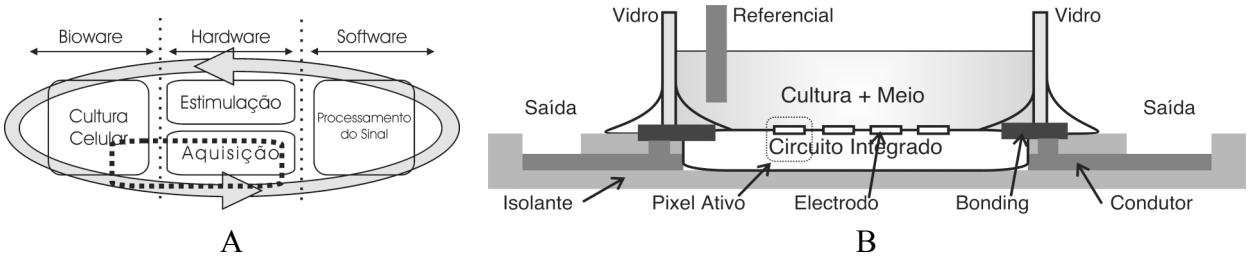

Figura P.05. Localização do pixel inteligente. A. No interior do laço fechado. B. Na matriz de eletrodos.

O *iP* é constituído por: um eletrodo, um pré-amplificador, um detector de atividade (Fig. P.06). Ele é concebido para melhorar a qualidade do sinal, a densidade na aquisição e o processamento dados. Deste modo, ele substitui um canal completo da aquisição do nosso *Hynet*.

O pré-amplificador é concebido seguindo o conceito de sensores à pixel ativo, o qual reduz a distância entre o eletrodo e o processamento de dados. Ele facilita igualmente o aumento do número e da densidade de pontos de aquisição, pois o sinal é suficientemente amplificado para ser multiplexado ou processado *in situ*.

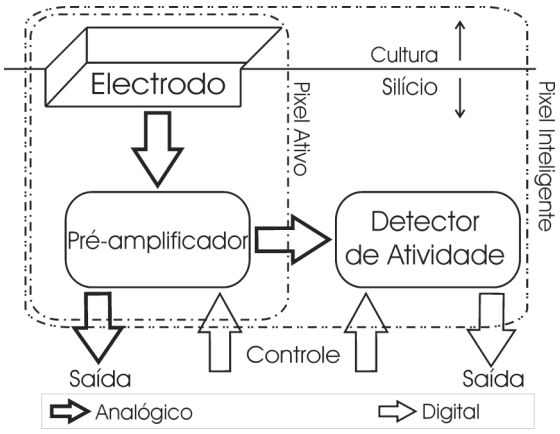

Figura P.06. O pixel inteligente.

Este amplificador deve ser capaz de amplificar um sinal biológico com muito ruído. Isto implica em uma concepção cuidadosa dos estágios de amplificação e filtragem. Ao mesmo tempo, para manter uma alta densidade de eletrodos, a superfície de silício que lhe é consagrada é muito limitada. Fig. P.07 apresenta a arquitetura compatível com esta especificações.

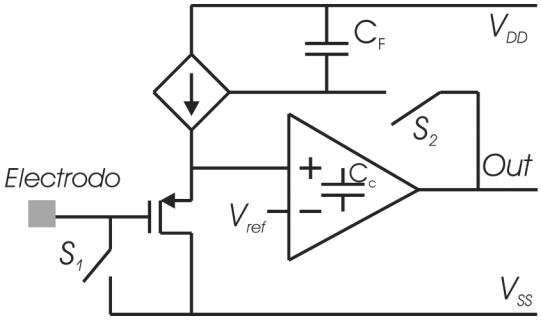

Figura P.07. Diagrama do pré-amplificador.

O amplificador operacional (OPA) utilizado contém um capacitor de Miller (Cc), o qual é responsável pela freqüência de corte alta. No modo amplificação, os interruptores S1 e S2 estão abertos. A saída (Out) é a imagem amplificada da tensão presente no eletrodo. No modo calibração, S2 está fechado. A tensão de offset do OPA e os efeitos da interface eletrodo-eletrólito são compensados, pois as duas entradas do OPA são à mesma referência Vref. Cf conserva o ponto de operação do circuito para o modo amplificação. S1 é fechado em caso de presença de um estímulo em um eletrodo vizinho. Nosso pré-amplificador apresenta as seguintes características (Tabela P.1)

Tabela P.1 Principais características do pré-amplificador.

Característica	Medida
Ganho	300 V/V (49 dB)
Ruído equivalente na entrada	10 μV_{rms} (1 - 10kHz)
Rejeição DC na entrada	± 430 mV
Freqüência de corte alta	10 kHz
Velocidade de varredura	1 V/µs
Distorção harmônica total	< - 30dB (1 kHz, 300 μV_{rms})
Rejeição ao ruído da alimentação	> 40dB
Impedância de entrada	> 1 TΩ (f < 100 kHz)
Consumação	45 µW média
Superfície	1300 μm^2

Com o intuito de testar nosso pré-amplificador, utilizamos o MEA-SG (Gerador de Sinais), de MCS, o qual simula a atividade neural. O sinal é primeiramente amplificado pelo MEA-1060 (também de MCS) e, em seguida, atenuado por uma ponte resistiva para simular um sinal não-amplificado. A etiqueta "Sinal MCS" (Figs. P.08.A) indica onde o sinal "MCS" (Figs. P.08.B et P.08.C) foi medido. A etiqueta "Nosso Sinal" (Figs. P.08.A) indica onde o sinal "Nosso Amplificador" (Figs. P.08.B et P.08.C) foi medido.

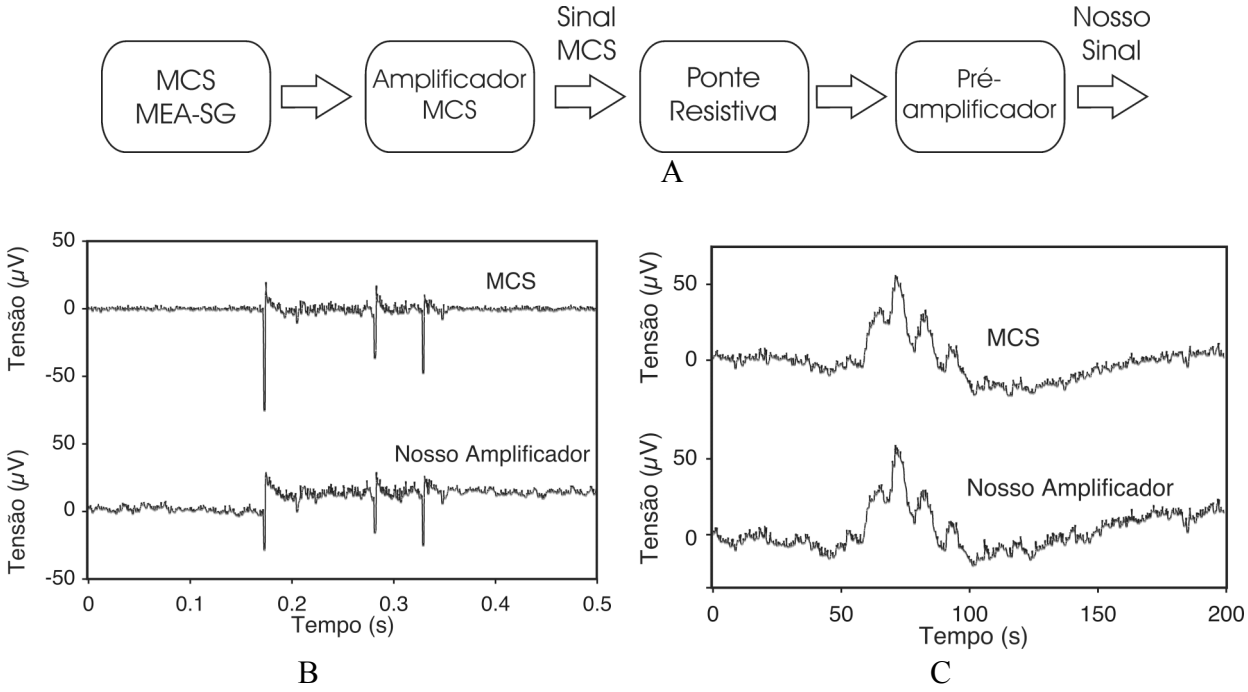

Figura P.08. Medidas com sinais neurais simulados. A. Diagrama. B. Potencial da ação artificial. A redução da amplitude do sinal do primeiro potencial de ação é devida à dupla filtragem em alta freqüência. C. Potencial de campo local. Os sinais do amplificador MCS são apresentados em cima e os do nosso amplificador, em baixo, nas figuras B e C. Os sinais apresentam as amplitudes equivalentes àquelas da entrada do pré-amplificador.

Integrado em um pixel ativo, nosso amplificador tem o potencial para aumentar a densidade e o número de pontos de aquisição. Para manter o funcionamento em tempo real do sistema, as performances temporais do processamento de dados também devem ser melhoradas.

A solução proposta é, evidentemente, o uso do detector de atividades presente no *iP*. Do mesmo modo que o pré-amplificador, o detector é presente tão próximo quanto possível ao eletrodo. Sua função é de detectar os potenciais de ação e ignorar os intervalos entre estes. O detector deve ser robusto às variações do sinal biológico e ter consumo e superfície compatíveis com um grande número e uma forte densidade de eletrodos.

O diagrama do circuito escolhido é o apresentado na Fig. P.09. Um limiar é aplicado ao sinal biológico na parte de decisão. O resultado é codificado em um bit afirmando um excesso ao limiar. Este limiar é definido como um múltiplo (N) do desvio padrão (SD) do sinal biológico e é atualizado em permanência pelo bloco de adaptação.

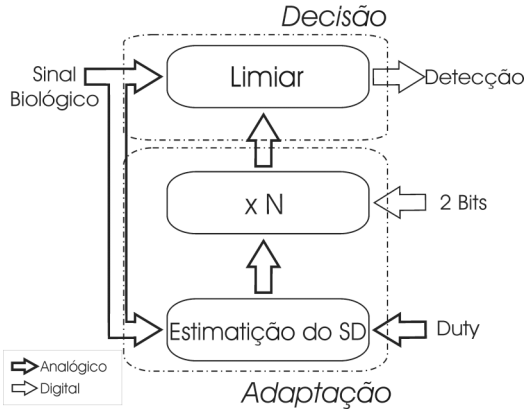

Figure P.09 O diagrama do detector.

O bloco de decisão deve imperativamente ser individual à cada pixel, mas a parte de adaptação pode ser deportada e comum a vários *pixels* no intuito de aumentar a densidade de eletrodos e diminuir a superfície e a consumação.

Finalmente, a Tabela P.2 apresenta as características do nosso detector.

O teste de cada parte do detector é efetuada separadamente. Primeiro, a adaptação do limiar é testada colocando uma entrada senoidal modulada (Fig. P.10). A adaptação se dá conforme o desejado, pois ela deve ser lenta para evitar a interpretação de sinais como ruído.

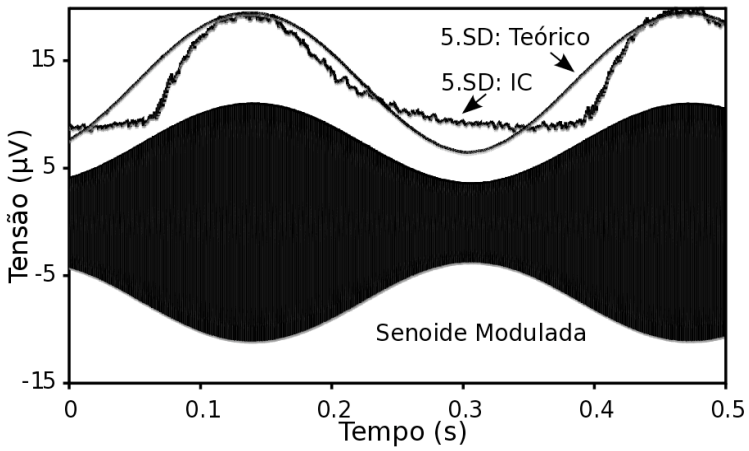

Figure P.10. Teste da adaptação.

Em seguida, a decisão é testada com sinais reais, provenientes de células Beta do pâncreas. A atividade espontânea dessas células é função da concentração de glicose do meio extracelular.

Tabela P.2 Características do detector.

Característica	Medida
Comparador	
Offset de entrada	< 450 µV
Freqüência	> 2 MHz
Atraso	< 0.2 µs
Superfície	150 μm^2
Consumo	27 µW
Decisão	
Superfície	300 μm^2
Consumo	54 µW
Adaptação	
Superfície	3200 μm^2 *a*
Consumo	45 µW
Pixel Inteligente	
Superfície	1600 μm^2
Consumo	100 µW
Pixel Inteligente + Adaptação	
Superfície	4800 μm^2 *a*
Consumo	145 µW

a superfície sem o capacitor, pois seu valor é ajustado conforme o experimento.

Um MEA contém a cultura celular num meio hiperglicêmico. A atividade é primeiramente amplificada pelo MEA-1060 de MCS e, em seguida, atenuada, sempre para simular um sinal não amplificado na entrada do amplificador. O sinal é transmitido ao detector, o qual acusa a presença ou ausência de atividade, codificado em um bit (Fig. P.11.A).

Fig. P.11.B apresenta a detecção de um potencial de ação. No momento em que o sinal excede o limiar, a detecção é efetuada. Fig. P.11.C mostra um outro registro. Se o limitar fosse escolhido como 5 vezes o SD, o último potencial teria sido ignorado. Esta figura também demonstra o interesse de uma dupla detecção, positiva e negativa.

C. Conclusão

A co-orientação deste doutorado é uma sinergia que, mais do que uma simples associação da experiência das duas equipes, conduziu à uma melhora sensível de todas as performances dos sistemas de cada equipe (Tabela P.3). A realização de uma futura Matriz de Ele-

trodos Inteligente, a partir da associação de milhares dos nossos *pixel* inteligentes, será um método de proporcionar avanços na pesquisa e nas aplicações da Bioeletrônica, em cada uma das equipes e de um jeito globalizado.

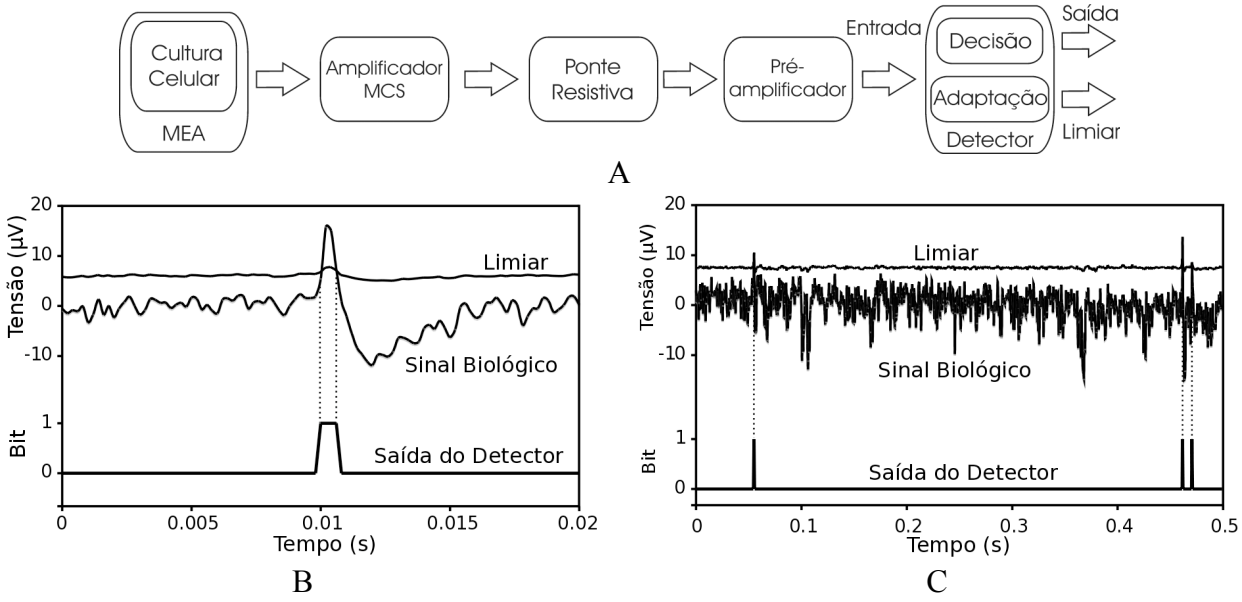

Figura P.11. Registro da atividade de células Beta do pâncreas em um meio hiperglicêmico. A. O diagrama do banco de medidas. B. A detecção de um potencial de ação. C. Um outro registro com vários potenciais de ação.

Tabela P.3 Resumo das melhorias apresentadas neste trabalho para cada um dos grupos.

Característica	Lugar	Antes	Depois
Hynet			
Fechamento de Laço	FR	Não	GUI
Pixel Ativo			
Pitch (µm)	SW	40	35
Ganho (V/V)	SW	100	300
Consumo (µW)	SW	83	45
Tecnologia	SW	CMOS 0.35 µm	CMOS 0.18 µm
	FR	Discreta	
Detecção			
Processamento	FR	Software	Hardware
	SW	Digital (FPGA)	Analógica & Integrada
Atraso (µs)	FR	25	< 1

Intelligent multielectrode arrays: improving spatiotemporal performances in hybrid (living-artificial), real-time, closed-loop systems. Guilherme Bontorin, September 2010.

Abstract: This thesis presents a promising new bioelectronics system, the *Hynet*. The *Hynet* is a Hybrid (living-artificial) Network, developed to study the long-term behavior of electrogenic cells (such as Neurons or Beta-cells), both individually and in a network. It is based on real-time closed-loop communication between a cell culture (bioware) and an artificial processing unit (hardware and software). In the first version of our *Hynet*, we use commercial Multielectrode Arrays (MEA) that limits its spatiotemporal performances. A new Intelligent Multielectrode Array (*iMEA*) is therefore developed. This new analog/mixed integrated circuit provides a large-scale, high-density, and adaptive interface with the Bioware, which improves the real-time data processing and the low-noise acquisition of the extracellular signal.
Keywords: Bioelectonics, Real Time, Closed-Loop, Hybrid Systems, LNA, High Density MultiElectrode Arrays (MEA), Neurons, Beta-cells, Analog ASICs.

Matrice d'électrodes intelligentes : un outil pour améliorer les performances spatiotemporelles des systèmes hybrides (vivant-artificiel), en boucle fermée et en temps réel.

Résumé : Cette thèse présente un système bioélectronique prometteur, l'*Hynet*. Ce Réseau Hybride (vivant-artificiel) est conçu pour l'étude du comportement à long terme des cellules électrogénératrices, comme les neurones et les cellules betas, en deux aspects : l'individuel et en réseau. Il est basé sur une boucle fermée et sur la communication en temps réel entre la culture cellulaire et une unité artificielle (Matériel, Logiciel). Le premier *Hynet* utilise des Matrices d'électrodes (MEA) commerciales qui limitent les performances spatiotemporelles du *Hynet*. Une nouvelle Matrice d'électrodes intelligente (*iMEA*) est développée. Ce nouveau circuit intégré, analogique et mixte, fournit une interface à forte densité, à forte échelle et adaptative avec la culture. Le nouveau système améliore le traitement des données en temps réel et une acquisition faible bruit du signal extracellulaire.
Mots-clefs : Bioélectronique, Temps Réel, Boucle Fermée, Systèmes Hybrides, Matrice Multi-électrodes (MEA) à Forte Densité, CMOS, Détection des potentiels d'action, Neurones, Cellules Bêta, ASIC Analogique.

Redes de eletrodos inteligentes: melhorando a performance espaço-temporal de sistemas híbridos (vivo e artificial), em laço fechado e em tempo real.

Resumo: Esta dissertação de doutorado apresenta um sistema bioeletrônico auspicioso, o *Hynet*. Esta Rede Híbrida (viva e artificial), é concebida para o estudo do comportamento à longo prazo de células eletrogeradoras (como neurônios ou células beta), em dois aspectos : individual e em redes. Ele é baseado na comunicação bidirecional, em laço fechado e em tempo real entre uma cultura celular (Bioware) e uma unidade artificial (Hardware ou Software). O primeiro *Hynet* é concebido, mas o uso de Matrizes de Eletrodos (MEA) comerciais limita a performance do sistema. Finalmente, uma nova Matriz de Eletrodos Inteligente (*iMEA*) é desenvolvida. Este novo circuito integrado fornece uma interface adaptativa, em alta densidade e grande escala, com o Bioware. O novo sistema melhora o processamento de dados em tempo real e a aquisição baixo ruído do sinal extracelular.
Palavras chave: Bioeletrônica, Tempo Real, Laço Fechado, Sistemas Híbridos, LNA, Matriz de Multi-eletrodos em Alta Densidade, Detecção de Potencial de ação, Neurônios, Células Beta, Circuito Integrado Analógico.